

4. VEHICLE CONFIGURATIONS

Several combinations of fuel cells and fuel processors are under consideration for vehicle applications. At this time, DOE programs focus the light-duty vehicle development on PEMFC systems. These systems are more suitable for light-duty vehicles because they offer higher power density, better performance on air, and lower temperature operation for rapid start up. The DOD Advanced Research Projects Agency has also aimed at fuel neutrality with the development of multi-fuel processors suitable for PEMFCs and SOFCs in addition to work on DMFCs (Patil). SOFC and DMFC development has not advanced to the point where fuel cell power output is large enough for vehicle applications. These may also have application for heavy-duty vehicles that could use a wider range of fuel cell types. This section reviews on-going vehicle development activities and presents case studies on fuel cell systems that would be feasible for light and heavy-duty vehicle applications. These case studies provide the basis for an assessment of vehicle emissions.

4.1 VEHICLE DEVELOPMENT PROGRAMS

4.1.1 Light-Duty Vehicles

All major automobile manufacturers are developing PEMFC systems for passenger cars. Each of the big three U.S. manufacturers is pursuing a cost-shared development program with the DOE as well as their own programs. European and Japanese auto manufactures also have development programs and are building prototype vehicles. Table 4-1 shows on-going fuel cell development activities that have applications for light-duty vehicles.

Several vehicle manufacturers have built prototype vehicles equipped with low temperature methanol-steam reformers. This configuration does not allow the fuel flexibility of a POX system; however, the effluent from the reformer is more suitable as a feed gas for PEMFCs since it contains a higher hydrogen concentration. GM/Delphi is building a low temperature reformer for a GM fuel cell powered car in a DOE program. Opel, the German subsidiary of GM, unveiled a fuel cell powered Sintra at the Geneva Auto show in March 1998. This methanol-fueled van is equipped with a low temperature steam reformer and a Ballard PEMFC. It does not use a battery for supplemental power and CO clean up is accomplished with a PROX system (Düsterwald). The vehicle has a 50 kW electric motor, 40 L fuel tank, water tank, and total unladen weight of 1800 kg. It accelerates from zero to 100 km/h (62 mph) in 20 sec and has a top speed of 150 km/h (95 mph) (HyWeb). A PEMFC powered Opel Zafira, shown in Figure 4-1, was also built to serve as a development platform (Adam Opel).

Daimler Benz has attracted considerable attention with its prototype fuel cell vehicles NECAR I, NECAR II, and NECAR 3. The first two vehicles were configured for dedicated hydrogen

operation. The fuel cell stack took up the entire interior of NECAR I in a Mercedes-Benz 190 van with a system power density of 167 W/L. NECAR II achieved a much more compact installation in a Mercedes-Benz V-class MPV van with a fuel cell power density of 1000 W/L.

Table 4-1. Fuel cell development efforts

Vehicle/System	Fuel Cell	Fuel	Power/Reformer/Storage ^a
GM PNGV, Opel Sintra 1800 kg	Ballard/GM PEM FC	Methanol	Delphi steam reformer 50 kW FC
Ford PNGV	IFC, H-Power, Plug Power, Energy Partners, Ballard PEMFC	Hydrogen Gasoline	Compressed, 5000 psi (330 atm) storage Multi-fuel POX studies
Chrysler PNGV	Allied Signal PEMFC Ballard PEMFC	Gasoline Hydrogen	Multi-fuel POX Compressed H ₂ , 10 kW FC
Mercedes Benz MDV NECAR I 3500 kg LDV NECAR II 2600 kg LDV NECAR 3 1750 kg	Ballard PEMFC Ballard PEMFC Ballard PEMFC	Hydrogen Hydrogen Methanol	Compressed H ₂ , 33 kW FC Compressed H ₂ , 50 kW FC Steam Reformer, PROX 50 kW FC
Breadboard system	Siemens PEMFC	Methanol	Halder Topsøe Steam Reformer, FZJ catalytic burner; AgPd membrane 50 kW FC
Toyota Prius Toyota RAV4	Toyota PEMFC	Hydrogen Methanol	Hydride storage, 20 kW FC 35 kW NiMH Battery, 35 kW motor
Renault Station Wagon	DeNora PEMFC	Hydrogen	Liquid hydrogen NiMH battery 30 kW FC
VW Joule III	Ballard PEMFC	Methanol	JM Hot-Spot POX, JM PROX, 50 kW FC planned
SOFC Utility Cart	DMFC	Diesel	Keele University experimental test vehicle < 5 kW
Laboratory Fuel Cell	JPL DMFC	Methanol	Currently < 1 kW
Laboratory Fuel Cell	LANL Direct PEMFC	Methanol	Currently < 1 kW
Laboratory Fuel Cell	Siemens DMFC	Methanol	Currently < 1 kW

^a FC = Fuel Cell, JM = Johnson Matthey



Figure 4-1. Opel Zafira powered with a methanol steam reformer (Adam Opel)

The NECAR 3, shown in Figure 4-2, is based on a Mercedes-Benz A-Class car. This proof of concept prototype vehicle is equipped with a methanol steam reformer. Daimler-Benz chose methanol over gasoline and diesel because the vehicle would be more efficient when operating on methanol and the reformer design is less complex with methanol (Heiler). The NECAR 3 is powered by two 150-cell Ballard stacks with a gross power of 50 kW which provides a top speed of 120 km/h (75 mph). The vehicle system is equipped with a compressor/expander that provides air for the fuel cell. The fuel cell uses about 75 percent of the hydrogen produced by the reformer and the balance is burned in a catalytic combustor to power the reformer and expander. The NECAR 3 uses a multi-stage selective CO oxidizer (PROX) to purify the gas mixture from the reformer.

In the NECAR 3, the reformer/fuel cell system is sufficiently large that the vehicle does not require any battery storage for tractive power and produces hydrogen on-line. Motor power is 33 kW continuous with 45 kW peak power capability. The NECAR 3 consumes 38 L of methanol over its 400 km (250 mi) range and is equipped with a 50 L fuel tank (Daimler-Benz). While the vehicle weighs 1750 kg, the NECAR 3 fuel cell and processor system is much more compact than systems on NECAR I and II. The height of the reformer system, shown in Figure 4-3, is 47 cm (18 in). The reformer is located in the rear of the vehicle with the two fuel cells in the floor section. Mercedes-Benz announced that they will offer a fuel cell powered car for sale to the public by the year 2005.



Figure 4-2. The Daimler-Benz NECAR 3 is equipped with a Ballard fuel cell and a methanol steam reformer (Photo courtesy Ballard Power Systems).

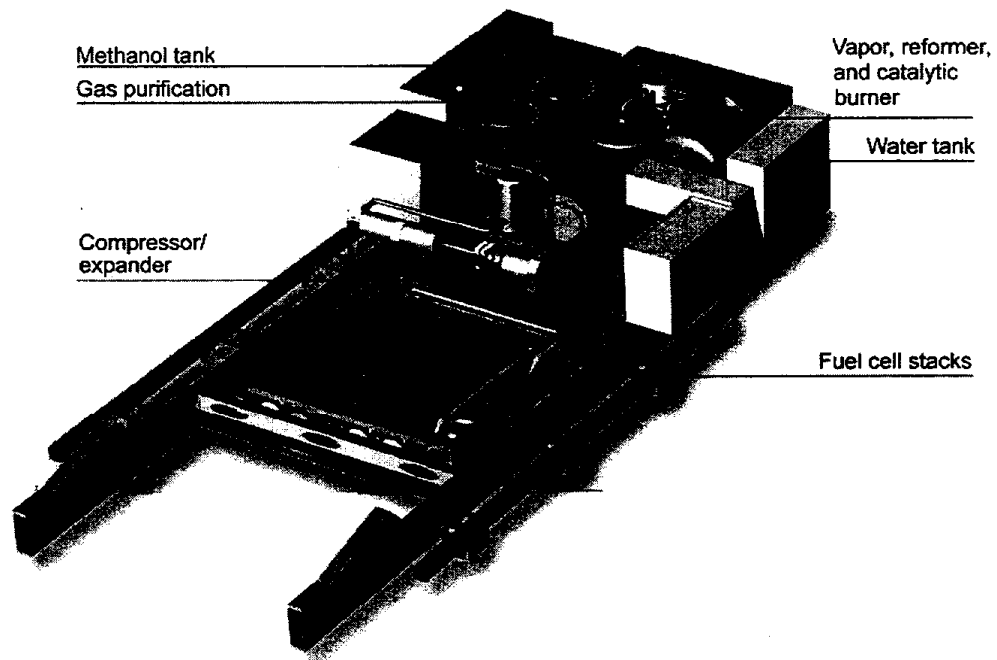


Figure 4-3. The methanol steam reformer and gas clean-up system is located in the rear of the NECAR 3 (Photo courtesy Ballard Power Systems, Daimler-Benz).

Toyota has produced several concept cars for dedicated hydrogen operation with hydride storage. Both the RAV4 and Prius have been configured as hybrid fuel cell vehicles. These vehicles are equipped with 20 kW PEMFCs and 35 kW electric motors. Toyota developed a hydride material that stores 2 kg of hydrogen in a 50 kg tank. The hydride structure has a greater capacity than other hydride alloys. Toyota also built a methanol fueled version of the RAV4 fuel cell hybrid. A low temperature steam reformer generates hydrogen to power the fuel cell.

The European Joule III project will use a Johnson Matthey Hot SpotTM catalytic autothermal reformer operating on methanol with a 50 kW Ballard PEMFC. The autothermal reformer approach offers the efficiency benefits of steam reforming combined with rapid start-up characteristics. The project will produce a prototype vehicle in the same size range as a Volkswagen Golf.

Other methanol fueled development projects include a PEMFC powered car with a steam reformer that has been built at Renault and a breadboard system at the FZJ. The FZJ system is unique because gas clean-up will be accomplished with a membrane, and the fuel cell will operate on pure hydrogen. Ford is developing a dedicated hydrogen PEMFC vehicle under the PNGV program. Several fuel cells were evaluated under this program including units from Energy Partners, IFC, H-Power, and Plug Power. IFC's ambient pressure fuel cell is particularly applicable for dedicated hydrogen systems where no waste anode gas must be burned (Meyer)¹. Ford has undertaken extensive studies with Directed Technologies Inc. (DTI) to evaluate hydrogen supply options and fuel cell efficiency. The advantages of hydrogen operation are zero emissions from the vehicle and an efficiency improvement of about 50 percent over a vehicle with an on-board fuel processor (Thomas); however, some of the efficiency benefit is reduced when hydrogen compression is considered.

Many of the fuel cell developers in the Ford DOE program are also participating in the development of POX/PEMFC systems. IFC is also working on a 50 kW gasoline powered POX/PEMFC vehicle power plant shown in Figure 4-4 (Meyer). This project team includes DOE, A. D. Little (Epyx), Texaco, UOP, and Modine. Ford has also worked with Plug Power on PEM stacks and fuel processor systems. Plug Power acquired fuel cell technology from in a joint venture with Mechanical Technology Inc. (MTI). This team with A. D. Little assembled a gasoline fueled POX/PEMFC system in October 1997 (Ernst).

In December 1997, Ford entered into a joint venture with Ballard Power Systems and Daimler-Benz (Roman). This venture established three companies that develop and manufacture fuel cells, fuel cell systems, and electric drivetrain systems. Ballard Power Systems retains majority ownership of the company that manufactures fuel cells. Daimler-Benz is the majority owner of dbb Fuel Cell Engines GMBH. This company will be responsible for fuel processors, air supply, and control subsystems. Ford is the majority owner of the company, ECo, which will further develop and commercialize electric drivetrains. An electric drive system consists of a traction

¹Uses for the unreacted hydrogen from a POX system are limited. As discussed later, waste anode gas helps power a compressor expander, which makes POX systems well suited for pressurized operation. A pure hydrogen fuel cell can recirculate hydrogen, so no waste anode gas is generated.

inverter, electric motor, and transaxle which converts electric power from the batteries and fuel cell system to tractive power.

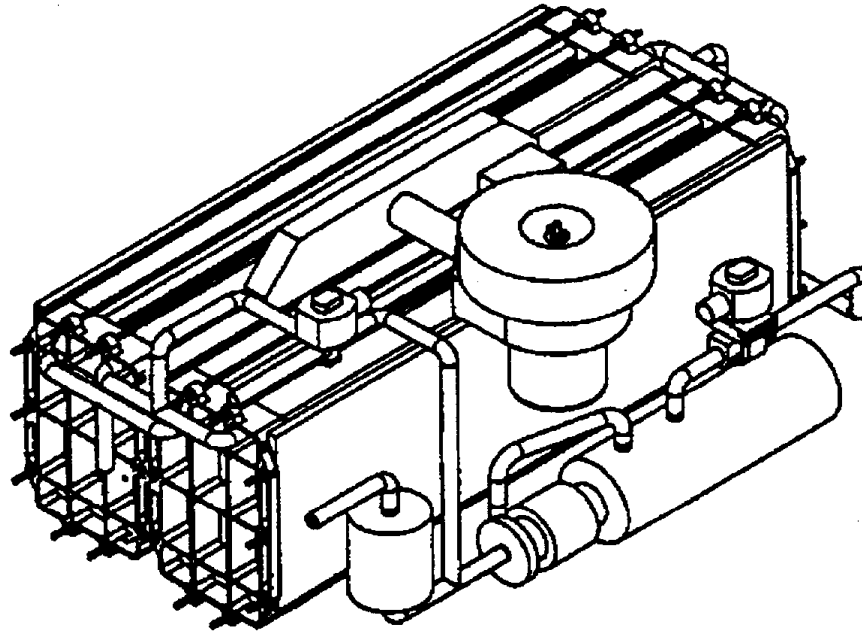


Figure 4-4. IFC 50 kW gasoline-air power plant for automotive applications

Another dedicated hydrogen vehicle started on-road operation in September 1997 under the Fuel Cell Electric Vehicle for Efficiency and Range (FEVER) project. DeNora, of Italy, provided a 30 kW PEMFC which was installed in a Renault station wagon. Hydrogen is supplied by a 115 kg liquid hydrogen tank which holds 8 kg of hydrogen. Nickel metal hydride batteries provide 2.8 kWh of energy storage. The vehicle has a top speed of 120 km/h (75 mph) and a range of 500 km (300 mi) (Hydrogen and Fuel Cell Letter).

Chrysler is pursuing the development of a multi-fuel POX system for PEMFCs. They are teamed with Allied Signal who is developing a PEMFC module for vehicles. A. D. Little (Epyx) is participating in the effort with their multi-fuel POX system. The fuel cell stack is packaged in a cylinder that fits in the tunnel formerly occupied by the exhaust system and drivetrain. Delphi Energy and Engine Management systems is also integrating a Ballard PEMFC with a gasoline fuel processor for Chrysler (Lancaster). At the 1997 Detroit Auto Show, Chrysler announced plans to complete a gasoline powered prototype vehicle for on-road operation in 1999.

DMFCs are not ready for vehicle demonstrations because the technology requires further development and scale-up work. A near term goal for DMFCs might be a hybrid utility vehicle with a small 5 kW fuel cell, with a 50 kW system for a passenger car requiring at least 5 more years of development.

4.1.2 Heavy-Duty Vehicles

Several fuel cell powered transit bus development programs are underway. The longest running project is headed by Georgetown University. The project was initially funded by the U.S. DOE, U.S. Department of Transportation (DOT), through the Federal Transit Administration (FTA) and the SCAQMD. The project initially focused on the development of a PAFC with a low temperature methanol steam reformer. Fuji provided both the reformer and fuel cell. PAFC/battery hybrid power plants were successfully installed and tested in three 9 M (30-ft) test bed buses (TBB). Figure 4-5 shows one of the buses. The 50 kW Fuji PAFC stack plus reformer can charge Saft nickel-cadmium (NiCd) batteries or can power the motor directly at part loads. The batteries provide power for grades and acceleration. A control system monitors the battery's state of charge (SOC), as well as traction power demand. When power is available from the fuel cell for charging and the battery is sufficiently discharged, the control system directs the fuel cell to charge the battery (Roan). The batteries also provide energy storage for regenerative braking. A summary of the Georgetown program and other programs is shown in Table 4-2.

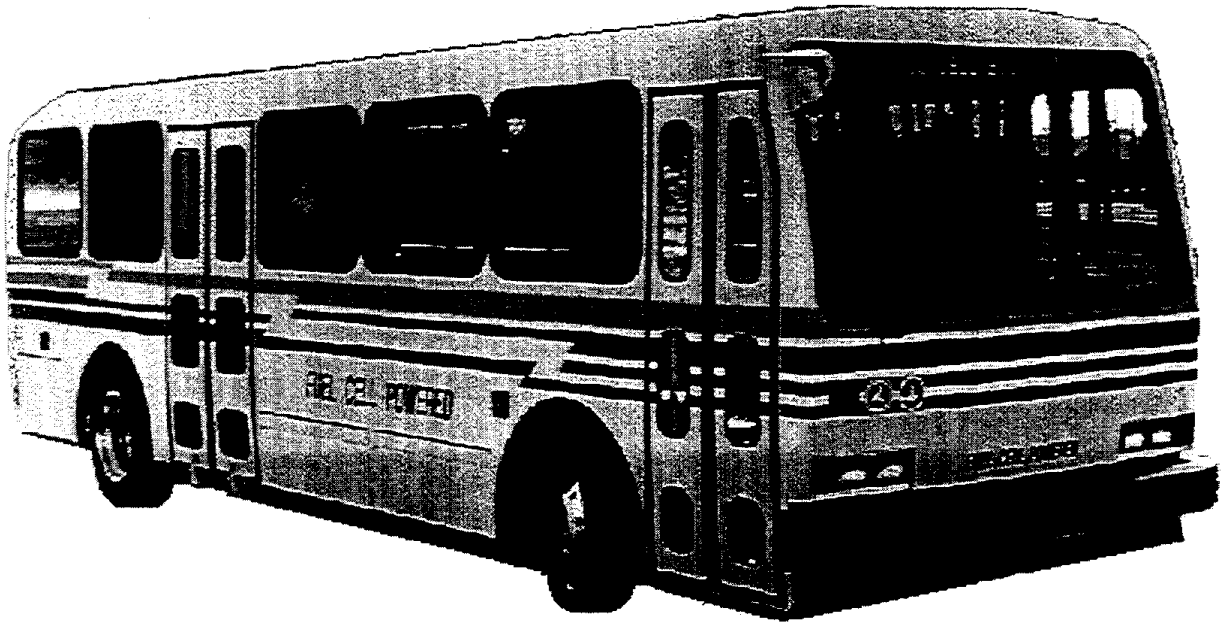


Figure 4-5. Three methanol fueled PAFC buses were built under Phase III of the Georgetown University program (Photo from NREL)

Table 4-2. North American fuel cell bus development programs

Project	Georgetown University Methanol Buses	DARPA Diesel Bus	Ballard Hydrogen Buses
Technology	<ul style="list-style-type: none"> • Phases I-III: Fuji PAFC (57 kW) with methanol steam reformer in three 30-ft buses (1994). • Saft Ni-Cd batteries • Phase IV: two 40-ft buses with different fuel cell technologies (1998) Ballard PEMFC with methanol SR. IFC PAFC with high temperature methanol SR • Electrosorce lead acid batteries 	<ul style="list-style-type: none"> • H-Power PEMFC • 6 month demonstration in a 32-ft Blue Bird bus with pure hydrogen fuel, 10 kW (1997) • Hydrogen Burner Technology multifuel POX reformer with integrated gas clean-up • 30 ft bus to be selected for diesel fueled operation, 60 kW (2000) 	<ul style="list-style-type: none"> • Ballard 120 kW PEMFC • directly fueled with compressed hydrogen, in a 32-ft El Dorado-National shuttle bus chassis (1993) • Phase II: 205 kW hydrogen-fueled Ballard PEMFC engine in a 40-ft New Flyer (D40LF) low floor bus (1995) • Phase III: 205 kW Ballard PEMFC 40-ft bus will then be demonstrated in Vancouver, Chicago and Los Angeles (1997)
Sponsors	<ul style="list-style-type: none"> • U.S. DOT/FTA • U.S. DOE • SCAQMD 	<ul style="list-style-type: none"> • DARPA • SMAQMD • CA ARB • SMUD 	<ul style="list-style-type: none"> • Canadian Federal government • Province of British Columbia • BC Transit • SCAQMD
Prime Contractor Subcontractors	<ul style="list-style-type: none"> • Georgetown University • IFC: PAFC with high temperature methanol SR • Ballard Power Systems: PEMFC with low temp methanol SR • Lockheed Martin Control Systems • Booz-Allen & Hamilton - system integration • TMC (Novabus) - bus chassis 	<ul style="list-style-type: none"> • H-Power • Hydrogen Burner Technology • McClellan Air Force Base • Singapore Technologies Automotive • Demonstration site to be determined 	<ul style="list-style-type: none"> • Ballard Power Systems • Science Applications International (SAIC): system integration • EDO: composite tanks for compressed hydrogen fuel

With funding from FTA, the Georgetown fuel cell bus project has moved into Phase IV. This phase seeks to commercialize 12 m (40-ft) transit buses with Ballard and IFC supplying both PEMFCs and PAFCs, and reformer systems. An IFC PAFC system was engineered into a Novabus RTS chassis (Brady). The fuel cell system is rated for 100 kW net (110 kW gross) power delivery, and it weighs 1730 kg. The reformer is a high temperature design based on IFC's stationary natural gas powered fuel cell. The reformer can operate on natural gas, naphtha, or LPG since reforming takes place at 800°C. As with the initial 30-foot TBB prototypes, this hybrid design will use batteries to store energy for load following and regenerative braking. An Electrosource lead acid battery pack provides storage capacity of approximately 49 kWh. The system, including battery housing, balance of system, and inverter, weighs 1820 kg. Lockheed Martin Control Systems is providing the power controls and propulsion system. The PAFC bus, with a seated capacity of 40 passengers, weighs 15,000 kg (17,950 kg GVW) and has a design range of 560 km (350 mi). The IFC bus first operated in 1997 and is undergoing development testing. Ballard (ddb) is developing a low temperature methanol steam reformer for use with their PEMFC. The fuel cell will also deliver 100 kW, and it will power a hybrid bus (Cooper).

Ballard Power Systems has built a series of prototype dedicated hydrogen buses leading to a commercial product. Direct hydrogen fueling eliminates the need for a reformer, and allows the fuel cell engine to follow load transients well enough that supplemental batteries are not needed. The advantages inherent in the relative simplicity of direct hydrogen fueled PEMFC stacks were underscored when an operational prototype of the Ballard bus was completed and road tested by early 1993, one year before the FTA program reached the same benchmark. While this vehicle incorporates dynamic (electric motor) braking, the braking energy cannot be stored for later use.

The initial Ballard prototype was a 10 m (32 ft) bus powered by a 90 kW PEMFC engine. In the second phase of the Ballard project, a more powerful 205 kW engine is being used, which is based on a new generation PEMFC with 2.5 times the power density of that used in the prototype bus (Howard). The more powerful stack was engineered into a 12 m (40 ft) Flyer (D40LF) low floor transit bus. This package is designed to meet FTA White Book performance standards and achieve a range of 400 km (250 mi) per hydrogen fill. A prototype of the Ballard 40-ft bus was delivered to Chicago Transit Authority on September 11, 1995 (Hydrogen and Fuel Cell Letter). Phase 3 demonstration buses were delivered to the Chicago Transit Authority and BC Transit in Vancouver. The 205 kW fuel cell engine is shown in Figure 4-6. The Phase 3 bus, shown in Figure 4-7, carries 60 passengers and has a range of 400 km (250 mi). The planned range for commercial buses is 560 km (350 mi) and will have a passenger carrying capacity of 75 passengers (Ballard).

In May 1997, Daimler-Benz unveiled its first dedicated hydrogen bus, called the NEBUS (new electric bus). The bus is also powered by the 205 kW Ballard PEMFC engine. The bus operates at various transit agencies in Germany.

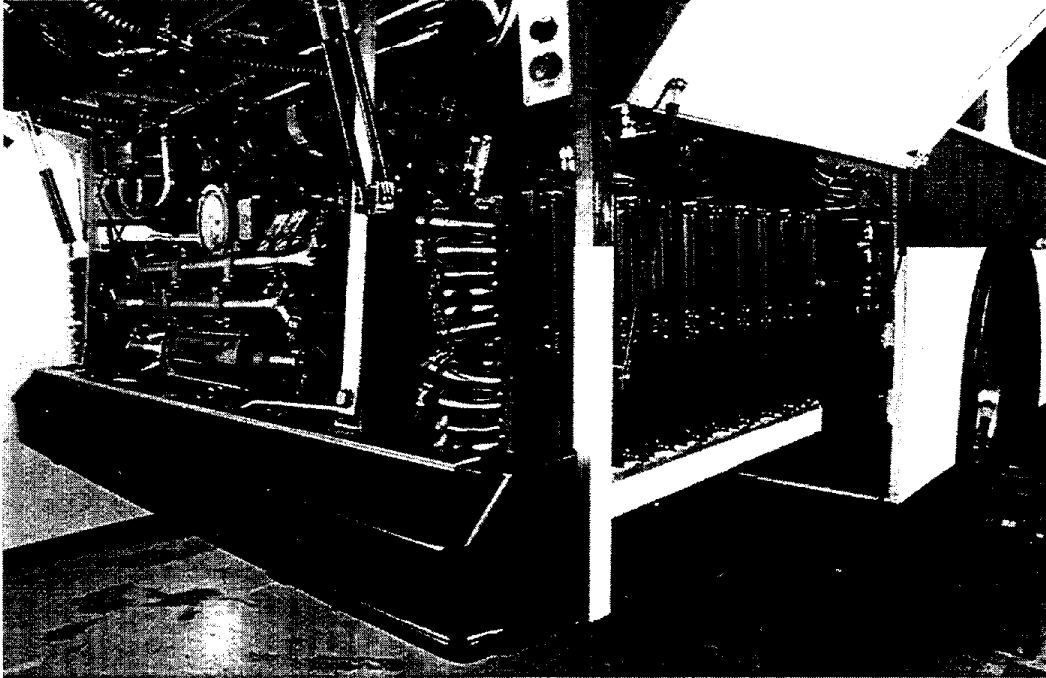


Figure 4-6. Ballard 205 kW fuel cell engine (Photos courtesy Ballard Power Systems)



Figure 4-7. Ballard dedicated hydrogen bus

4.2 FUEL CELL VEHICLE CONFIGURATIONS FOR CASE STUDIES

Case studies of light and heavy-duty fuel cell vehicles were developed to evaluate vehicle emissions and assess effects of different fuel, fuel processor, and vehicle configurations. The vehicle configuration provides input for a vehicle energy consumption and emissions model. Table 4-3 identifies the fuel cell/reformer combinations that were investigated. Because light-duty vehicle operation is dominated by stop and go driving with frequent short trips, PEMFC and DMFC vehicle configurations are the basis for light-duty vehicle case studies. These fuel cells operate at low temperatures and, therefore, do not incur substantial energy penalties for start up. The CO₂ tolerance, status of technology, and fast start up capability make PEMFCs the principal option for passenger cars. DMFCs, if scaled up and further developed, would be attractive options for passenger cars. Heavy-duty vehicles operate over longer duty cycles where energy losses from start up have a smaller effect and higher temperature fuel cells are options.

Table 4-3. Fuel cell vehicle configurations for case studies

Fuel	Vehicle	Reformer	Processing	Fuel Cell	Case Studies
Gasoline	LDV	POX	PROX	PEMFC	Table 4-6
Diesel					Table 4-7
LPG					
CNG					
Ethanol Methanol					
Methanol	LDV	Low temperature steam reformer	Membrane	PEMFC	Table 4-8
Methanol	LDV	ATR/low temperature steam reformer	PROX	PEMFC	
Methanol	LDV	Steam reformer	PROX	PEMFC	
Methanol	LDV	—	—	DMFC	
Methanol	HD bus	Low temperature steam reformer	—	PEMFC	Table 4-13
Methanol CNG	HD bus	High temperature steam reformer	—	PAFC	
Diesel	HD bus	POX	PROX	PEMFC	
Diesel	HD bus	POX	—	SOFC	

4.3 LIGHT-DUTY VEHICLE CASE STUDIES

Detailed analytical simulations of reformer/fuel system performance were performed for two light-duty vehicle options: a PEMFC with multifuel POX and a PEMFC with a methanol steam reformer. Relevant comments concerning system performance issues are also provided for DMFC systems. Detailed analytical simulations of reformer/fuel cell system performance were formed for the fuel and fuel processor combinations listed in Table 4-3. Various hybrid options are considered for a gasoline POX/PEMFC system while the other fuels are evaluated with the same fuel cell size and hybrid strategy. The analysis of the multi-fuel POX and ATR systems are considered together since the operation of HBT's POX system includes steam injection. The ATR under development by Epyx uses a catalyst to enhance reforming in the presence of steam. The operating conditions of a POX system and an ATR overlap. At the time of this study, insufficient data was available to distinguish performance and potential future emission differences between a POX system with steam injection and an ATR, also with steam injection and a reforming catalyst. Specific calculations are based on a non-catalytic system with a high temperature POX section.

Three technology options involving low temperature methanol steam reforming were considered. Low temperature steam reforming allows for the development of several unique approaches for gas reforming and gas clean up. Most methanol steam reformer systems (NECAR 3, Opel, Toyota, GM) rely on heat transfer between the reformer burner and the reformer. The hybrid steam reformer/ATR developed by Johnson Matthey allows for a rapid start up of the fuel processor while a conventional steam reformer may take longer to warm up. A membrane system is possible with a steam reformer system since the reformer can produce a relatively high concentration of hydrogen at high pressure. This system is under development at the FZJ.

The evaluation of a fuel cell/reformer system is based on a process flow diagram, flow simulation model, and estimates of vehicle weight for different configuration options. The parameters from this analysis provide input to a model of emissions and energy demand over different driving cycles. Modeling a fuel cell system requires an assessment of the system power requirements as well as the fuel cell/reformer components. This evaluation is an iterative process where the performance of the fuel cell system affects the weight of vehicle components which affects power demand from the fuel cell system. The vehicle configurations are presented first. The vehicle energy demands and weight estimates for light-duty vehicle options are described in Section 4.3.1. The process flow diagram and system integration considerations along with the simulation modeling assumptions are given in Section 4.3.2. Fuel consumption for light-duty vehicle case study results are presented in Section 4.3.3. Results of the case studies are presented in Section 6.

4.3.1 Light-Duty Vehicle Energy and Weight Modeling

A conceptual design of a light-duty passenger car provided the basis for determining parameters for modeling the vehicle and components. The vehicle weight affects fuel consumption and reformer size and affects start-up emissions. A light-duty vehicle model is shown in Figure 4-8. The vehicle is configured as either a pure fuel-cell-powered vehicle or a serial hybrid with

battery, flywheel, or ultracapacitor energy storage. The weight of the following components was predicted according to the vehicle power requirements.

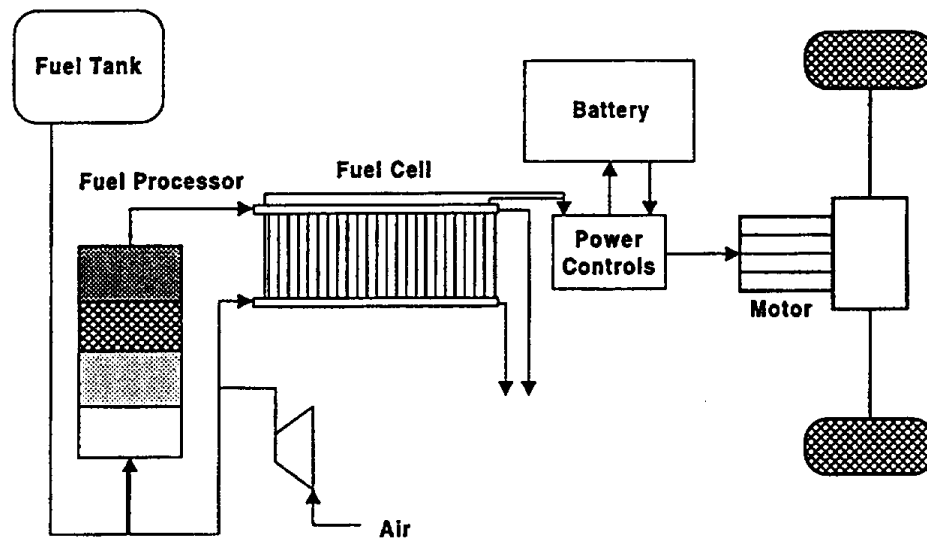


Figure 4-8. Simplified fuel cell vehicle system with on-board fuel processor

- Base vehicle without engine (glider)
- Fuel cell
- Fuel processor
- Radiator and water storage
- Traction battery
- Power controller
- Electric motor and transmission

The weight of the vehicle components depends on the performance requirements of the vehicle. The vehicle design is based on a mid-sized American passenger car with modest performance capabilities. Minimum acceleration for zero to 60 mph (96.6 km/h) is 11 seconds. Hill climbing capability is a 4 percent grade at 100 km/h for at least 15 km. The acceleration requirement determines the maximum power which must be met by the combined output of the fuel cell and battery. The hill climbing requirement typically does not constrain total power output since the power required for acceleration is much greater than the power required to sustain a constant speed during a hill climb. However, for systems with small fuel cells and large batteries, hill climbing requires a large battery for energy storage.

Figure 4-9 shows the predicted acceleration performance for a fuel cell vehicle with electric drive compared to a gasoline powered vehicle. The fuel cell vehicle curve is based on a constant motor power output after the initial first second of acceleration. The speed versus time curve in Figure 4-9 is calculated from the power that is available from the motor after air resistance and road loads are taken into account. The motor power affects the peak fuel cell and battery power requirements. Because electric motors can generate much more torque at low speeds, the fuel cell vehicle has the capability to accelerate more quickly than a gasoline powered vehicle with a spark-ignited engine. This result is significant because it allows for acceleration at a constant rate at peak power. Therefore, a somewhat heavier fuel cell powered vehicle can achieve the same 0 to 100 km/h acceleration as a conventional vehicle with the same maximum power output. While reformer response time may produce a delay in power output, a fuel cell powered vehicle with battery or capacitor storage is expected to have very good low speed acceleration.

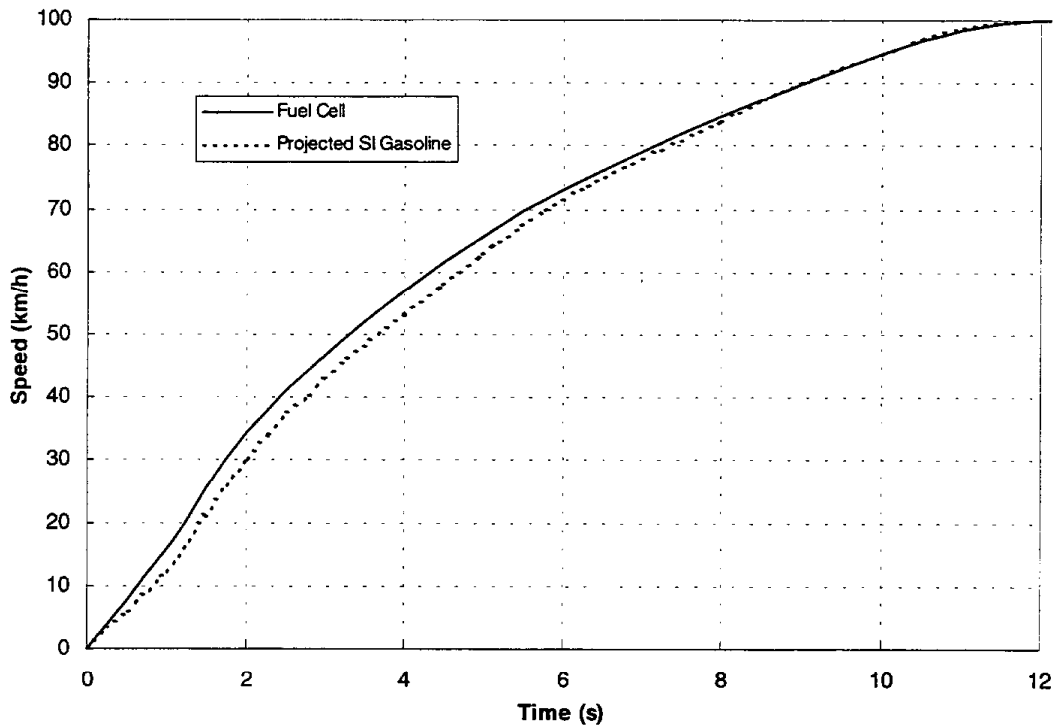


Figure 4-9. Passenger car acceleration performance

The power required for acceleration is the key parameter that affects the size of the vehicle power train components. The force, F , that must be overcome during acceleration is determined from the following relationship:

$$F = \frac{1}{2} C_D A_f \rho V^2 + mg \sin\theta + C_{rr} mg \cos\theta + m dV/dt$$

where:

C_D = vehicle drag coefficient

A_f = vehicle frontal area (m^2)

ρ = air density ($1.18 \text{ kg}/m^3$)

V = vehicle speed (m/s)

m = vehicle mass (kg)

g = gravitational constant ($9.8 \text{ m}/s^2$)

Θ = angle of grade

C_{rr} = coefficient of rolling resistance = $C_{rs} + C_{rd}V$

where C_{rs} - static rolling resistance coefficient (dimensionless) and C_{rd} = dynamic rolling resistance coefficient (s/m)

dV/dt = change in speed (m/s^2)

Road load power (RLP) is the product of force and velocity:

$$RLP = F V$$

Vehicle mass was derived from an analysis of vehicle component weights, which depended on the power density values shown in Table 4-4. The size of system components was based on a two passenger load and the weight of the vehicle including the fuel and fuel tank. The efficiency of system components in Table 4-5 affected the size of the fuel cell and supplemental traction battery. A model of vehicle component mass determined the fuel cell, fuel processor, and battery size based on road load power requirements.

Both fuel cell only and hybrid configurations were evaluated. The vehicles are classified according to battery size. The system with no battery is referred to as fuel cell only. The system with a small battery that provides peak power with the fuel cell following the road load is referred to as the fuel cell dominant hybrid. The opposite approach is a large battery that follows the driving load with a small fuel cell, referred to as a battery dominant hybrid. The load sharing hybrid has a fuel cell and battery with equal power capabilities. Table 4-6 shows the analysis results for gasoline POX/PEMFC power plants. The conclusion is that the net weight increase relative to the gasoline IC engine ranges from about 100 to 250 kg. This conclusion is generally applicable to other current reformer/fuel cell combinations.

Table 4-4. Specific power of vehicle powertrain components (kW/kg)

Component ^a	PEMFC POX	PEMFC Methanol ATR	PEMFC/Methanol SR		DMFC
			Membrane	PROX	
Fuel cell	0.85	0.9	1.0	0.95	0.25
Fuel Processor Weight	0.7	0.65	0.65	0.6	—
Motor, Transmission	1.5	1.5	1.5	1.5	1.5
Power Controls	1.5	1.5	1.5	1.5	1.5
Battery, NiMH	0.25	0.25	0.25	0.25	0.25

^a Gottesfeld reports achievable power density of 0.25 kW/kg for DMFC and 1.0 kW/kg for H₂ PEMFC. Leidjeff-Hey indicates a development target of 0.5 to 1.25 kWh/kg target for passenger car PEMFCs. PEMFC values are adjusted for effect of reformate on power output. DOE goal for fuel processor is 0.6 kW/kg which has been achieved by ADL for an ATR/POX system. Motor, transmission, radiator, and controls based on year 2004 projections from James. Edwards reports power density of 1.0 kW/kg for Johnson Matthey Hot Spot™. Reh reports a goal of 0.35 kW/kg for a Fuel Cell and Fuel Processor System.

Table 4-5. Efficiency of electric drivetrain components²

Component	Efficiency (%)
Transmission	95
Motor	90
Battery in (charge)	87
Battery out (discharge)	87
Electric motor/ Controller	80

²Ogden estimates 80% battery round trip efficiency. Burke reports a 90% round trip for thin film lead acid pulse batteries and 55% round trip for NiMH pulse batteries. Lai reports 85.7% charging and 92% discharging (78.8% round trip) for current fed management and 87.7% charging, 86.4% discharging (75.8% round trip) for voltage fed management. Wimmer (1998b) reports measured efficiency values for IFC PAFC bus components: 94% DC to DC converter; 94% motor controller; 65% DC motor efficiency; and 79% battery.

Table 4-6. Component and vehicle mass for gasoline POX/PEMFC model passenger car

Component	Baseline LDV Gasoline ICE	Gasoline Fuel Cell Only	Gasoline Fuel Cell Dominant Hybrid	Gasoline Load Sharing Hybrid	Gasoline Battery Dominant Hybrid	Gasoline Fuel Cell Dominant Hybrid
Fuel Cell/Engine Type	Spark ignited	PEMFC	PEMFC	PEMFC	PEMFC	PEMFC
Fuel Processor		POX PROX	POX PROX	POX PROX	POX PROX	POX Methanation
Fuel Cell Power (kW)	—	75	60	40	20	60
Battery Net Power (kW)	0	0	19	40	64	19
Motor power (kW)	75	68.4	70.5	72.1	74.6	70.5
Glider Weight (kg)	930	930	930	930	930	930
Passenger Load (kg)	140	140	140	140	140	140
Engine/Fuel Cell Weight (kg)	162	88.2	70.6	47.1	23.5	75.0
Fuel Tank Weight (kg)	40	32.0	32.0	32.0	32.0	32.0
Tank Capacity (L)	50	40	40	40	40	40
NiMH Traction Battery Weight (kg)	0	0	90	193	300	90
Radiator, Water tank (kg)	13.0	21.4	17.1	11.4	5.7	17.1
Fuel Processor Weight (kg)	0	126	101	67	34	96
Power Controls (kg)	0	45.6	47.0	48.1	49.8	47.0
Motor, Transmission (kg)	50.0	68.4	70.5	72.1	74.6	70.5
Vehicle Design Weight (kg)	1335	1452	1498	1541	1589	1498
Vehicle Test Weight (kg)	1265	1382	1428	1471	1519	1428
Net Weight over ICE (kg)	0	117	163	205	254	163

The fuel cell only configuration has the advantage of operating at a lower average load on the fuel cell; therefore, the fuel cell produces a higher voltage and is more efficient although the fuel processor efficiency is reduced at lower loads. DOE's goal for POX PEMFC vehicle development is a fuel cell only system with no battery energy storage. Operating a vehicle in this mode will prove challenging as the ability of a fuel processor to follow transient load changes is unknown. Adding an energy storage device with about 15 kW of peaking power reduces the fuel cell power to 60 kW (fuel cell dominant hybrid in Table 4-6). A battery or ultracapacitor would be a desirable form of energy storage as these can provide power during start up and as well as acceleration while a flywheel is unlikely to store power for an extended shut down. An advanced battery, such as a lead acid pulse battery or a nickel metal hydride (NiMH), would be available in the near term. A vehicle with a NiMH battery weighs 90 kg more than the baseline vehicle. Replacing the battery with an ultracapacitor saves 40 kg in vehicle weight. Ultracapacitors will be more desirable long term options since they will result in cost and weight savings. The effect of this weight savings on emissions would be minimal and was not considered in this study. Regenerative braking capability is still feasible with an ultracapacitor since the total energy from

Table 4-7. Component and vehicle mass for alternative fueled POX/PEMFC model passenger car (fuel cell dominant hybrid configuration)

Component	Diesel	LPG	Ethanol	CNG ^a	CNG	Methanol
Fuel Cell/Engine Type	PEMFC	PEMFC	PEMFC	PEMFC	PEMFC	PEMFC
Fuel Processor	POX PROX	POX PROX	POX PROX	POX PROX	POX PROX	POX PROX
Fuel Cell Power (kW)	60	60	60	60	60	60
Battery Power (kW)	21	19	19	22	24	20
Motor power (kW)	70.8	70.5	70.9	72.8	75.3	71.6
Glider Weight (kg)	930	930	930	930	930	930
Passenger Load (kg)	140	140	140	140	140	140
Engine/Fuel Cell Weight (kg)	70.6	70.6	70.6	70.6	70.6	70.6
Fuel Tank Weight (kg)	37.6	31.9	38.9	67.0	103.9	69.6
Tank Capacity (L)	40	55	45	120	190	80
NiMH Traction Battery Weight (kg)	92	90	92.5	102.4	115.0	95.8
Radiator, Water tank (kg)	17.1	17.1	17.1	17.1	17.1	17.1
Fuel Processor Weight (kg)	101	101	101	100.8	100.8	100.8
Power Controls (kg)	47.2	47.0	47.3	48.6	50.2	47.7
Motor, Transmission (kg)	70.8	70.5	70.9	72.8	75.3	71.6
Vehicle Design Weight (kg)	1506	1498	1508	1549	1603	1543
Vehicle Test Weight (kg)	1436	1428	1438	1479	1533	1473
Net Weight over ICE (kg)	171	163	173	214	268	186

^a Range limited to 420 km (260 mi).

The properties of methanol allow for greater flexibility in fuel processing. The catalytic dissociation of methanol and steam occurs at 260°C while temperatures around 700°C are required for steam reforming of other fuels. Autothermal reformers (ATRs) and steam reformers (SRs) can result in improved fuel processing efficiency. DMFCs would result in a simplified power plant system. Table 4-8 shows the weight of vehicles with methanol ATRs, methanol SRs, and DMFCs. The 60 kW SR/PROX system reflects the NECAR 3 design and the 20 kW SR/PROX system reflects the Toyota hybrid design. The power density of the PEMFC operating on methanol SR product gas was estimated to be 5 percent greater than that of a PEMFC operating on POX reformat. This improvement in power density is offset by a lower power density for the fuel processor system. The net effect is an increase of 164 to 183 kg over a conventional vehicle. The weight of the pure methanol PEMFC cell vehicle is similar to that of configurations with power augmentation. Projections of power density for a DMFC are 0.25 kW/kg (Halpert 1997b) compared to values closer to 1.0 kW/kg for gaseous PEMFCs. The reduced power density of the DMFC results in a heavier vehicle; however, the fuel cell power

system is substantially simpler than other configurations. For the DMFC, a battery dominant hybrid would weigh about as much as a fuel cell only vehicle since the battery must provide both peak power for acceleration and energy storage for hill climbing. An ultra capacitor could reduce the weight of a DMFC vehicle because the ultra capacitor has such a high power density. Other energy storage options such as pulse batteries with greater power density at the expense of energy density would also be suitable for fuel cell powered vehicles.

Table 4-8. Component and vehicle mass for methanol fuel cell passenger car (low temperature ATR, SR, and DMFC systems)

Component	Methanol Fuel Cell Dominant Hybrid	Methanol Fuel Cell Dominant Hybrid	Methanol Fuel Cell Dominant Hybrid	Methanol Battery Dominant Hybrid	Methanol Fuel Cell Only	Methanol Battery Dominant Hybrid
Fuel Cell/Engine Type	PEMFC	PEMFC	PEMFC	PEMFC	DMFC	DMFC
Fuel Processor	ATR/PROX	SR/membrane	SR/PROX	SR/PROX	—	—
Fuel Cell Power (kW)	60	60	60	20	72.9	20
Battery Power (kW)	20	20	20	60	0	61
Motor power (kW)	71.4	71.3	71.4	70.5	72.8	72.0
Glider Weight (kg)	930	930	930	930	930	930
Passenger Load (kg)	140	140	140	140	140	140
Engine/Fuel Cell Weight (kg)	66.7	60.0	63.2	21.1	291.6	80.0
Fuel Tank Weight (kg)	47.9	47.9	47.9	47.9	47.9	47.9
Tank Capacity (L)	55	55	55	55	55	55
NiMH Traction Battery Weight (kg)	94.7	94.1	94.7	202.1	0.0	208.0
Radiator, Water tank (kg)	17.1	17.1	17.1	5.7	18.2	5.0
Fuel Processor Weight (kg)	102.6	107.1	105.3	35.1	0.0	0.0
Power Controls (kg)	47.6	47.5	47.6	47.0	48.6	48.0
Motor, Transmission (kg)	71.4	71.3	71.4	70.5	72.8	72.0
Vehicle Design Weight (kg)	1518	1515	1517	1499	1549	1531
Vehicle Test Weight (kg)	1448	1445	1447	1429	1479	1461
Net Weight over ICE (kg)	183	180	182	164	214	196

The vehicle weight estimates provide input into the model of vehicle energy consumption and emissions. Advances in vehicle construction materials and manufacturing as well as improvements in aerodynamics are being considered as means of improving vehicle fuel economy. The objective of these vehicle weight estimates is to provide a basis for comparing different fuel cell configurations. The estimates correspond to aggressive weight reductions for vehicles manufactured in the year 2005, but are by no means the lowest vehicle weights that are projected for future fuel cell powered vehicles. The vehicle weight projections provide a basis for estimating fuel processor weight and warm up energy requirements as well as a consistent basis for determining vehicle load for driving simulations. DMFCs are not as advanced as the

other technology options in Figure 4-8 and represent a more long-term estimate of a vehicle system.

4.3.2 Process Descriptions and Modeling Assumptions

The process mass and energy balance simulation combined in-house models and a chemical process analyses to determine the energy consumption and emissions. The model determines the reformer gas inlet and exit compositions, CO removal, gas humidification, fuel cell hydrogen reaction, water recovery, excess anode hydrogen combustion, and compressor/expander performance. The following covers the system descriptions and model assumptions for the POX/PEMFC system, the methanol steam reformer/PEMFC, and the DMFC system.

POX/PEMFC System Description

A schematic diagram of a POX/PEMFC system is shown in Figure 4-10. Fuel, air, and steam react in the POX reactor to form a mixture of nitrogen, hydrogen, CO, CO₂, and traces of hydrocarbons, methane, and ammonia. Water is injected to quench the POX gas mixture. CO reacts with steam in the HTS and LTS, and final traces of CO are reduced in a PROX and/or methanation reactor. POX systems are suited for pressurized operation because excess fuel from the fuel cell anode cannot be burned in the reformer. The PEMFC consumes hydrogen from the anode gas mixture, and the remaining gas passes through a condenser and is burned in a catalytic burner. Oxygen-depleted air from the fuel cell cathode reacts with the waste anode gas. The catalytic burner is the principal source of emissions from this system. Exhaust from the burner (at 3 atm) passes through an expander which drives a turbo-compressor to provide air for the POX and fuel cell.

The selection of components and operating conditions for a fuel cell system affects its efficiency and operability. For example, the complexity, cost, and energy consumption of compression equipment must be weighed against the improvement in efficiency. Key parameters in a POX/PEM FC system that affect the complexity and efficiency include the following:

- System pressure
- Humidification and water recovery
- Fuel type
- Sulfur removal
- CO cleanup system
- Operating stoichiometry

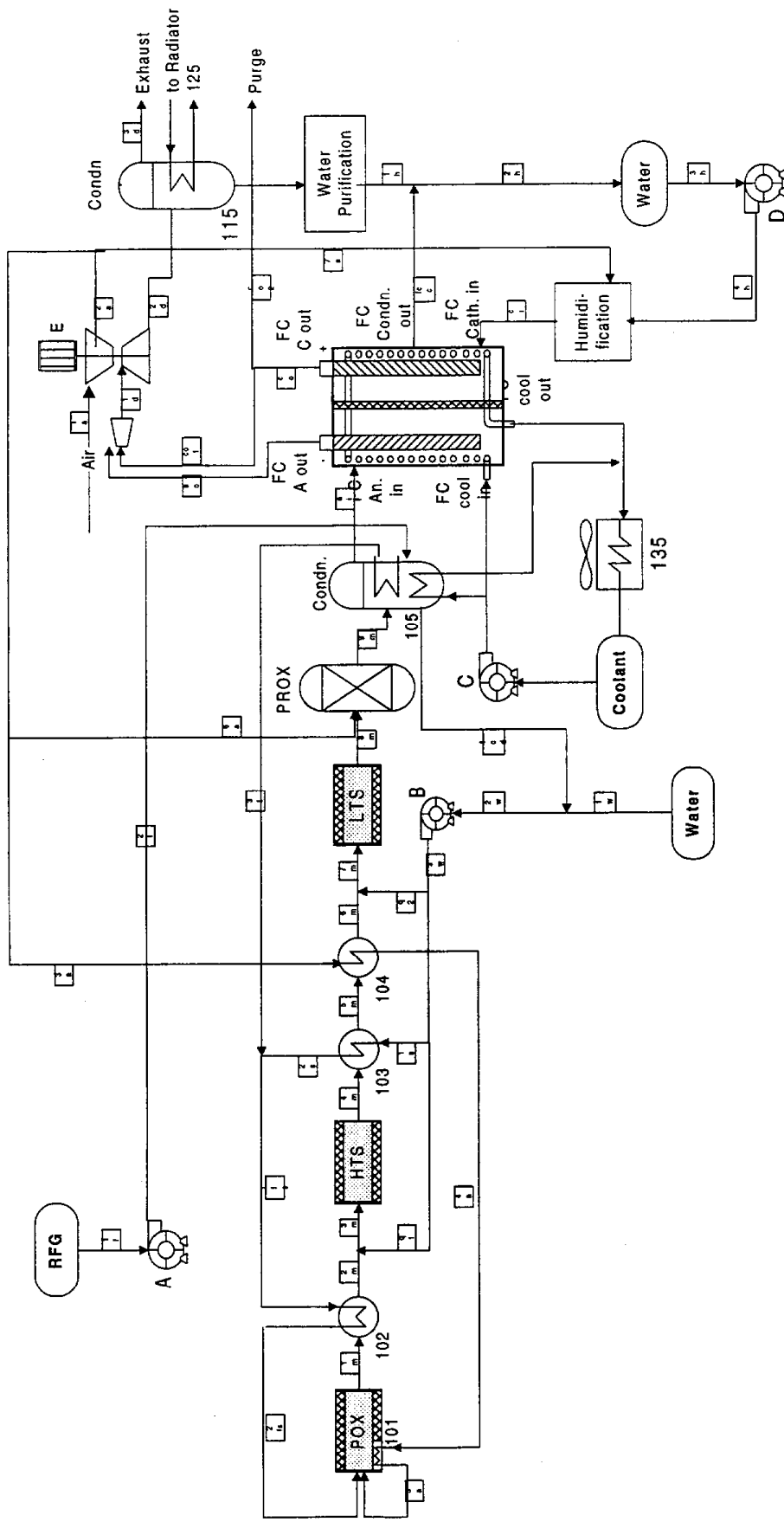


Figure 4-10. Process flow diagram for POX system with PEMFC

The fuel cell stack operating pressure affects system efficiency because the cell output voltage increases at elevated pressures. This effect has led to the development of more efficient compressor/expanders. However, the compressor/expander system adds complexity and cost to the fuel cell system. The complexity of providing compressed air has led to the development of low pressure fuel cell stacks.

PEMFC humidification and water recovery is an important system consideration that favors operation at 3 atm. The feed gas to the PEMFC must be sufficiently humid to prevent drying of the cell membrane in comparison to the values shown in Table 3-6. The fuel volume for the gasoline and diesel fuel cell vehicles was reduced to 40 L. This fuel volume provides a slightly higher range than that of the conventional gasoline vehicle. Fuel tank size is important since it not only affects vehicle range but also affects fuel spillage assumptions discussed in Section 6.2. The fuel tank volume represents a compromise between reducing vehicle weight and providing additional range. It was estimated that the benefits of achieving additional range outweighed the benefits of further reductions in fuel tank size. Commercial passenger cars with diesel IC engines tend to achieve a greater range than gasoline vehicles. This trend indicates that manufacturers do not choose to reduce fuel tank size if storage size is not an issue. Similarly, in this study, the size of the diesel tank is held the same as that of the gasoline fuel cell vehicle. LPG, methanol, ethanol, and CNG have a lower energy density than gasoline. Fuel tank volumes were calculated to achieve the same range as the gasoline fuel cell vehicle. The result is fuel tank storage volumes ranging from 55 to 59 L for the liquid fuels and 190 L for CNG. The fuel volumes correspond to the fuel energy shown in Table 3-7. As discussed in Section 4, methanol steam reformer vehicles are more efficient than POX fuel cell systems. Consequently the fuel tank size for this type of vehicle does not need to be as large as that for a methanol POX system. The tank size was also calculated for a CNG vehicle with reduced range. The ratio of partial pressure of water vapor (mole water/mole total gas) to the vapor pressure of water at a given temperature determines its relative humidity. A given quantity of water vapor (on a mole basis) provides the same relative humidity at 1 atm or 3 atm since the vapor pressure of water depends upon temperature only and not pressure. Therefore, the amount of water required as a percentage of the total gas stream is lower at 3 atm and humidification is less critical. Higher operating pressures also make water recovery and radiator sizing more practical for a high pressure system. The combination of improved efficiency, humidification, and water recovery favor the 3 atm system for PEMFCs.

The temperature and relative humidity of ambient air also affect water recovery. Hot dry air reduces the moisture available in the cathode and places a greater load on the radiator for water recovery. Menzer evaluated the water balance for a PEMFC system over a range of ambient temperatures, relative humidity, and fuel cell pressures. The analysis showed an excess water recovery for 3 atm systems for operating temperatures up to 45°C.

CO removal also affects the performance of the PEMFC system depending upon the approach used. Fuel processor developers aim to produce a feed gas with no more than 20 ppm CO which is within the expected performance characteristics of a PROX unit. However, other approaches such as methanation or advanced LTS reactors may be able to provide a feed gas that contains 100 ppm or less while reducing the weight, complexity, and air injection requirement for a PROX. Such a system would be suitable for CO tolerant fuel cells (containing higher levels of

ruthenium catalyst). The system weight would be lower; however, the fuel cell efficiency would also be somewhat lower.

The stoichiometric ratio, λ , affects the efficiency of the POX system as discussed in Section 3. Lower stoichiometric ratios result in higher CO and hydrogen production; however, soot forms if the reactor temperature is too low. The choice of stoichiometric ratio depends on the reformer design and operating load. One design criteria is the desire to maintain a constant velocity and high temperature within the burner. At part loads, heat losses are greater and the overall gas flow rate is low. These considerations would require a higher stoichiometric ratio which would result in a higher adiabatic flame temperature and compensate for heat losses. Total gas flow is reduced at low load operation which would affect the performance of heat exchangers that preheat the POX inlet air. A higher air preheat can be achieved at low loads which offsets somewhat the requirement for increasing the stoichiometric ratio. These parameters are factored into the evaluation of reformer performance and efficiency over the range of operating loads.

POX/PEMFC Modeling Assumptions

The fuel cell system model determines fuel demand, system mass flow, and efficiency over the range of operating loads. The process simulation model combines in house models to determine the mass and energy balance for the fuel cell system. The REFORINP model determines fuel, air, and steam inputs to the reformer and exit compositions, CO removal, gas humidification, fuel cell hydrogen reaction, water recovery, excess anode hydrogen combustion, and compressor/expander performance. The flowrates are adjusted on an iterative basis to satisfy the following primary criteria:

- Hydrogen into the fuel cell meets electric demand
- Waste anode gas is sufficient to power the compressor expander
- Sufficient water is recovered to provide fuel processor feed
- Fuel, air, and steam inputs to the fuel processor provide sufficient hydrogen for the fuel cell

The reformer is represented as a constant enthalpy reactor where the equilibrium product gas compositions are determined by minimizing the Gibb's free energy for a constrained chemical composition. The temperature and enthalpy of air, fuel, and steam entering the POX are predicted from heat transfer constraints in the system flow model. Heats of formation for the fuel inputs are calculated from fuel heating values (Table 3-2). Equilibrium fuel processor gas compositions are calculated with the Acurex Chemical Equilibrium (ACE) model (Powars). The equilibrium gas compositions are adjusted to reflect estimates of actual POX reactor performance. The recovery of heat is modeled to allow for elevated temperatures in the POX unit. Increasing the POX temperature improves reaction kinetics which improves the rate of fuel conversion to CO and hydrogen and reduces unconverted methane (sometimes referred to as methane slip) (Woods). The final exit gas compositions and reactor temperatures are determined

using heat recovery assumptions after unconverted methane and heat losses are taken into account.

Temperature changes and gas compositions during CO removal and gas humidification in the HTS are then determined. Water requirements for the POX quench are determined from the POX exit gas enthalpy and target HTS inlet temperature. Sulfur removal occurs either before or after the HTS in a zinc oxide bed. Temperature conditions are optimal for sulfur removal after the HTS; however, steam inhibits the reaction of H₂S with the zinc oxide. This detail does not significantly affect the process flow analysis. CO conversion and exit temperatures in the HTS and LTS are based on the water gas shift equilibrium at the target reactor temperature after taking into account pinch point limitations. Final CO removal is performed in a methanation or PROX reactor, or combination of both steps. In addition to removing CO, the heat of reaction from methanation and CO oxidation raises the gas temperature. Excess oxygen also reacts with hydrogen to generate heat. Removing reaction heat is an important feature in the CO removal system because rising shift catalyst temperatures will lead to CO formation through the reverse water gas shift reaction. Methanation consumes three moles of hydrogen per mole of CO. For the PROX reaction, approximately 2 moles of air are injected for every mole of CO that is removed. The excess air consumes hydrogen to form water vapor. The model accounts for these processes.

Exit gas from the PROX is cooled and excess water is condensed from the gas stream and returned to the water storage tank. Purification of the recycle water will likely be required prior to recycling into the reformer system. The simulation model determines the gas temperature and humidity prior to entering the fuel cell. A higher fuel cell anode feed temperature increases the moisture level and helps reduce drying of the membrane.

Hydrogen dissociates on the anode and protons pass through the membrane to react with oxygen in the cathode air to form water vapor. The anode is supplied with 15 to 20 percent excess hydrogen to help maintain a high power output from the fuel cell. An uneven distribution of anode gas can cause sections of the fuel cell to be starved of hydrogen unless excess hydrogen is provided. The fuel cell load determines the current density and cell voltage. Hydrogen consumption and heat rejection within the fuel cell are determined from the fuel cell performance curves in Section 2. For POX/PEMFC systems, a fuel cell voltage curve that represents the POX fuel processor effluent is used. The voltage curve, combined with fuel cell area and number of cells, determines current and fuel cell efficiency over the range of operating loads. Hydrogen demand and heat rejected from the fuel cell is determined from fuel cell efficiency.

Water recovery is modeled for the fuel cell anode and cathode prior to combustion in a catalytic burner. The burner exhaust drives an expander which powers a compressor, and the excess gas is cooled to recover additional water. Expander power output and compressor power requirements are modeled from performance curves shown in Section 3. The compressor provides air for the POX reactor and for the fuel cell cathode. These systems operate at 3 atm which results in a significant power demand from the compressor. The expander powers the compressor. Unreacted hydrogen from the fuel cell anode is combusted in a catalytic burner with excess anode air and this gas mixture drives the compressor. The fuel cell system model calculates the compressor and expander power demands to verify that sufficient power is available from the

expander. Recovering water in a condenser upstream of the burner minimizes the radiator load required for final water recovery. The fuel cell produces more water than required by the reformer; so, some water can be lost in the vehicle exhaust.

The mass and energy balance from the fuel cell system model determines fuel cell hydrogen demand, reformer fuel input, and burner fuel input for different vehicle loads. These parameters allow for a calculation of fuel cell system efficiency and provide input for an emissions model.

Low Temperature Methanol Steam Reformer with PEMFC Description and Modeling Assumptions

Figure 4-11 is the flow diagram of the methanol steam reformer/PEMFC system. In this system, water and methanol are evaporated with waste heat from the burner, and react over a catalyst bed to produce hydrogen, CO₂, and CO. The CO is removed in the LTS and PROX reactors, and enters the fuel cell anode. Waste anode gas containing hydrogen and CO₂ provides fuel for the steam reformer burner. Methanol fuel is used to warm up the burner, and can also provide supplemental energy during fuel cell operation. However, burning methanol in the burner would increase emissions.

The methanol steam reformer and membrane combination in Figure 4-12 produces pure hydrogen for a PEMFC. This system has the advantage of operating the fuel cell more efficiently on hydrogen. Unused hydrogen can be recirculated back to the fuel cell so the cell can operate at a lower fuel utilization (higher anode stoichiometry). Some of the hydrogen must be bled off as a burner fuel to prevent build up of trace contaminants. The extent of bleed off must be adjusted to reflect the CO levels that escape through the membrane to prevent unacceptable CO buildup. The membrane effluent is burned in the steam reformer. Epyx has achieved a steady-state hydrogen production efficiency of 78 percent when operating on gasoline and 84 percent when operating on ethanol. Start-up times are currently reported as 10 minutes with developments underway to improve start-up, transient operation, packaging, and system size. Epyx packaged their fuel processor with a Los Alamos National Laboratory PROX and a Plug Power PEMFC to demonstrate an integrated PEMFC system that produced 10 kW_e of power. The low temperature steam reformer requires little compression energy for the reformer input because these inputs are liquid methanol and water. A compressor/expander is used to provide pressurized air for the fuel cell cathode.

The combination of methanol steam reformer with PROX provides reformat rather than pure hydrogen to a PEMFC. The anode effluent is burned in the steam reformer. The PROX effluent provides a more dilute gas mixture than the membrane. The system may be simpler to operate than a membrane and represents a more conventional technology. The membrane technology for vehicle applications is still in an early state of development.

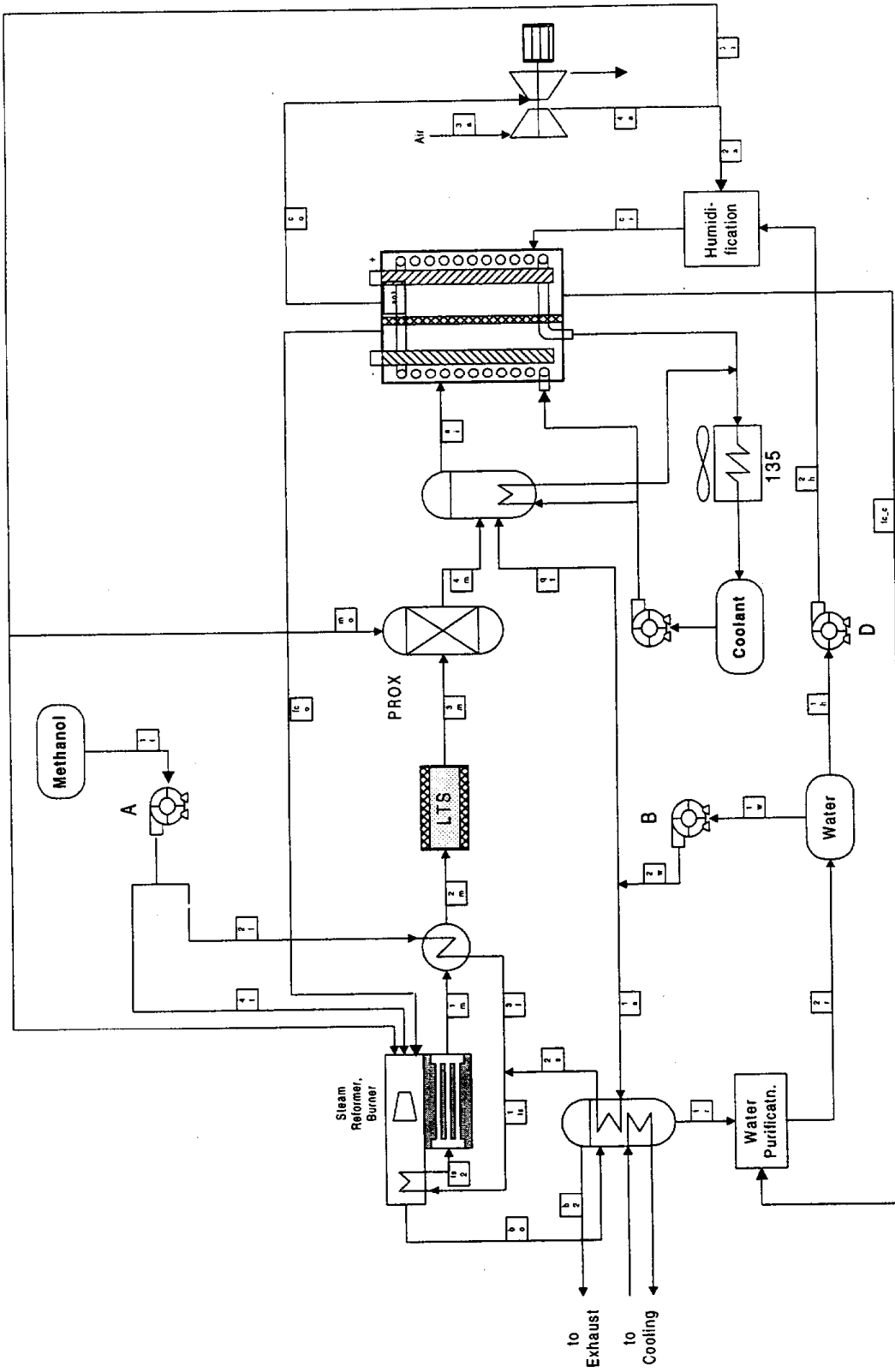


Figure 4-11. Process flow diagram for methanol steam reformer system with PROX and PEMFC

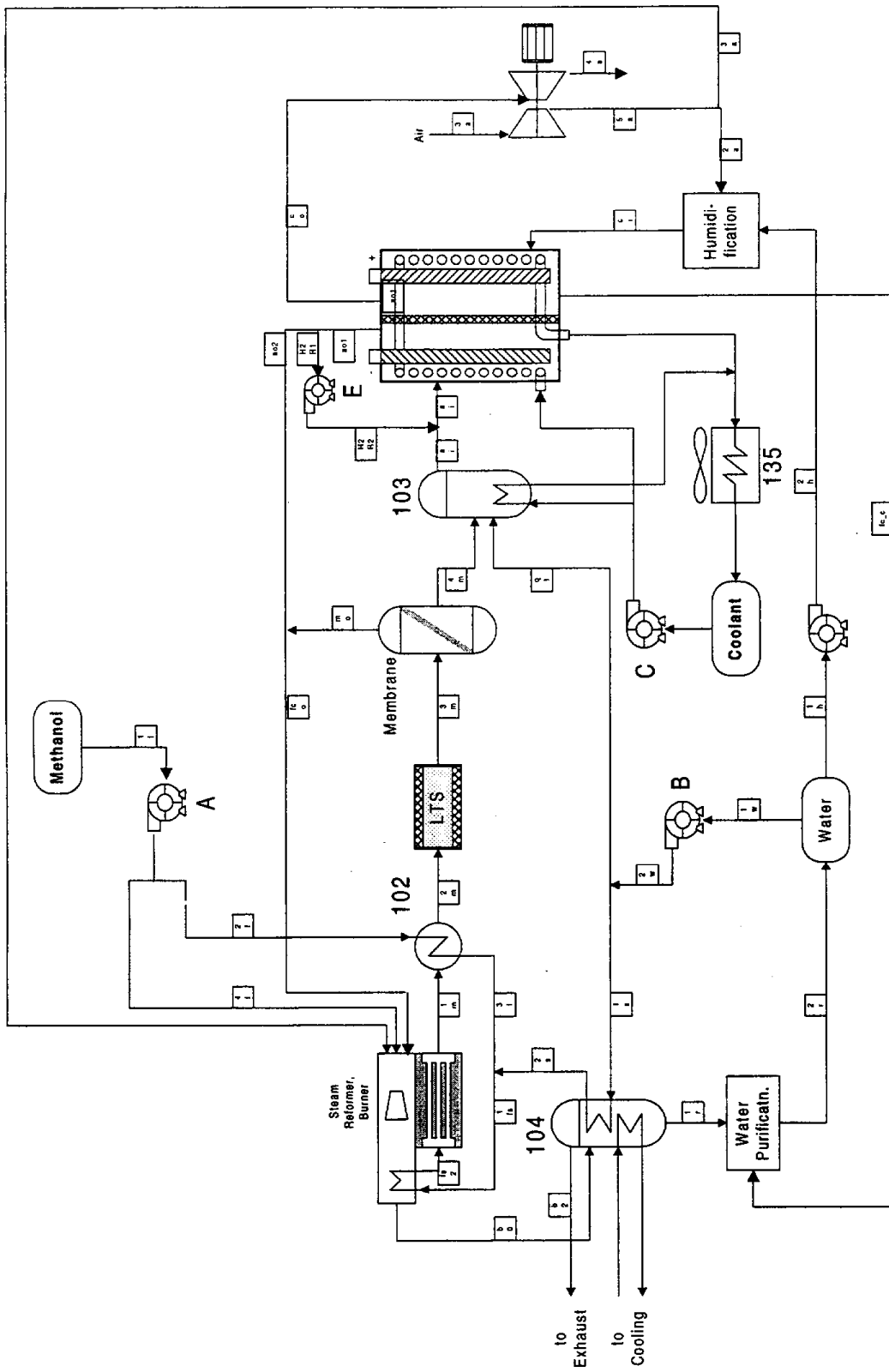


Figure 4-12. Process flow diagram for methanol steam reformer system with membrane and PEMFC

Direct Methanol Fuel Cell Case Study Descriptions

While the DMFC has not been developed to the 20 to 50 kW size required for passenger cars, it represents an attractive option. The DMFC produces no combustion emissions. Preliminary testing shows no partial oxidation emissions from methanol that dissociates on the cathode (Halpert). An evaluation of DMFC system performance provides fuel consumption and allows for a comparison of fuel cycle emissions.

The configuration for a DMFC system is shown in Figure 4-13. The fuel cell generates power when a mixture of methanol and water is circulated through the anode and air passes through the cathode side of the fuel cell. The DMFC system uses an electric fuel and water circulation pump and air blower which contribute to a parasitic load on the power plant system. Water is required for the anode side reaction from methanol to CO_2 . A methanol water mixture helps minimize methanol carry over through the fuel cell membrane. The methanol water mixture is circulated back to a storage tank and a condenser recovers water from the cathode. Dissolved CO_2 escapes from the methanol water mixture and is purged from the tank. Methanol from the vehicle storage tank is added to the mixture tank to maintain a 3 percent methanol/water mixture. The methanol concentration can be measured with a combination of methanol sensor and by detecting a drop in voltage output from the fuel cell. The DMFC system is simple compared to other fuel cell and fuel processor systems. DMFCs do not require reformers; however, fuel cell stack development requires much more development work for vehicle applications. The power density of DMFCs is also considerably less than that of PEMFCs.

4.3.3 Performance Results for the Light-Duty Vehicle Case Studies

Figure 4-14 shows the predicted fuel cell and overall efficiency for a POX/PEMFC system operating on gasoline for different load conditions. The fuel cell and overall efficiency for a methanol SR system are also shown. The higher fuel cell efficiency is based on the performance curve discussed in Section 2.5.1. The higher efficiency of the methanol SR combined with the higher fuel cell efficiency results in a greater overall efficiency compared with the POX system.

For the POX/PEMFC system, fuel cell efficiency affects the overall system performance because the fuel cell is more efficient at low loads than at high loads. The fuel cell efficiency also affects the load on the radiator. Compressor efficiency (Figure 3-28) and reformer conversion efficiency are lower at low loads which reduces the effect of higher fuel cell efficiency. At low loads, the POX unit would be operated at a leaner stoichiometry in order to increase temperatures and gas velocities. Higher temperatures make up for the greater percentage of heat losses. The fuel processor stoichiometries for different load conditions are shown in Table 4-9.

The fuel cell power output and energy input requirements was estimated over different driving cycles. The driving cycle for EPA and ARB vehicle emission certification is referred to as the Federal Urban Driving Schedule (FUDS), shown in Figure 4-15. The FUDS cycle includes stop and go driving with relatively low load requirements.

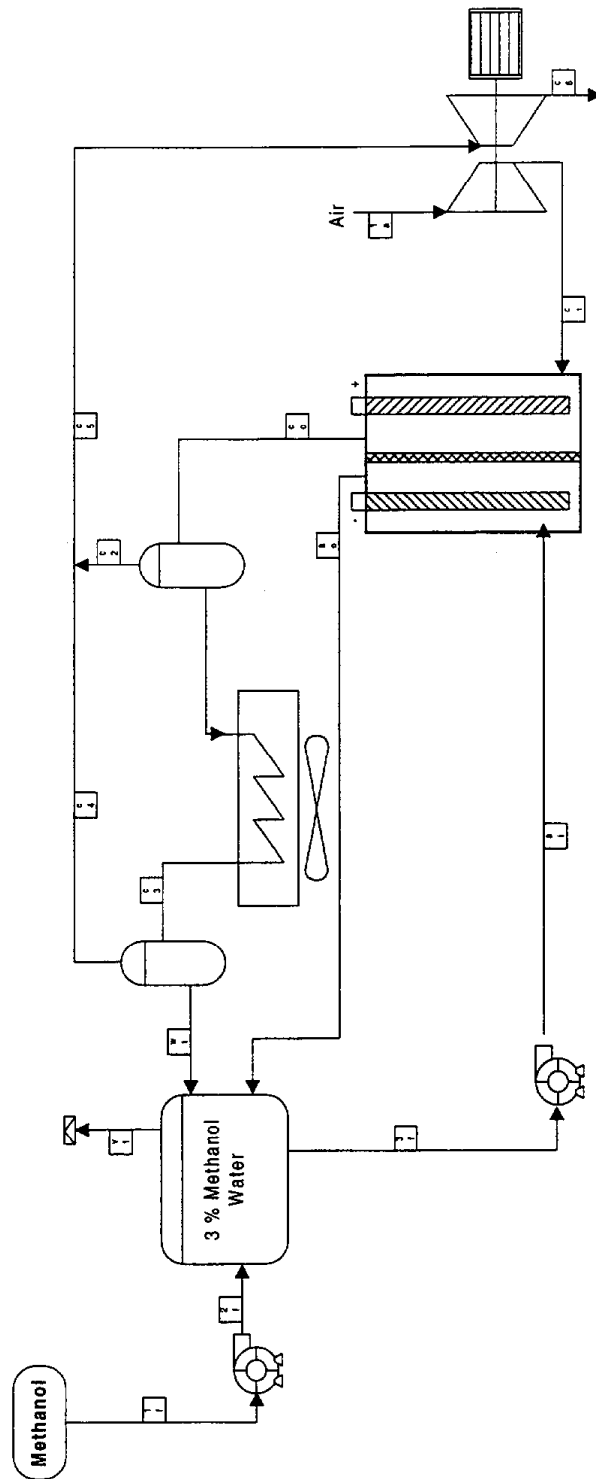


Figure 4-13. Process flow diagram for DMFC system

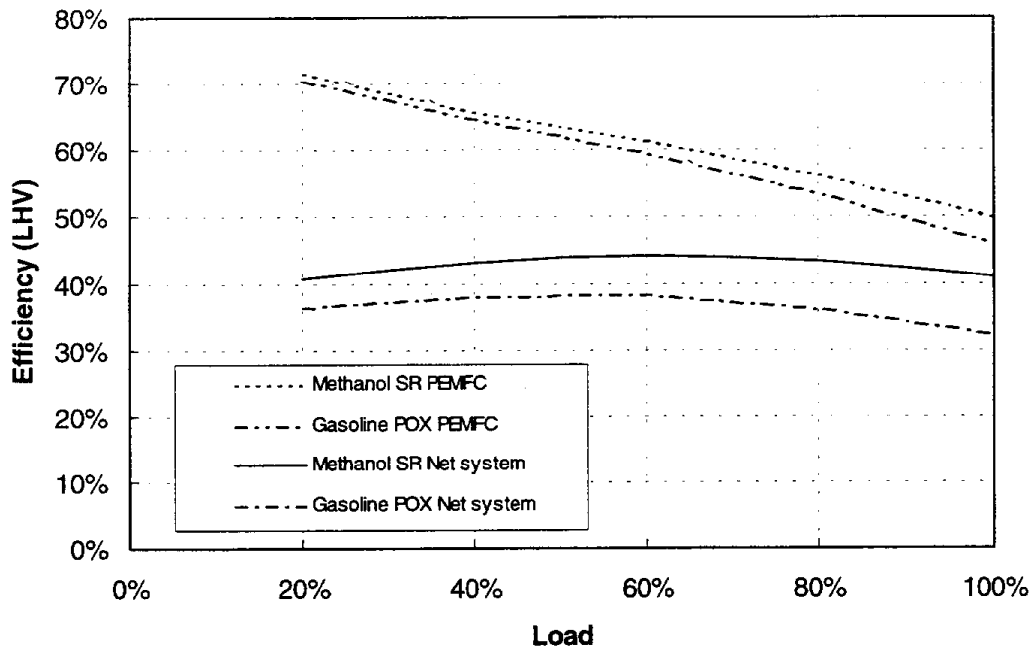


Figure 4-14. Effect of load on fuel processor efficiency

Table 4-9. Effect of load on fuel cell system performance for gasoline POX/PEMFC system

Fuel Cell Output (kW)	20	30	60
<u>Gasoline POX</u>			
Load (%)	33	50	100
System efficiency (%)	36.5	38.1	32.4
Fuel processor stoichiometry, λ	0.42	0.36	0.33
Condenser load (kW)	7.8	14.5	16.2
Radiator load (kW)	12.5	37.2	70.1

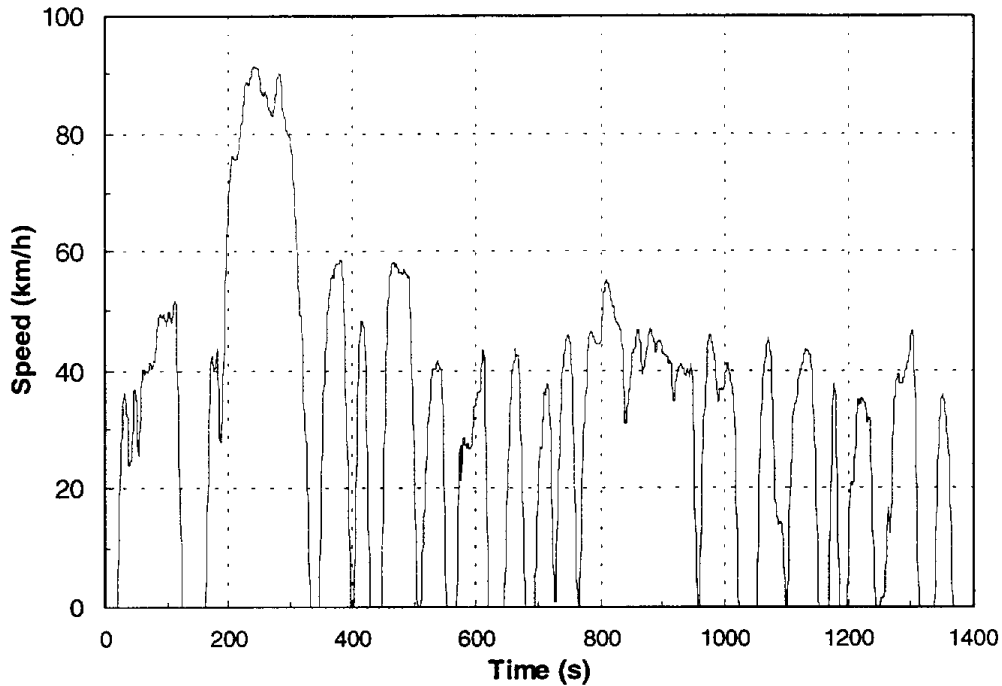
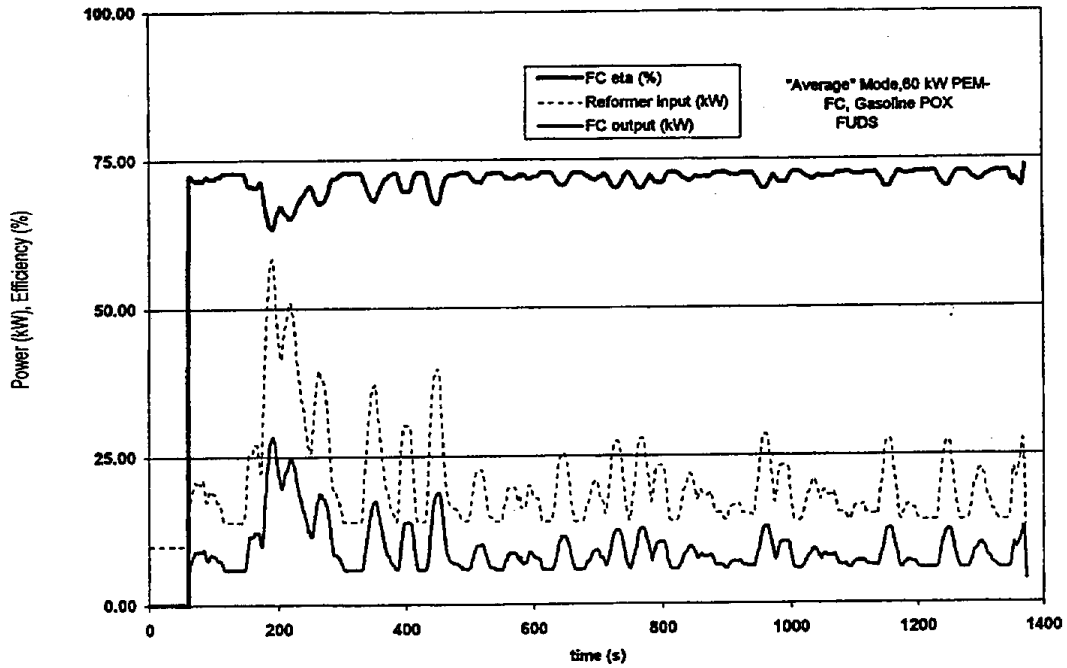


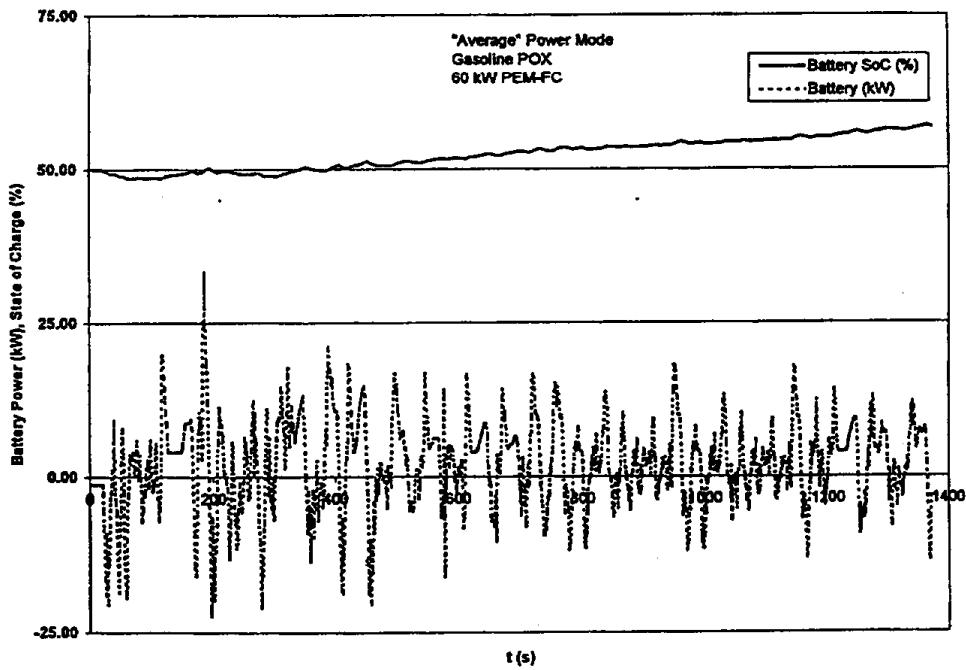
Figure 4-15. Federal Urban Driving Schedule (FUDS cycle)

The vehicle driving cycle model, CYCLEMASTER, determines road power demand from the vehicle weights described in Section 4.3.1 and a drag coefficient of 0.25. The static and dynamic rolling resistance coefficients are 0.0121 and 1.42×10^{-5} s/m respectively. Total fuel cell power output is determined after the battery contribution and parasitic loads are considered. These road load parameters are conservative. Values that result in lower power demand are often projected (Ogden).

Figure 4-16(a) shows the second by second fuel cell power demand over the FUDS cycle for a 60 kW gasoline POX/PEMFC vehicle. The vehicles are classified according to battery size. The system with no battery is referred to as fuel cell only. The system with a small battery that provides peak power with the fuel cell following the road load is referred to as the fuel cell dominant hybrid. The opposite approach is a large battery that follows the driving load with a small fuel cell, referred to as a battery dominant hybrid. The load sharing hybrid has a fuel cell and battery with equal power capabilities. Fuel cell power output depends upon the system operating strategy. Two operating strategies referred to as average power management and peak power management were evaluated for the fuel cell dominant hybrid with a 60 kW fuel cell. The average power management approach reduces the rate of transient load changes in the reformer. The fuel cell and reformer produce a more “averaged” power output. The fuel cell power demand is based on the charging strategy for the battery and estimate of response time for the fuel cell and fuel processor system. Battery power, shown in the bottom of the figure depends on the power management for the vehicle. The battery makes up for a delay in the fuel cell/reformer



a. Fuel cell



b. Battery power

Figure 4-16. Fuel cell and battery power output for 60 kW gasoline POX/PEMFC/PROX system (fuel cell dominant hybrid in Table 4-6) (average power management, FUDS cycle)

power output and power demand beyond the fuel cell capacity. The CYCLEMASTER model assumes that the fuel cell system must maintain a minimum power level of about 10 percent of the maximum power output. Heat losses and compressor inefficiency would make idle operation at lower loads very challenging. Some of the “idle” power output is consumed by parasitic loads and excess power is used for battery charging. Battery sizing for the hybrid configuration is driven by specific power. Therefore, the battery for a hybrid has ample energy storage capacity, even with a 60 kW fuel cell, and rapid charging is not necessary. Therefore, the power management system for the vehicle is not driven strongly by battery state of charge (SOC), but rather by opportunity charging when the fuel cell is at low load and high efficiency. Regenerative braking also charges the battery. The energy consumption calculated for the vehicle takes into account a credit or deficit for the SOC if the value changes from the beginning to the end of the driving cycle.

Figure 4-16(a) illustrates the fuel cell performance (output and efficiency) and reformer energy input for the average power management approach. The energy management system smooths the fuel cell power demand to eliminate rapid load changes and place more of the burden of load changes on the battery. This approach avoids the sharp spikes in reformer fuel input.

Figure 4-17 shows the fuel cell performance and reformer input for the same fuel cell system as in Figure 4-16 but using the peak power management approach. This energy management approach uses the battery to provide only peak power that the fuel cell and reformer cannot deliver. The net result is much more rapid spikes in reformer fuel demand. The advantage of the peak power management approach is reduced battery charging losses. Once the reformer performance is taken into account, net fuel cell system efficiency decreases slightly at lower loads. The disadvantage of the peak power management approach is increased load changes which are difficult for the reformer to follow. The peak power management approach did not result in a significant change in predicted fuel consumption.

Figure 4-18 shows the fuel cell power output, reformer input, and fuel cell efficiency for the battery dominant hybrid with a 20 kW fuel cell. The fuel cell is able to meet most of the power demand of the FUDS cycle. Fuel cell power output follows the driving cycle with a smoothing of load to reduce adverse affects of transient operation. The battery dominant hybrid operates at a lower average fuel cell efficiency but is able to take advantage of increased regenerative braking.

The fuel economy for the light-duty vehicle case studies is shown in Table 4-10. The 20 kW fuel cell results in lower fuel consumption than that of the 60 kW fuel cell over the FUDS cycle. This effect occurs for several reasons. Start-up energy requirements are lower for the smaller reformer in the 20 kW system. The minimum power output during idle is lower for the 20 kW system which reduces idle energy consumption. The 20 kW fuel cell can meet much of the power demand over the FUDS cycle; so, power demand from the battery is relatively low and battery losses do not play as large a role.

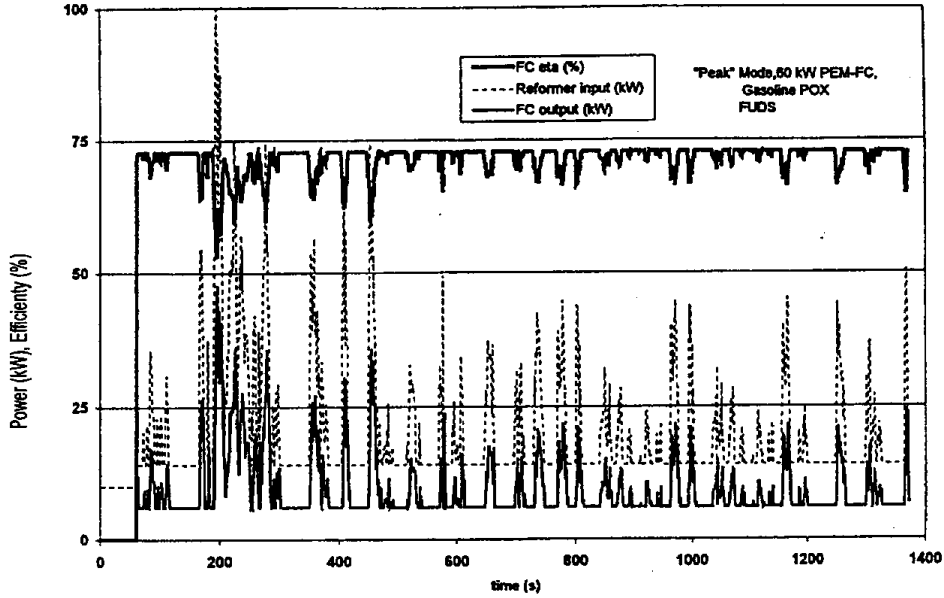


Figure 4-17. Fuel cell power output for 60 kW gasoline POX/PEMFC/PROX system (fuel cell dominant hybrid in Table 4-6) (peak power management, FUDS cycle)

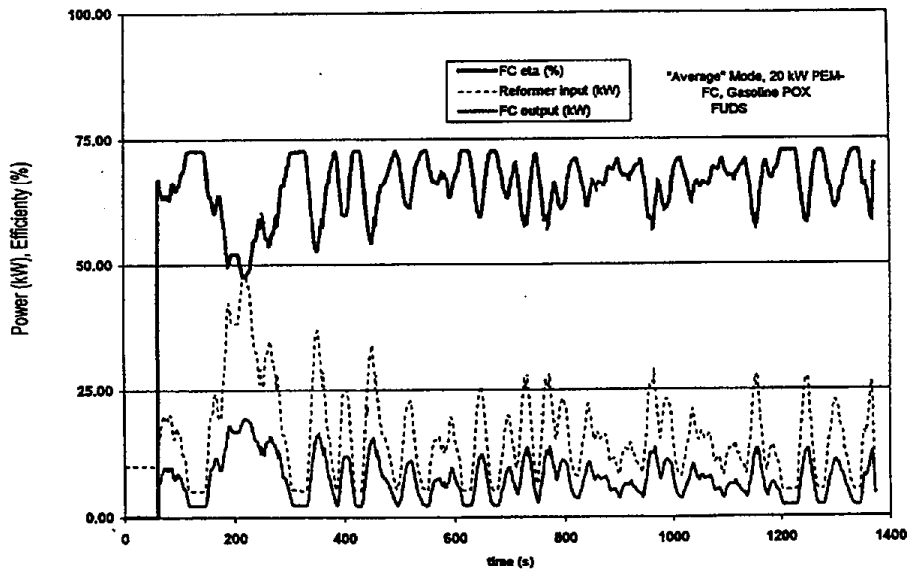


Figure 4-18. Fuel cell output for 20 kW gasoline POX/PEMFC/PROX system (battery dominant hybrid in Table 4-6) (average power management)

Table 4-10. Summary of fuel consumption over various driving cycles

Fuel	Fuel Cell/ Engine Power	Fuel Cell/ Engine	Fuel Processor	Cycle	Energy Consumption (kJ/km)	Fuel Consumption (L/100 km)	Fuel Economy (mpg) ^a
Baseline LDV	73 kW	Spark ignited	—	FUDS	3034	9.6	24.6
Gasoline ^b	75 kW	PEMFC	POX PROX	FUDS	2155	6.9	34.6
Gasoline ^b	60 kW	PEMFC	POX PROX	FUDS	2110	6.7	35.3
Gasoline ^b	60 kW	PEMFC	POX PROX	HFET	1785	5.68	41.8
Gasoline ^b	60 kW	PEMFC	POX PROX	ECE	1800	5.7	41.4
Gasoline ^b	40 kW	PEMFC	POX PROX	FUDS	2025	6.4	36.8
Gasoline ^b	20 kW	PEMFC	POX PROX	FUDS	1940	6.2	38.4
Gasoline ^b	20 kW	PEMFC	POX PROX	HFET	1707	5.4	43.6
Gasoline ^b	20 kW	PEMFC	POX PROX	ECE	1710	5.4	43.6
Gasoline ^b	60 kW	PEMFC	POX Methanation	FUDS	2090	6.7	35.7
Diesel ^c	60 kW	PEMFC	POX PROX	FUDS	2130	6.8	35.0
LPG ^c	60 kW	PEMFC	POX PROX	FUDS	2090	6.6	35.7
Ethanol ^c	60 kW	PEMFC	POX PROX	FUDS	2090	6.6	35.7
CNG low range ^c	60 kW	PEMFC	POX PROX	FUDS	2120	6.7 ^d	35.2
CNG ^c	60 kW	PEMFC	POX PROX	FUDS	2160	6.9 ^d	34.5
Methanol ^f	60 kW	PEMFC	POX PROX	FUDS	2100	6.7	35.5
Methanol ^e	60 kW	PEMFC	ATR PROX	FUDS	1770	5.6	42.1
Methanol ^e	60 kW	PEMFC	SR/membrane	FUDS	1590	5.1	46.9
Methanol ^e	60 kW	PEMFC	SR PROX	FUDS	1610	5.1	46.3
Methanol ^e	20 kW	PEMFC	SR PROX	FUDS	1569	5.0	47.5
Methanol ^e	73 kW	DMFC	—	FUDS	1660	5.3	44.9
Methanol ^e	20 kW	DMFC	—	FUDS	1630	5.2	45.7

^aMiles per equivalent gallon of gasoline.

^bCase studies in Table 4-6.

^cCase studies in Table 4-7.

^dkg/100 km.

^eCase studies in Table 4-8.

Table 4-10 shows that ethanol, LPG, and methanol POX/PEMFC systems have better fuel economy relative to most gasoline and diesel due to their improved fuel processor efficiency. The fuel economy for CNG is lower than that of the other alternative fuels since the vehicle weight is greater. Reducing the weight of the CNG vehicle at the expense of range improves fuel economy. The PEMFC with a methanol steam reformer and ATR also achieve an improved fuel economy compared to the POX cases.

Figure 4-19 compares the fuel consumption for selected 60 kW systems presented in Table 4-10 with a passenger car powered by a gasoline (RFG) IC engine. The methanol steam reformer vehicle uses about one-half the energy as the gasoline-powered IC engine vehicle. This result depends largely on fuel consumption assumptions for the IC engine vehicle and may vary by approximately 20 percent. The result is not unexpected; however, because the fuel cell powered vehicles benefit from improved power plant efficiency and regenerative braking.

The vehicle weight and fuel consumption estimates in this study are within the range of other estimates shown in Table 4-11. Odgen projects heavier near term values with a 1050 kg glider and lighter weights with correspondingly lower fuel economy including future vehicle design considerations. Volvo projects a lighter vehicle with a relatively heavy glider (Ekdunge).

Some researchers have suggested that a cycle based on the FUDS with 1.25 times the speed would be more representative of real world driving conditions. The ECE cycle, shown in Figure 4-20, is used for vehicle certification in Europe. The cycle is less random and is useful for observing the effects of transient operation on model predications. Figures 4-21 and 4-22 show the effect of higher loads on fuel cell efficiency. During the high-speed portion of the cycle, the 20 kW fuel cell operates at its lowest efficiency. The overall fuel consumption for the ECE is about 15 percent lower than the FUDS cycle due to the lower loads early on in the cycle. Fuel consumption was also evaluated over the EPA highway cycle shown in Figure 4-23. This cycle requires a greater use of batteries for the hybrid so the 60 kW system is more efficient for highway driving.

4.4 HEAVY-DUTY VEHICLE CASE STUDIES

In heavy-duty applications, start-up time is not as critical an issue, because these vehicles operate in general for long periods between shut-down. Driving in urban areas requires a lot of acceleration and deceleration. Accordingly, the fuel cell power output, and with that, the amount of hydrogen needed to provide sufficient electrical power to meet the road load, varies to a great extent. In a hybrid system, extra power needed due to reformer delay might be drawn from the onboard battery, however, non-hybrid systems would need a reformer that could provide sufficient hydrogen, according to the change in road-load, with close to no delay. On a hybrid, with on-board reforming, the battery acts as a load buffer between the demand and the reformer fuel cell system.

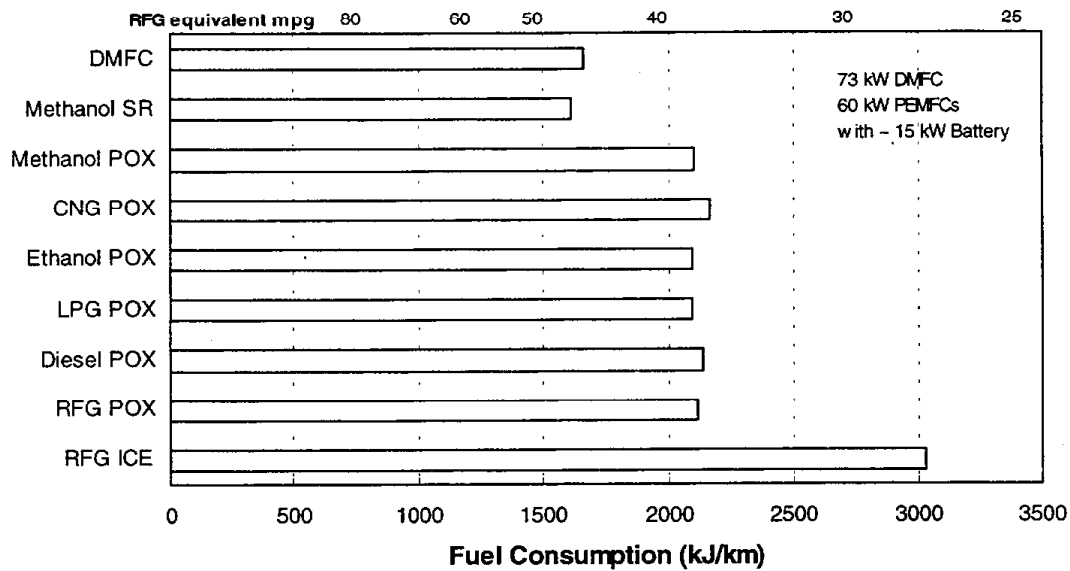


Figure 4-19. Light-duty vehicle fuel energy consumption for 60 kW fuel cell. Miles/gal are shown on a gasoline equivalent basis (FUDS cycle).

Table 4-11. Comparison of light-duty vehicle weight and energy consumption projections

	This Study ^a	Princeton (Ogden)		Volvo (Ekduge)
		Low Weight	Baseline	
<u>Gasoline POX System (Tables 4-6, 4-10)</u>				
Peak fuel cell and battery power (kW _e)	79	89.4	160	—
Glider Weight (kg)	930	800	1050	—
POX Vehicle (kg)	1498	1395	2560	—
FUDS Fuel Economy (kJ/km)	2110	1140	2000	—
<u>Methanol SR System (Tables 4-8, 4-10)</u>				
Peak Fuel cell and battery power (kW _e)	80	83.7	156	116
Glider Weight (kW)	930	800	1050	1130
Methanol SR Vehicle (kg)	1517	1287	2485	1755
FUDS Fuel Economy (kJ/km)	1610	1200	2490	1800

^aFuel cell dominant hybrids with PROX gas clean-up and PEMFC.

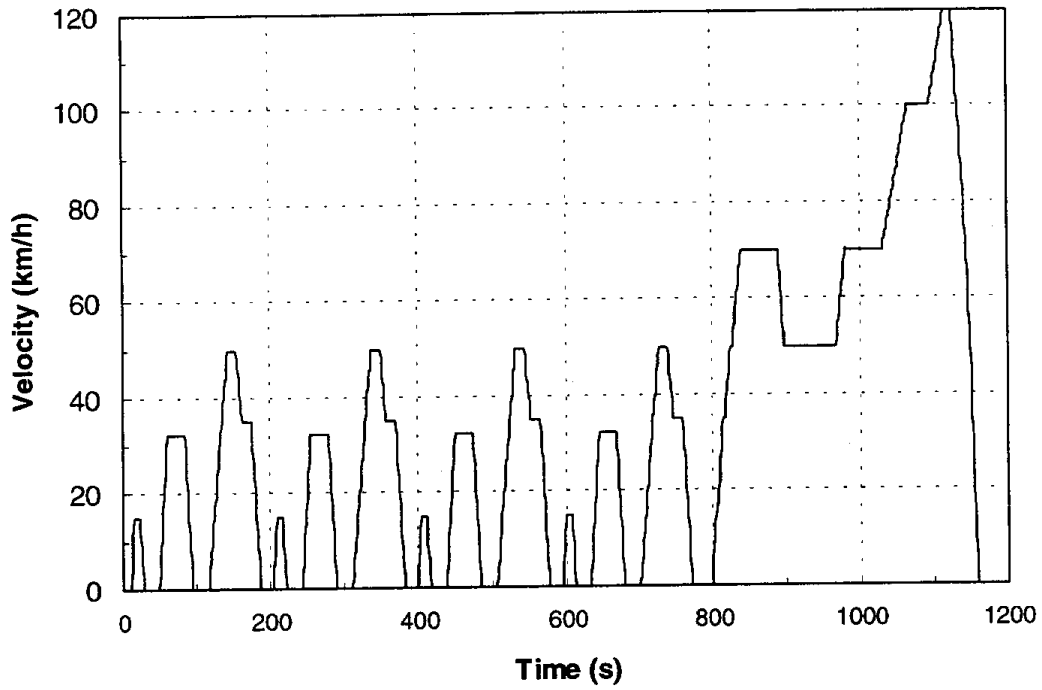


Figure 4-20. European ECE driving cycle

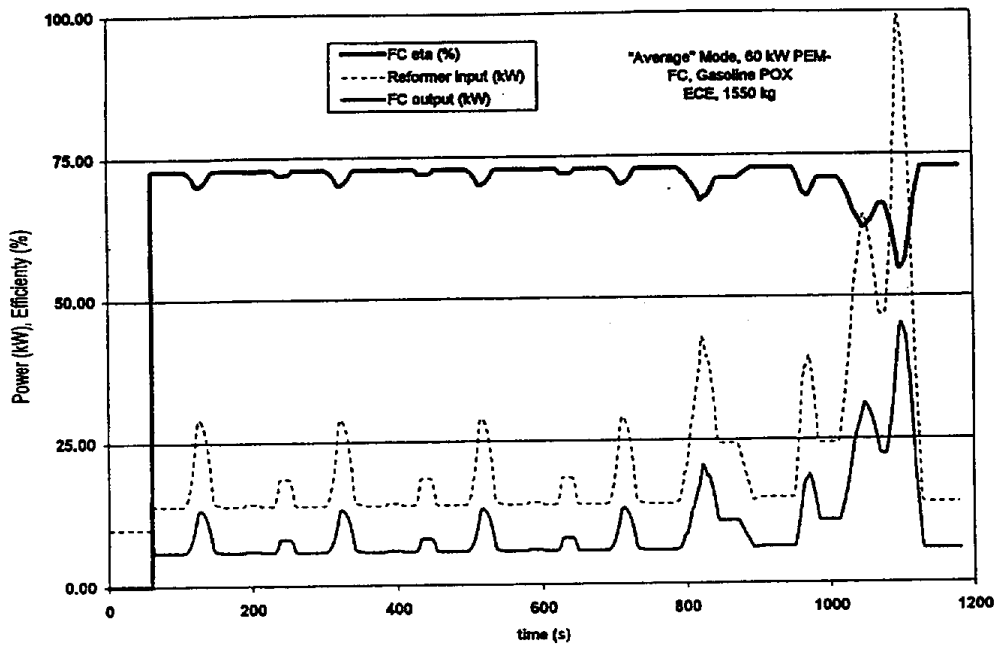


Figure 4-21. Fuel cell power output for 60 kW gasoline POX/PEMFC system (average power management)

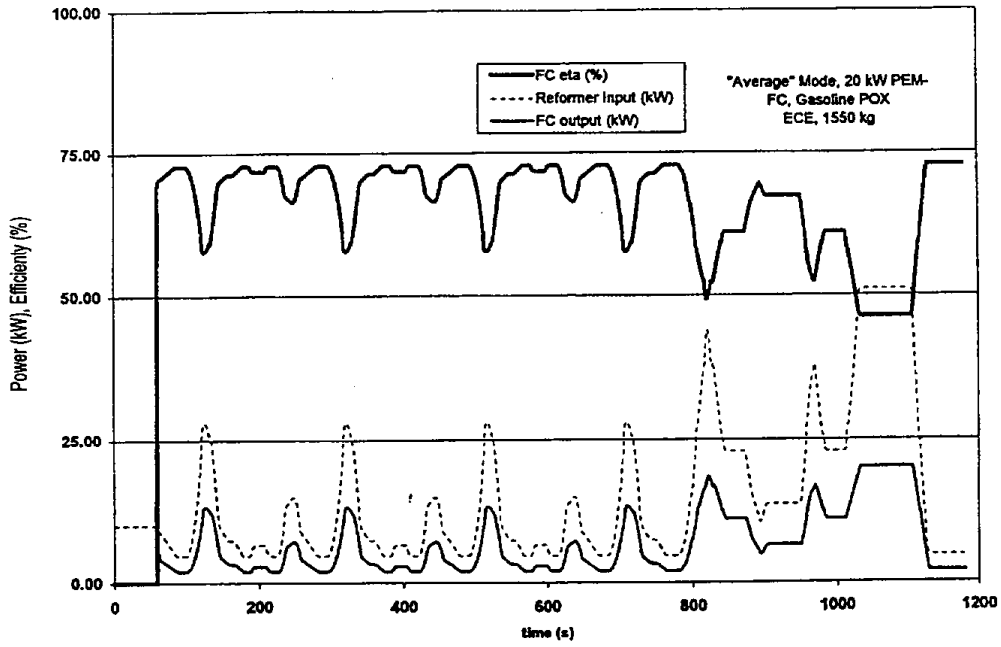


Figure 4-22. Fuel cell power output for 20 kW gasoline POX/PEMFC system (average power management)

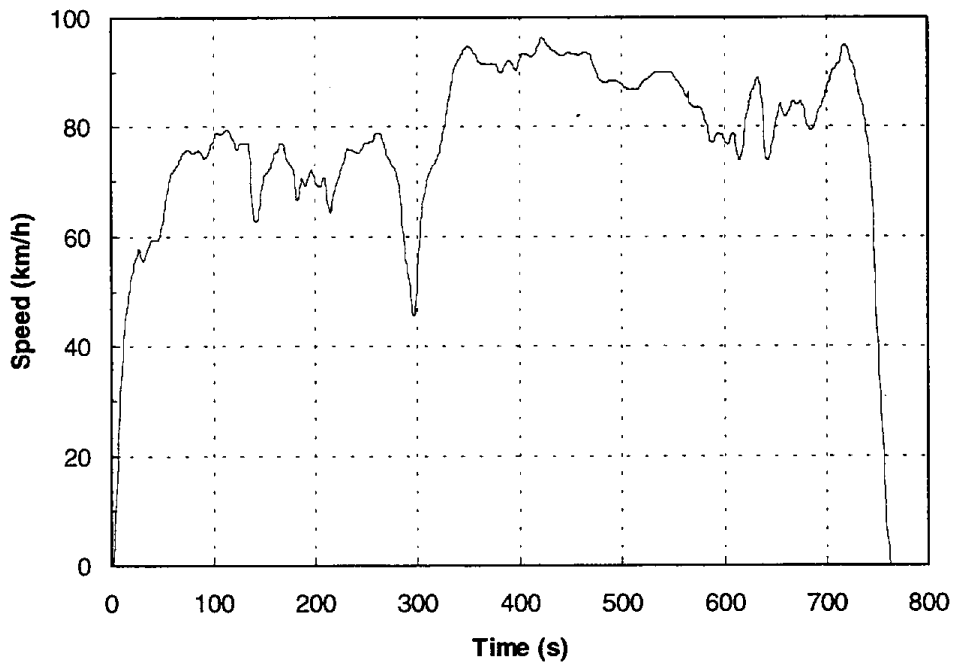


Figure 4-23. Highway fuel economy test (HFET) driving cycle

All of the options have some tradeoffs so several of these options are viable candidates. Packaging constraints and response time requirements make high temperature steam reformers poor choices for passenger cars. The high operating temperature of a PAFC may preclude PAFCs from passenger car operation, however, the fuel cell can operate directly on the product of reformer gas without further clean up. PEMFCs are more efficient than PAFCs; however, these require low levels of CO and other contaminants. PAFC systems built to date have demonstrated higher total system efficiency values; however, integration of PEMFC systems are evolving rapidly. Direct methanol fuel cells do not require reformers, however the technology currently is very bulky and has not been scaled up beyond about 1 kW. SOFCs have the potential for high power density, yet these also require further development. SOFCs could operate with higher efficiency and are even less sensitive to contaminants. Solid oxide fuel cells operate at such high temperatures that the fuel cell exhaust can produce additional power in a turbine.

Weight estimates for heavy-duty buses are presented in Section 4.4.1. The process flow diagram and system integration considerations along with simulation modeling assumptions are given in Section 4.4.2. Fuel consumption for heavy-duty case studies are presented in Section 4.4.3.

4.4.1 Heavy-Duty Vehicle Energy and Weight Modeling

A conceptual design for a heavy-duty bus provided the basis for modeling the vehicle and components. The weight of the following components was predicted according to the vehicle power requirements (see Table 4-12).

- Base vehicle without engine (glider)
- Fuel cell
- Fuel processor
- Radiator and water storage
- Traction battery
- Power controller
- Electric motor and transmission

The weight of the vehicle components depends on the performance requirements of the vehicle. The vehicle design is based on a 12 m (40 ft) transit bus meeting FTA white book specifications for acceleration, shown in Figure 4-24. The results of the energy model are shown in Table 4-13.

Table 4-12. Component and vehicle mass for heavy-duty transit buses

Component	Diesel ICE	Methanol Fuel Cell	Methanol Hybrid	Methanol Hybrid	CNG Hybrid	Diesel Hybrid	Diesel Hybrid
Fuel Cell/Engine Type	CI	PEMFC	PEMFC	PAFC	PAFC	PEMFC	SOFC
Fuel Processor	—	LT SR	LT SR	HT SR	HT SR	POX	POX
Fuel Cell Power (kW)	205	205	100	100	100	100	100
Glider Weight (kg)	12000	12000	12000	12000	12000	12000	12000
Passenger Load (kg)	1400	1400	1400	1400	1400	1400	1400
Engine/Fuel Cell Weight (kg)	710	573	411	550	467	467	467
Fuel Tank Weight (kg)	560	348	348	348	1222	320	320
Tank Capacity (L)	700	400	400	400	1000	400	400
Traction Battery Weight (kg)	0	0	800	800	800	800	800
Radiator, Water tank (kg)	50	103	50	50	50	50	50
Fuel Processor Weight (kg)	0	956	685	917	718	718	718
Power Controls (kg)	0	281	281	281	281	281	281
Motor, Transmission (kg)	314	421	421	421	421	421	421
Vehicle Design Weight (kg)	15034	16081	16396	16766	17358	16456	16456
Net Weight over ICE (kg)	0	1047	1362	1733	2325	1423	1423

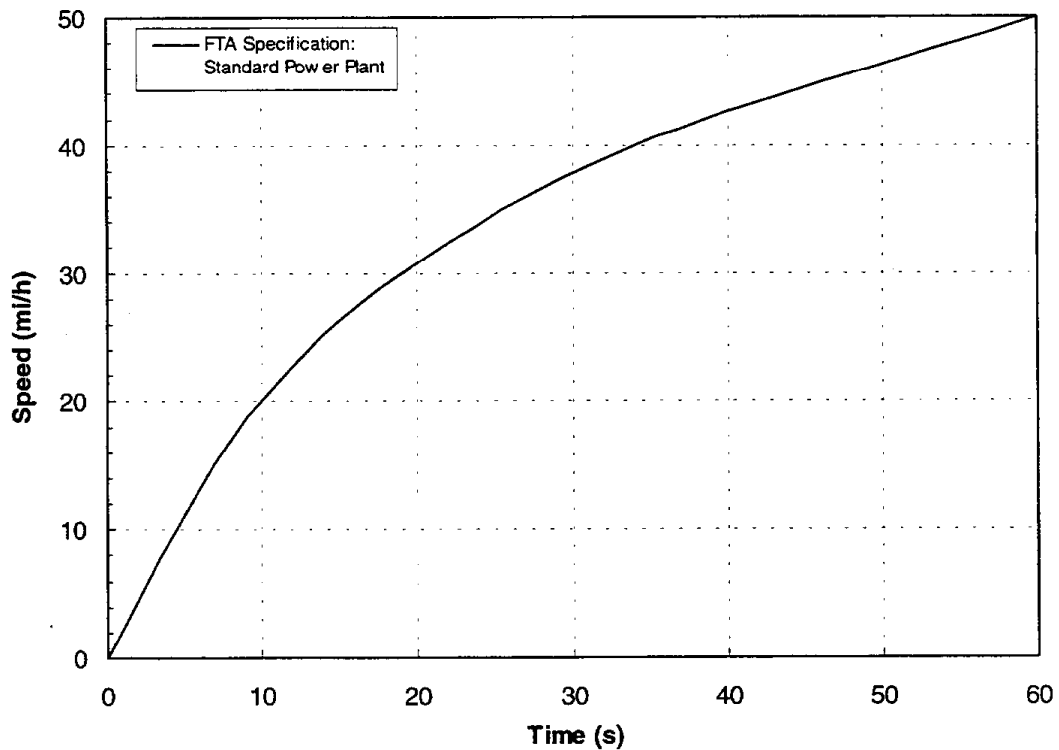


Figure 4-24. FTA minimum acceleration

Table 4-13. Heavy-duty vehicle fuel consumption

Fuel	Fuel Cell/ Engine Type		Fuel Processor	Cycle	Energy Consumption (kJ/km)	Fuel Consumption (L/100 km)	Fuel Economy (mpg) ^a
Diesel	Direct injection ICE		—	CBD	22516	61.3	3.87
Methanol	Fuel Cell	PEMFC	Low Temp. SR	CBD	16085	101.5	5.41
Methanol	Hybrid	PAFC	High Temp. SR	CBD	14965	94.4	5.82
Diesel	Hybrid	PEMFC	POX	CBD	16808	45.8	5.18
Methanol	Hybrid	PEMFC	Low Temp. SR	CBD	14538	91.8	5.99
Diesel	Hybrid	SOFC	POX	CBD	13455	36.6	6.47
CNG	Hybrid	PAFC	High Temp. SR	CBD	16299	34.5 ^b	5.35
Diesel	Direct injection ICE		—	Sch. D	25600	69.7	3.40
Methanol	Fuel Cell	PEMFC	Low Temp. SR	Sch. D	18288	115.4	4.76
Methanol	Hybrid	PAFC	High Temp. SR	Sch. D	16519	104.3	4.96
Diesel	Hybrid	PEMFC	POX	Sch. D	18553	50.5	4.42
Methanol	Hybrid	PEMFC	Low Temp. SR	Sch. D	16048	101.3	5.13
Diesel	Hybrid	SOFC	POX	Sch. D	14852	40.4	5.52
CNG	Hybrid	PAFC	High Temp. SR	Sch. D	17992	38.1 ^b	4.84

^a Miles per diesel equivalent gallon.

^b kg/100 km.

4.4.2 Heavy-Duty Vehicle Simulation Modeling

Case studies for heavy-duty vehicles include a PEMFC with a low temperature methanol steam reformer and a POX fuel processor, a PAFC with high temperature steam reformer, and an SOFC with a POX fuel processor. The first three process configurations represent fuel cell systems that are under currently under development. Ballard (dbb) is providing a 100 kW PEMFC system with a low temperature steam reformer for the Phase IV Georgetown program. The IFC methanol PAFC is currently being tested on the road. H-Power is developing a PEMFC system with an HBT diesel fueled POX fuel processor. SOFCs have the potential for delivering high power densities and can operate on diesel fuel which makes these attractive for vehicle applications and evaluation in this study.

The process configuration for the PEMFC systems were described in Section 4.3. The process flow diagrams in Figures 4-10 and 4-11 were applied to the heavy-duty vehicle case studies. Separate analyses were performed for the PAFC and SOFC case. The fuel processor options for PAFC and SOFC systems as well as the specific case studies evaluated in this study are presented in the following discussion.

4.4.2.1 Phosphoric Acid Fuel Cell Systems

While PAFCs are bulkier than PEMFCs, these fuel cells have the advantage of being more tolerant to CO in the anode gas feed. This feature makes PAFCs suitable for operation with a wide range of fuel processors without supplemental CO clean-up. The PAFC catalyst is sensitive to sulfur poisoning, therefore operation on gasoline, diesel, natural gas, or LPG will require some degree of sulfur removal while no sulfur removal is required for methanol or ethanol operation. The same fuel quality considerations apply to PEMFC systems.

Several PAFC systems have been built for operation with different fuels and fuel processors. The Fuji system operates on methanol with a low temperature reformer. IFC builds natural gas and LPG fueled systems with a high temperature steam reformer for stationary power generation. IFC also delivered a unit for the Phase IV Georgetown project that operates in methanol.

While the high temperature reformer takes longer to warm up and requires more insulation than a low temperature reformer, it has the advantage of being less sensitive to fuel quality. Trace contaminants such as hydrocarbons and ethanol will be reacted in the reformer.

The case study for the PAFC system is based on a high temperature steam reformer operating methanol or CNG. The system, shown in Figure 4-25, includes a steam reformer, low temperature shift reactor with feed that goes directly to the PAFC. CO clean up and humidification are not required. Waste gas from the anode fuels the steam reformer. The system is based on an atmospheric reformer and PAFC. Since pressurization requirements are modest, electric blowers provide air for the fuel cell anode and reformer burner. Methanol and water are fed into the reformer with a liquid pump, which has a low power requirement compared to air compression. The IFC PAFC system is configured for the reformer burner to operate only on waste anode gas. Since methanol is not fed directly into the burner, hydrocarbon emissions are minimal. Since the PAFC can tolerate CO and hydrocarbons from the reformer product gas, no further clean-up such as a PROX is required.

4.4.2.2 Solid Oxide Fuel Cell Systems

The SOFC operating on diesel may be an attractive alternative for heavy-duty vehicles. The fuel cell can operate with the low levels of sulfur found in diesel fuel and actually generates power from the conversion of sulfur to SO₂. The SOFC operates at temperatures from 650 to 800°C and produces a high temperature exhaust. Therefore, an SOFC system can work well when integrated with a turbine that can take advantage of the high temperature exhaust stream from the fuel cell.

Figure 4-26 illustrates the SOFC system for the case study. A POX system generates CO and hydrogen for the fuel cell. Reforming is not performed on the fuel cell in order to achieve a more compact design and minimize the thermal stress from endothermic reforming and exothermic reaction on the same surface. A turbine provides electrical power for the hybrid bus system and also provides air for the fuel cell cathode. Water recovery is more difficult from the dilute exhaust of the turbine, so an on-board water tank provides demineralized water for steam feed. The inconvenience of needing to add water to the bus is offset by the reduction in cost and complexity of a large heat exchanger for recovering and purifying water. Steam is generated from

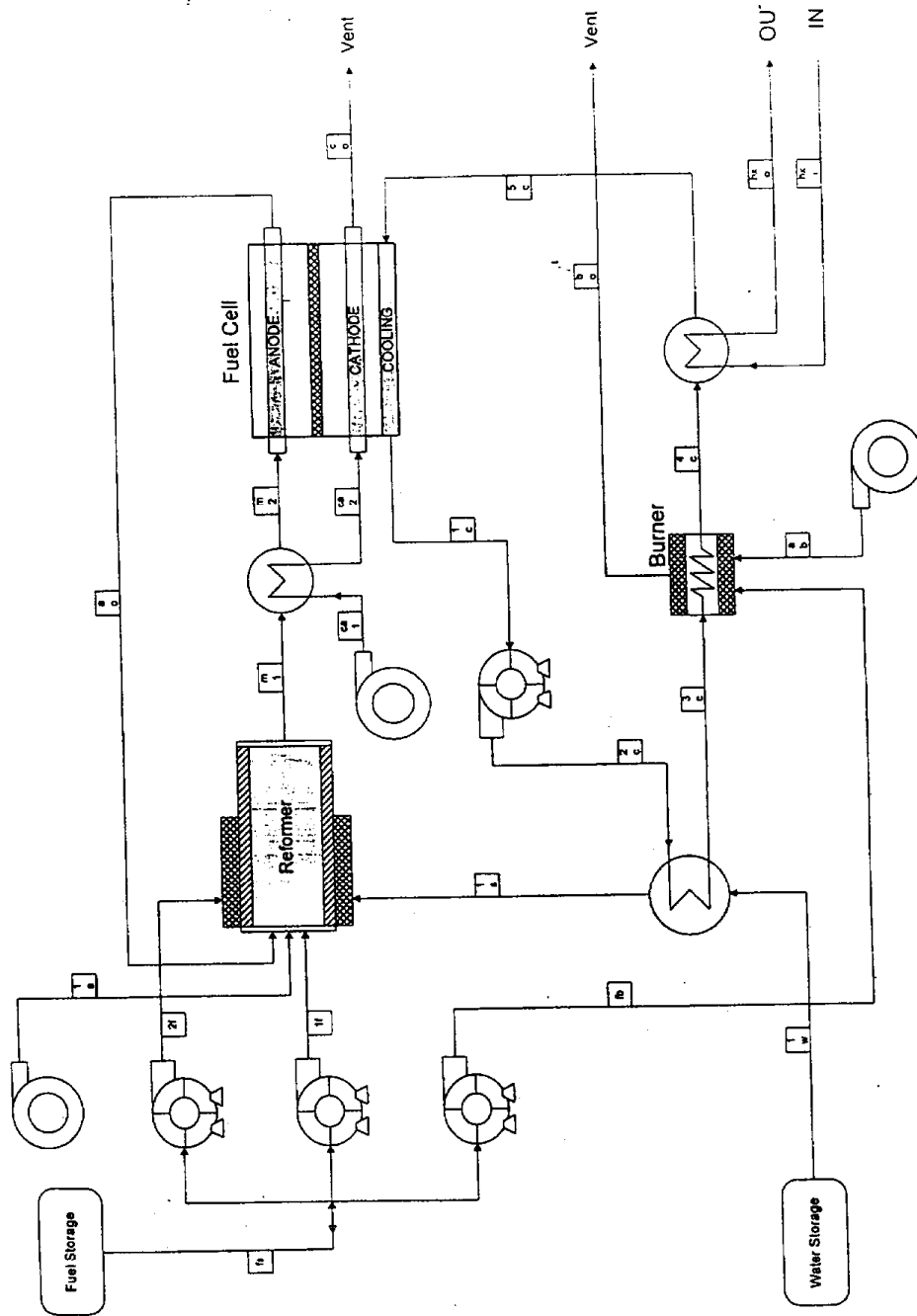


Figure 4-25. Process flow diagram for PAFC with high temperature steam reformer

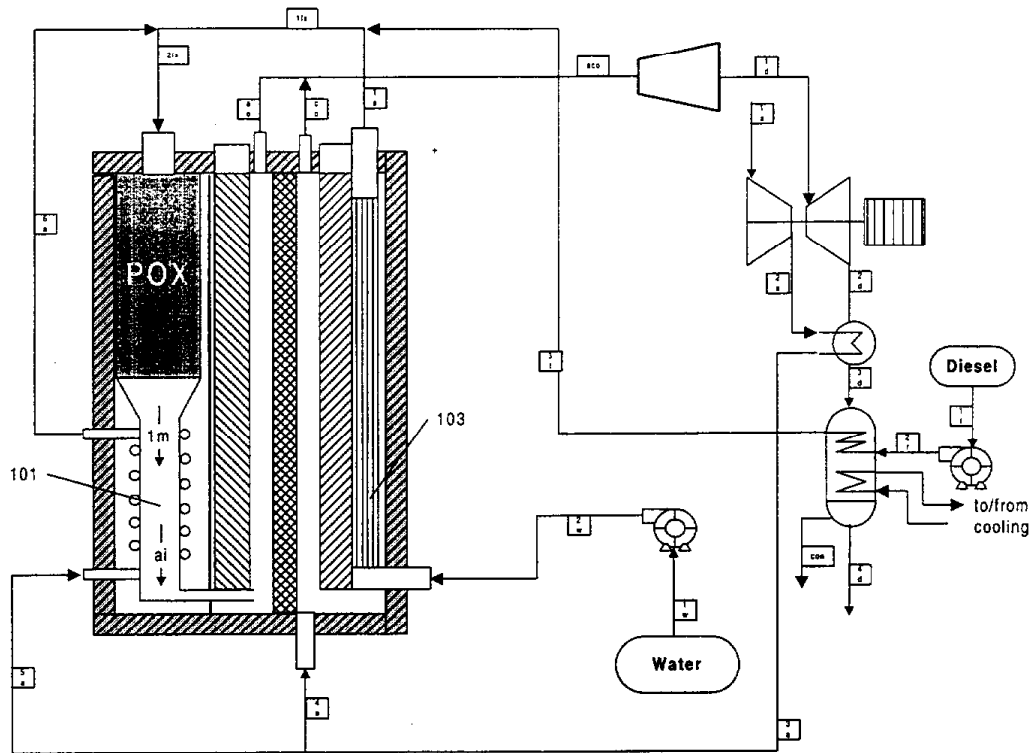


Figure 4-26. Process flow diagram for POX/SOFC system

waste heat and added to the POX reactor to minimize soot formation and improve hydrogen yield.

The POX reactor incorporates integrated heat recovery to increase the reactor temperature and minimize unreacted methane in the POX effluent. Methane and hydrocarbons that do not react in the POX can also react with oxygen on the SOFC. The SOFC system provides three opportunities to convert hydrocarbons. The POX reactor, SOFC, and finally the combustion turbine.

4.4.3 Performance Results for Heavy-Duty Vehicle Case Studies

Figure 4-27 shows the overall efficiency for the heavy-duty vehicle case studies. The SOFC system has the highest efficiency over much of the load range since the fuel cell and turbine are both able to recover power from the reformed fuel. The PEMFC system is potentially more efficient than the PAFC system due to the higher voltage output of the fuel cell, however, this improvement in efficiency is yet to be demonstrated in a vehicle application. The balance of system requirements for the PEMFC are more complex because a compressor provides 3 atm air for the fuel cell. Table 4-13 shows the projected vehicle weight and fuel consumption for the heavy-duty vehicle case studies.

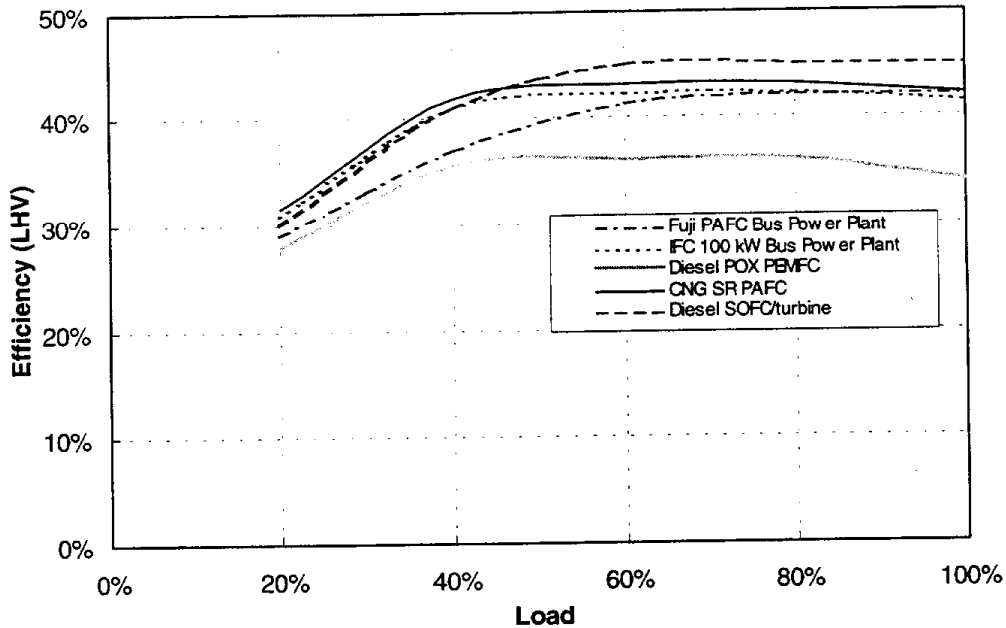


Figure 4-27 Fuel cell/reformer efficiency of heavy-duty vehicle systems (LHV basis)

The Central Business Cycle (CBD), shown in Figure 4-28 is often used for testing transit buses. While no vehicles are certified to this cycle, it has gained widespread popularity for chassis dynamometer emission testing. The cycle is based on a series of acceleration to 20 mph, cruise, and deceleration events. This driving pattern is typical of transit bus operation. Figure 4-29 shows the EPA Heavy-Duty On-Road Driving Schedule (Schedule D), which is an on-road representation of the transient engine dynamometer cycle used for certifying heavy-duty engines. The rate of acceleration in the cycle is based on the performance of a typical heavy-duty truck. In practice, many heavy-duty vehicles are able to meet the acceleration requirements of this cycle with their engine and transmission configurations.

Figure 4-30 shows the energy consumption for different heavy-duty bus cell configurations over the CBD cycle. All of these figures are for 100 kW hybrid configurations. The efficiency of the fuel cell and fuel processor affects fuel consumption. The energy consumption takes into account regenerative braking over the driving cycle. During braking portions of the drive cycle, the force from deceleration of the vehicle's mass is greater than air resistance and friction. A portion of this work is recovered through regenerative braking for hybrid buses. In the case of a conventional IC engine, the brakes must absorb all of this energy. For hybrid configurations, a fraction of the braking work is recovered. A total recovery of 36 percent of the available regenerative power is estimated for the CBD cycle. This factor takes into account battery round trip losses (charging and discharging), power storage limitations of the power controls and batteries, and braking requirements of the vehicle. Regenerative braking reduces the total power demand by 10 percent over the CBD cycle.

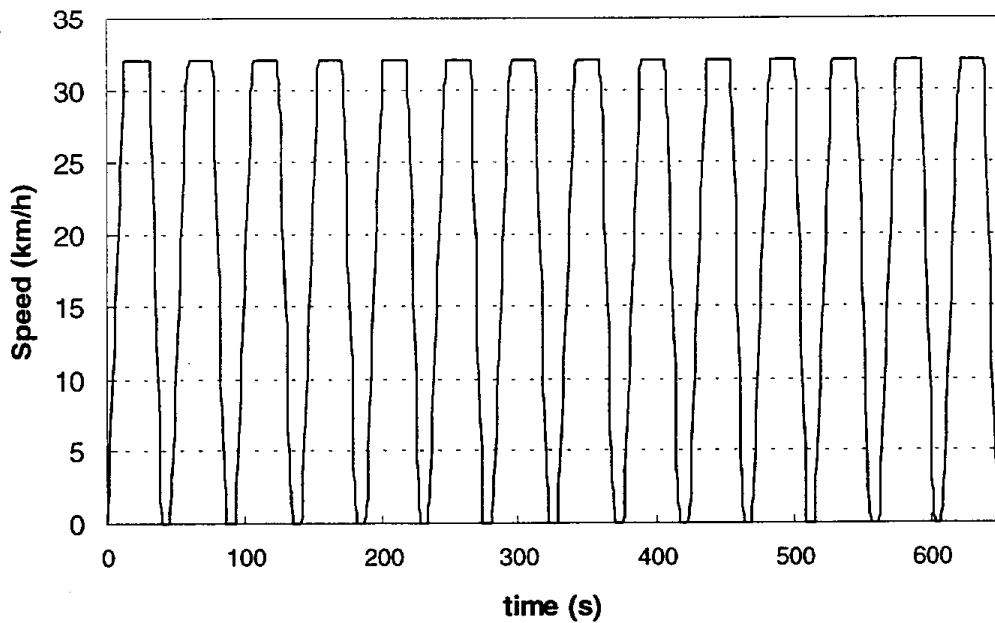


Figure 4-28. Central Business District Cycle (CBD) for heavy-duty vehicle testing

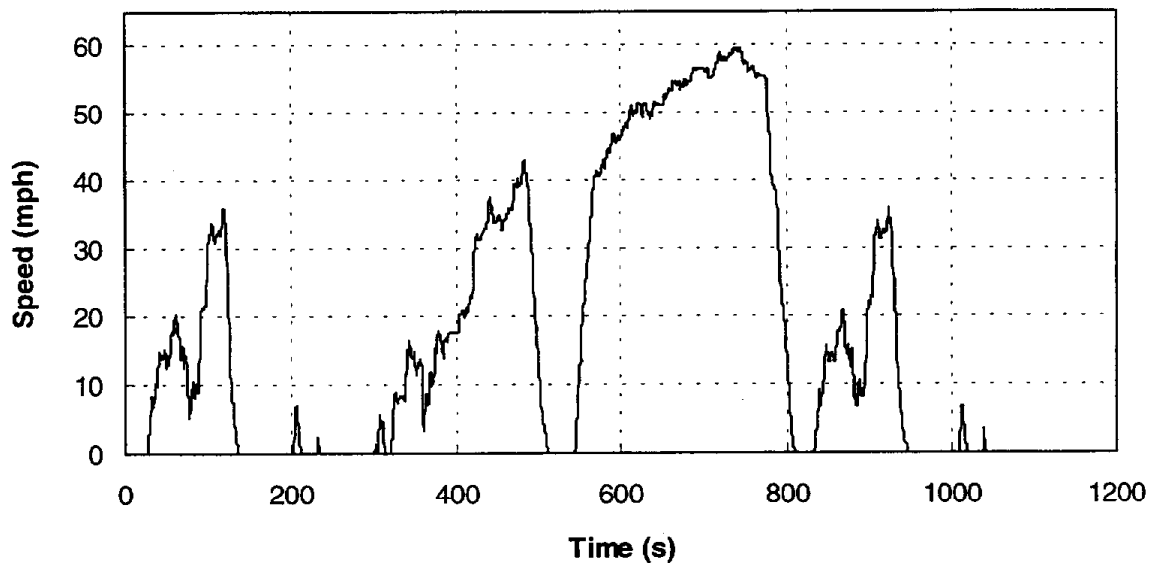


Figure 4-29. The EPA Schedule D cycle for heavy-duty vehicle testing is based on the EPA transient engine test procedure

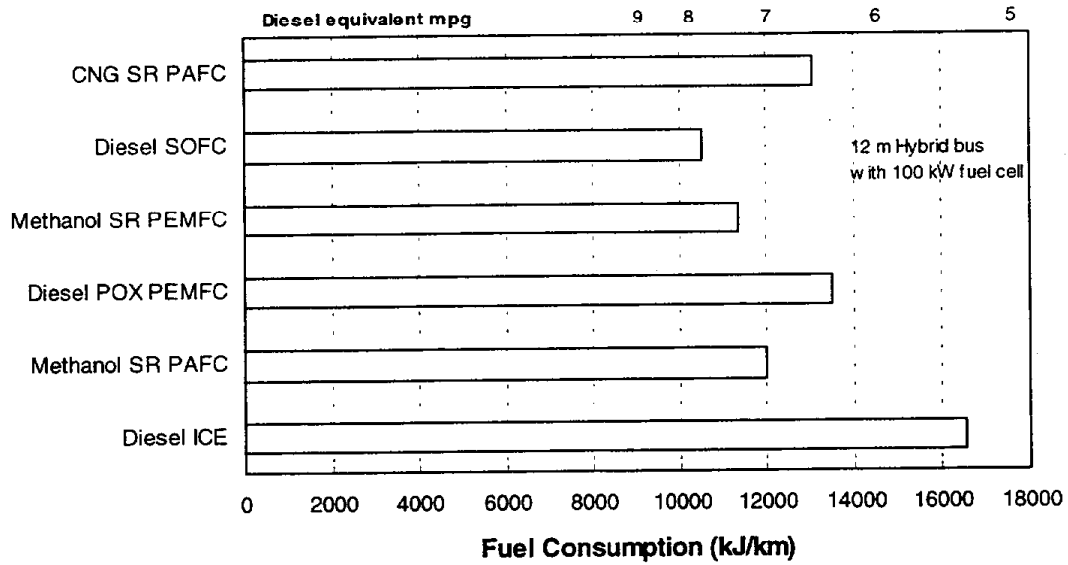


Figure 4-30. Fuel consumption for heavy-duty buses for the CBD cycle

Table 4-12 shows the estimated energy consumption over the Schedule D cycle. The driving cycle includes acceleration to higher speeds and has a higher average power requirement than the CBD cycle. The regenerative braking recovery factor is reduced to 28 percent over the Schedule D cycle to take into account the control systems limited ability to absorb all of the power over four rapid decelerations.

5. EMISSION DATA

The principal sources of emissions from fuel cell powered vehicles with on-board hydrocarbon fuel reformers are the combustion devices needed to heat the fuel cell and the reformer. The burners combust the vehicle fuel during start up and the anode gas during normal operation. Measurements of emissions from burners, reformer subsystems, and fuel cell systems provide information for the overall vehicle emissions assessment, which is described in Section 6.

In this section, emission data are presented for methanol steam reformer systems, a natural gas steam reformer, and a partial oxidation system. As part of this project ARCADIS Geraghty & Miller measured emissions from one Fuji PAFC-powered bus (DOE/DOT Phase III test bed bus [TBB-2]). Georgetown University and West Virginia University measured the emissions from the TBB-3. Lastly, ARCADIS Geraghty & Miller measured the waste gas combustion emissions from a Phoenix Gas Systems (subsidiary of HBT) stationary POX system. The data from these tests are summarized in Sections 5.1, 5.2 and 5.3, respectively. Additional emissions data were obtained from a review of literature and from in-house ARCADIS Geraghty & Miller test data. These additional sources of information, which are presented in Sections 5.4, 5.5, and 5.6, include emissions data for the FZJ methanol steam reformer, ONSI stationary PAFC power plant, and other burners and engines.

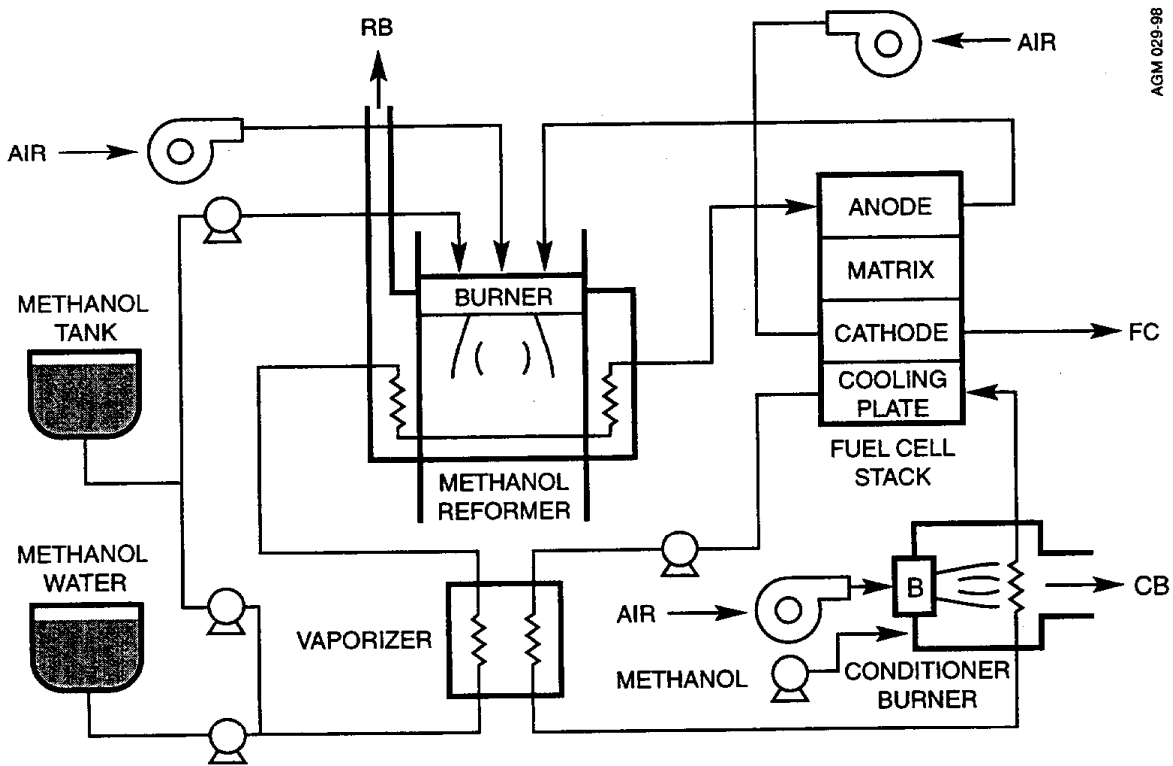
5.1 METHANOL PAFC TBB-2 EMISSIONS

ARCADIS Geraghty & Miller tested the Fuji PAFC-powered TBB-2 at the Energy Technology Engineering Center (ETEC), a subsidiary of Boeing North American, in September 1996. The TBB-2 included a Fuji methanol steam reformer and Fuji PAFC. Design parameters are shown in Table 5-1. The fuel cell and reformer flow schematic is shown in Figure 5-1. The system includes three emission sources: a reformer burner, a fuel cell temperature conditioner burner, and the fuel cell cathode. The reformer is fed with a mixture of methanol and water that is blended and stored on the bus. Another tank stores pure methanol, which is used to power two conditioner burners that warm up the fuel cell and reformer until hydrogen supply is established.

The fuel cell conditioner burner does not operate once the fuel cell is heated to operating temperature. After start up, the blower on the burner continues to remove heat through a cooling plate on the fuel cell. After the reformer produces hydrogen, the reformer burner burns anode and tailgas and supplemental methanol (referred to as reformer burner trim) when the anode gas does not provide enough energy for the reformer. Future fuel cell powered buses are expected to operate without a conditioning burner or burner trim fuel input.

Table 5-1. Phase III methanol PAFC TBB-2 parameters

Parameter	Value
Length	9 m (30 ft)
Curb weight	11,300 kg (26,000 lb)
Test weight	13,400 kg (31,111 lb)
Fuel cell system	Fuji PAFC with methanol SR
Water/methanol mixture	1.5 mol/mol
Fuel cell power	57 kW
Motor power	90 kW
Battery	Saft NiCd



AGM 029-98

Figure 5-1. Phase III methanol PAFC TBB-2 flow schematic (Booze Allen)

Figure 5-2 shows the PAFC power plant adjacent to the rear of the bus. The air blowers for the reformer burner, conditioner burner, and cathode air supply are visible in the photo. These blowers generate the flow for the TBB's exhaust system.

Emissions from the TBB-2 were measured with the vehicle operating in a stationary mode at ETEC. The Fuji PAFC system was operated at three power levels with the bus batteries absorbing the fuel cell's power output. Testing occurred at idle and moderate load conditions, which corresponded to fuel cell power output levels of 11, 19, and 27 kW. Testing at higher power levels was not possible because the power absorbing capability of the battery system was limited. Testing also occurred during start up periods.

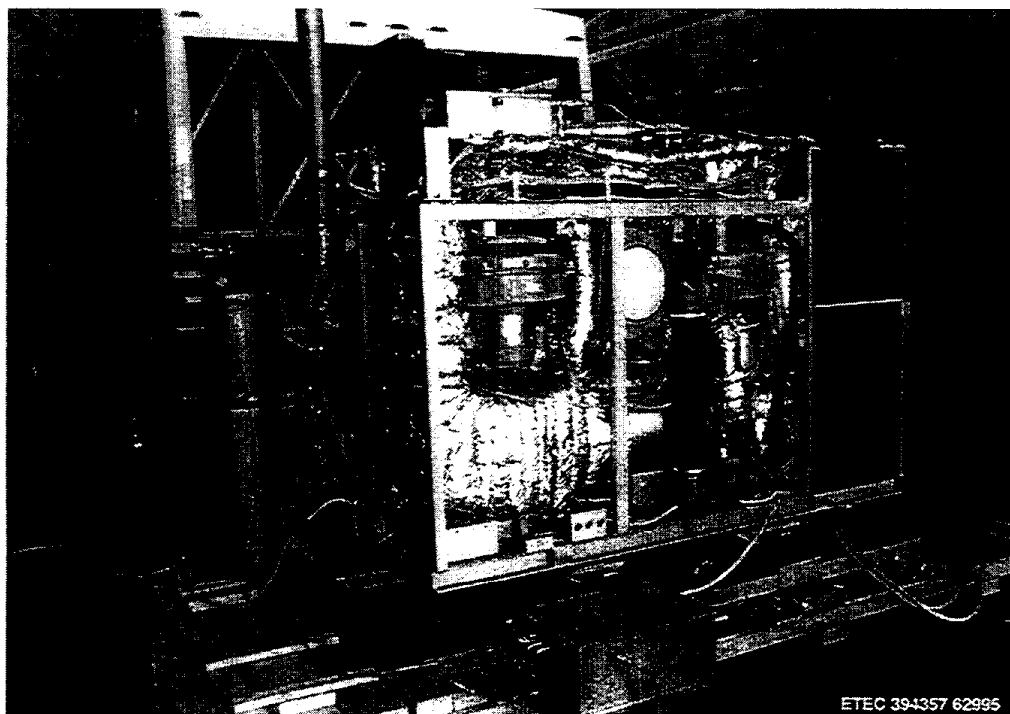


Figure 5-2. Fuji steam reformer and PAFC package for the DOE/DOT Phase III methanol TBB-2

ARCADIS Geraghty & Miller performed sampling and analysis using a mobile emission sampling laboratory according to ARB Test Method 100 — Continuous Emissions Monitoring. A manifold was constructed to collect integrated-average exhaust samples from the three emission sources on the bus. At certain times, the sources were sampled individually. Instruments were calibrated during the course of the day to assure that instrument drift was within test method criteria. A data logger collected the instrument data, and average values were recorded at one-minute intervals. During each sampling run, ARCADIS Geraghty & Miller measured exhaust temperature, CO₂, NO_x, CO, and total hydrocarbons (THC). Moisture content

was measured at two load conditions. The following system operating parameters were also recorded at the start and end of each sampling run.

- Time
- Battery state of charge (SOC)
- Battery voltage (V)
- Fuel cell Power (kW) output

Figure 5-3 shows these operating parameters for the testing conducted on September 4, 1996. The fuel cell power values at the beginning and end of each test condition are shown as triangles. The battery voltage and SOC are also shown during the testing period. Figure 5-3 also includes calculated values for the energy input into the battery in units of MJ. These values are parallel to the SOC data, providing an independent validation of the SOC measurement.

The average emission concentration results for the Phase III methanol PAFC TBB-2 tests are listed for each test condition in Table 5-2. Figures 5-4 and 5-5 show data points for the testing on September 4, 1996. The emissions during start up, when the burners are fueled with methanol, are detailed in Figure 5-4. Figure 5-5 shows the emission results at different process locations during steady operation at various load conditions.

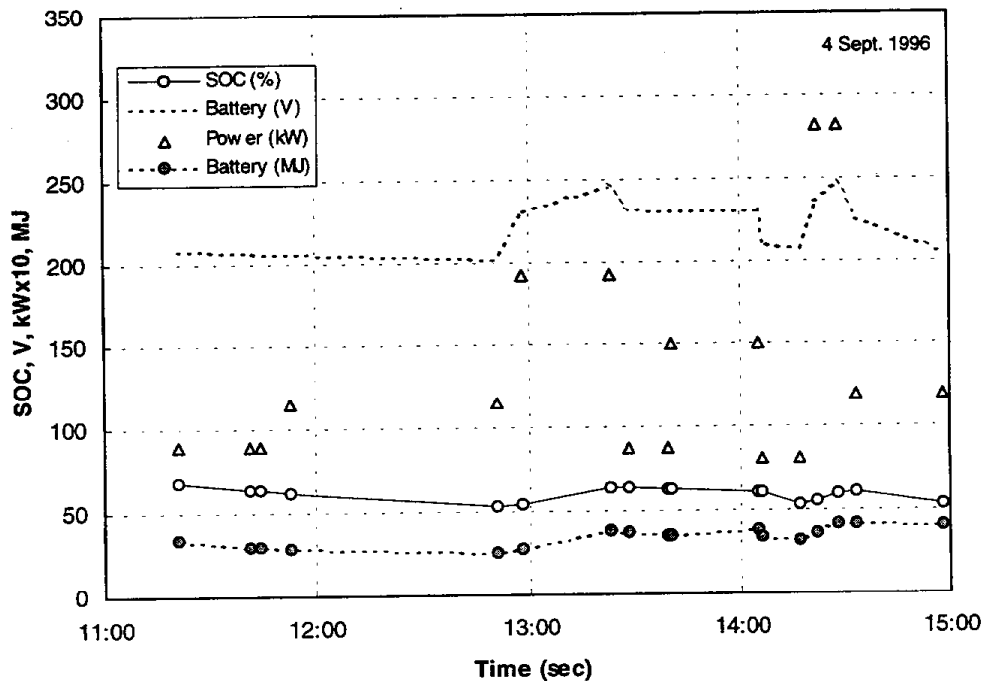


Figure 5-3. Operating parameters for Phase III methanol PAFC TBB-2 tested at ETEC

Table 5-2. Emissions at start up and steady load condition (dry basis)

Test Condition	Sample Location ^a	O ₂ (%)	CO ₂ (%)	CO (ppm)	NO _x (ppm)	THC (ppm)	Power (kW)
Start up	M	16.8	3.2	276	4.3	47.7	—
Idle	M	17.2	2.7	52	<1	5.4	11
25% load	M	15.3	3.9	136	<1	6.2	19
50% load	M	16.9	3.1	165	1.2	22.3	27
Start up	CB	8.7	1.8	38	<1	5.3	—
Idle	CB	20.8	0.2	3	<1	2.9	11
Idle	FC	15.8	1.2	51	<1	8.4	11
25% load	FC	13.4	0.6	11	<1	6.9	19
Idle	RB	17.8	2.3	94	<1	0.9	11
25% load	RB	19.4	3.0	351	<1	29.1	19

^aRB=Reformer burner, FC=Fuel cell cathode, CB=Fuel cell conditioner burner, M=Manifold. The manifold combines all three emission sources.

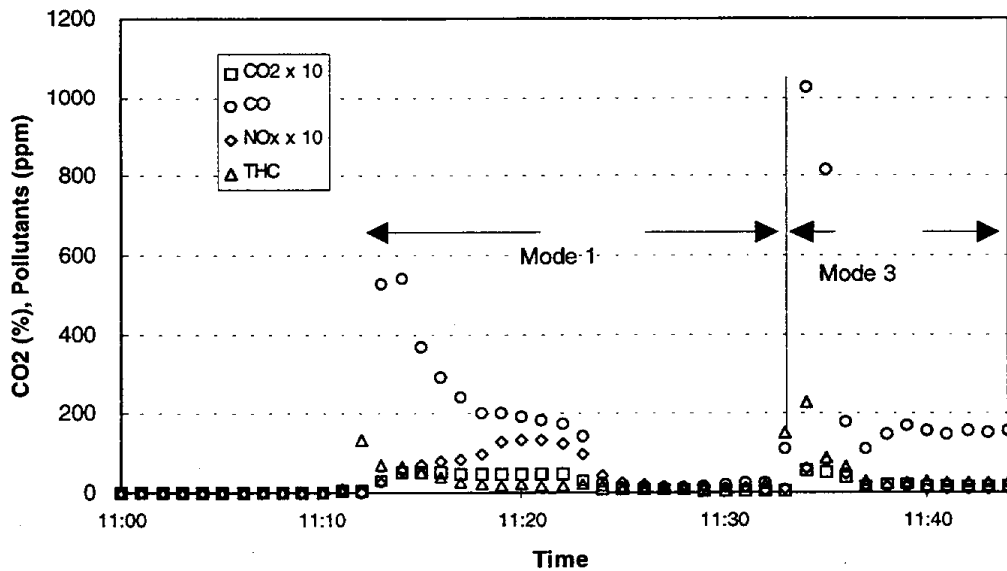


Figure 5-4. TBB-2 start up emissions, 4 September 1996

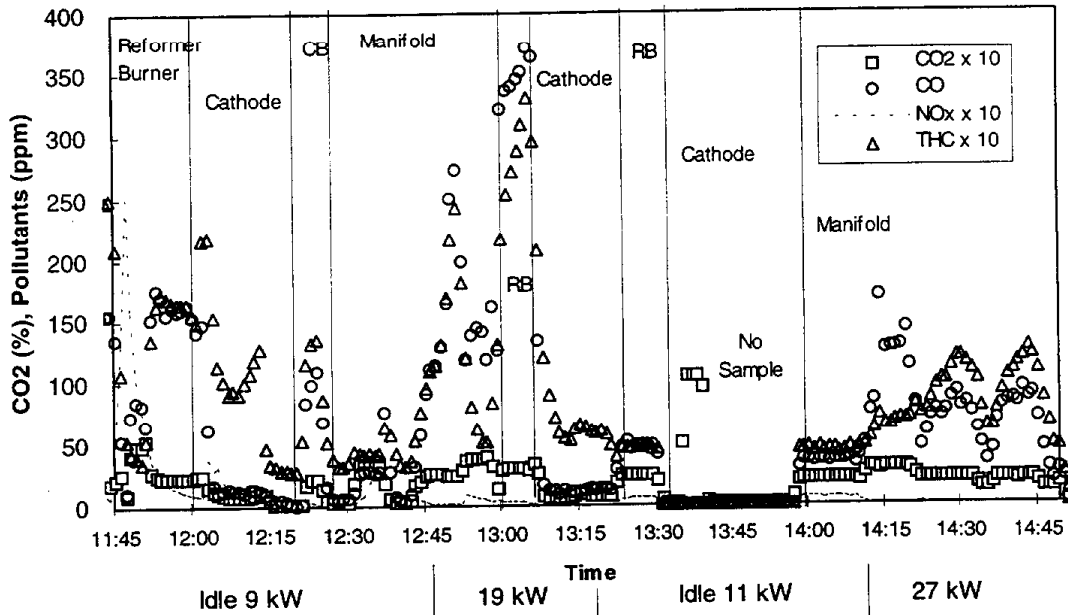


Figure 5-5. TBB-2 steady state emissions, 4 September 1996

A review of the data from the ETEC testing of the Phase III methanol PAFC TBB-2 indicates the following:

- The manifold data average values in Table 5-2 show that CO and HC emissions were lower during no load and part load operations. The emissions observed from the fuel cell cathode exhaust (FC) were unexpected because the reaction of hydrogen with oxygen occurs on the cathode. The source of CO, CO₂, and HC from the fuel cell cathode could be migration across the fuel cell or background emissions.
- An initial spike in NO_x emissions can be observed from the reformer burner at the beginning of testing. Afterwards, NO_x emissions were below 1 ppm except during low load operation when supplemental fuel was added to the burner. NO_x levels were undetected for much of the reformer burner's operation.
- The reformer burner is the principal source of emissions with some CO and HC observed from the fuel cell cathode and the conditioning burner during startup.
- The conditioning burner operates primarily during start up. When the conditioning burner was tested after the fuel cell warmed up, the CO₂ was negligible which indicated that no combustion was occurring. Traces of hydrocarbons and CO were measured in the conditioning burner which may have been related to exhaust from the reformer burner entering the air inlet.

- Moisture content was measured from the manifold sampling location during one no load and one composite no load and 27 kW operation event. Over a 24 min. sampling period with 7 min. of 25 kW operation, 6 min. of ramp up to load, and the balance of time at idle, the moisture content was 7.0 percent. The moisture content for a separate idle measurement was 5.6 percent.

Data from the steady state testing are presented on a mass basis and compared to other heavy-duty engines data in Table 5-3. The Fuji PAFC values are based on the measurements from the manifold. Exhaust mass flow was calculated from fuel flow and CO₂ concentrations and emissions are presented on a mass per kWh_e of fuel cell electrical power output basis. These emissions are well below heavy-diesel engine standards that are shown on a mass per kWh of shaft power over the transient driving cycle. This comparison is valid because one kWh_e provides about the same level of vehicle tractive power as one kWh of shaft power¹. NO_x from the fuel cell power plant is one thousandth of the diesel engine standard while CO and THC are also well below the standards.

Table 5-3 also shows steady-state emissions data from the Phase IV Georgetown PAFC power plant. The IFC 100 kW power plant was delivered for installation in a Novabus RTS bus in January 1998. The fuel cell system is more responsive than its stationary power plant predecessors and can achieve a power ramp up of 20 percent per second (Callaghan).

5.2 PAFC BUS CHASSIS DYNAMOMETER TESTING

A second DOE/DOT PAFC bus (TBB-3), operated by Georgetown University, was tested on the University of West Virginia (WVU) mobile chassis dynamometer in early 1997 to measure the emissions from a PAFC methanol bus. This portable laboratory simulates the road load for on-road driving. The system measures emissions with a dilution tunnel and collects data on a real time basis. Data from the emission testing were provided by Georgetown University (Wimmer, 1997) and reported in an SAE publication (Wimmer 1998a). The TBB-3 was tested during start-up and at three constant load conditions (25, 50, 75 percent) with the power absorbed by load banks. Testing was also performed over the Central Business District (CBD) and Arterial (ART) Cycles.

¹Engine work in kWh must be transmitted through the engine and transmission to provide work to meet the road power demand. The power converter and motor absorb about the same losses of the fuel cell power before it is power at the wheels.

Table 5-3. Comparison of steady-state emissions from PAFC power plants with heavy-duty diesel engine emission standards

Source ^a	NO _x	CO	THC	PM
Fuel Cell Power Plant (mg/kWh _e)				
Fuji PAFC 9 kW ^b	14	1290	210	NM
Fuji PAFC 19 kW ^b	11	2690	230	NM
Fuji PAFC 27 kW ^b	3.6	1540	90	NM
Fuji PAFC 25/75 kW ^c	40	3850	120	13
IFC PAFC ^c	ND	20	10	13
HD Engines (mg/kWh)				
1998 Bus Standard (g/kWh)	5360	20780	1740	67
1997 DDC Diesel S50 w. cat.	6300	1200	130	54
1997 DDC S50 CNG	2550	3485	1070	40

^a Fuel cell power plant data is shown on a g/kWh of electric power basis. Bus power in kWh is shaft power over the transient cycle.

^b Data from ARCADIS Geraghty & Miller CEM testing, NM = not measured

^c Data from Wimmer (1998b).

^d ND = no data.

Figure 5-6 shows the exhaust gas concentrations and operating parameters over the CBD cycle. The bus was driven over 14 acceleration and cruise events (0 to 20 mph). The fuel cell does not respond quickly to the load but rather responds to the state of charge (SOC) of the batteries. The initial and final SOC were the same for the CBD test event. At the start of driving, fuel cell power is below 20 kW and ramps up to over 40 kW at the end of the test. Energy is initially drawn from the batteries and the SOC drops over the first half of the dynamometer test cycle and then increases over the end of the test. The fuel cell operated for about 150 sec after the end of driving to recharge the batteries to the initial SOC. The addition of methanol as reformer fuel is indicated as burner or reformer trim. At the beginning of operation, burner trim is maximum, then ramps down, and increases towards the end of the test. CO emissions were much higher during periods when the burner was combusting supplemental methanol.

Table 5-4 summarizes the WVU test data for the PAFC TBB-3 and includes comparable emissions data for a typical diesel bus. NO_x emissions were less than 1 percent of those from the diesel buses, and hydrocarbon emissions were also lower. CO emissions were nominally the same levels. Particulate emissions were below the detection limit.

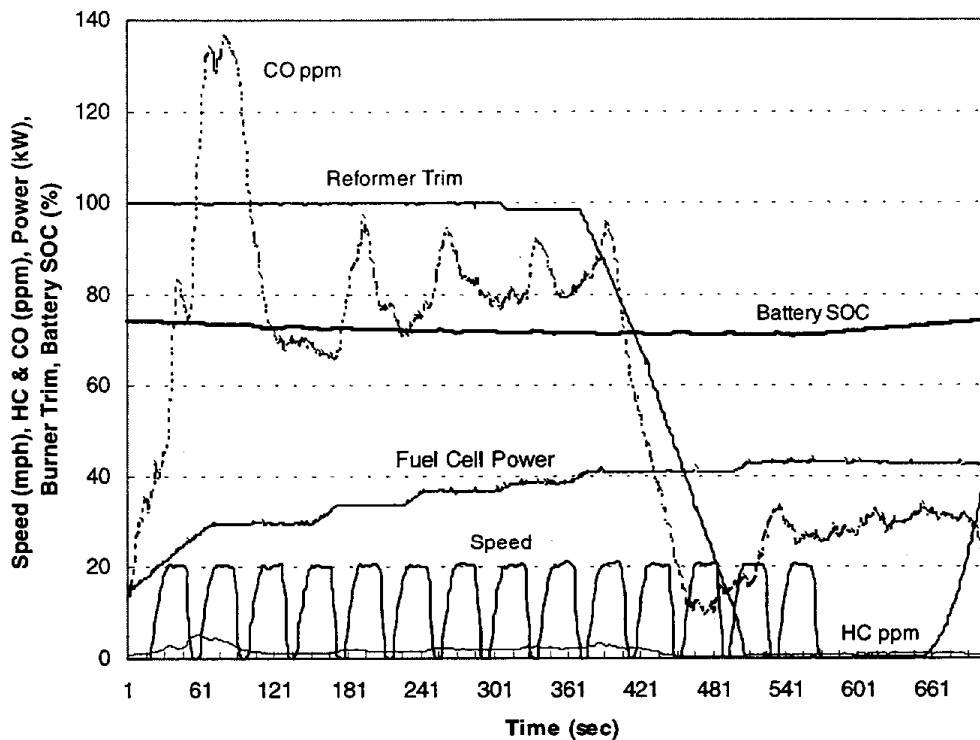


Figure 5-6. PAFC methanol TBB-3 emissions and operating data, CBD cycle (Wimmer)

Table 5-4. Chassis dynamometer emissions from DOE/DOT methanol PAFC bus

Cycle	NO _x (g/mi)	HC (g/mi)	CO (g/mi)	Fuel Economy (MJ/km, [mpg] ^a)
PAFC Bus				
CBD ^b	0.01	0.21	7.8	20.2 [2.35]
CBD	0.05	0.28	9.0	22.0 [2.15]
ART ^c	0.01	0.96	14.6	23.9 [1.98]
ART	0.01	0.57	8.4	27.4 [1.73]
Typical diesel bus CBD ^d	20	1	8	22.5 [3.8]

^a MJ lower heating value, miles per gallon methanol for fuel cell bus, miles per gallon diesel for diesel bus

^b CBD = Central Business District

^c ART = Arterial

^d Data for 12-m, 15,000 kg transit bus (Bass, Unnasch (1995))

The results for the Fuji PAFC bus from both the ETEC testing and the WVU testing show a substantial improvement over diesel emissions, particularly NO_x and particulate. While the Fuji system is not a full size configuration, the results indicate that emissions are reduced substantially. The operation of the Fuji PAFC buses depends upon the programming and tuning of the control systems on the bus (Green). The control logic and fuel supply for the fuel cell power plant have a significant effect on hydrocarbon and CO emissions while NO_x and particulate emissions are uniformly low. The fuel economy in mpg is one half that of the diesel bus; however, the energy consumption (MJ/km) is the same as that of a 12 m (40 ft) diesel bus.

5.3 HBT UOB™ PARTIAL OXIDATION (POX) SYSTEM TEST DATA

In this project, ARCADIS Geraghty & Miller tested an HBT underoxidized burner (UOB™) industrial hydrogen generation system to provide data on emissions from components of a POX system. The HBT UOB™ system is shown in Figure 5-7. The UOB™ consisted of a POX, a high temperature shift reactor (HTS), a condenser unit, pressure swing adsorption (PSA) gas clean up unit and a waste gas flare. The objectives of the testing were to determine the composition of hydrocarbon emissions, evaluate the effect of load changes, and quantify the emissions from the burning waste gas. The system that was tested operates at 10 atm. It is fabricated from vessels certified to meet ASME standards with separate POX and HTS sections. The operating parameters for the UOB™ system are shown in Tables 5-5 and 5-6.

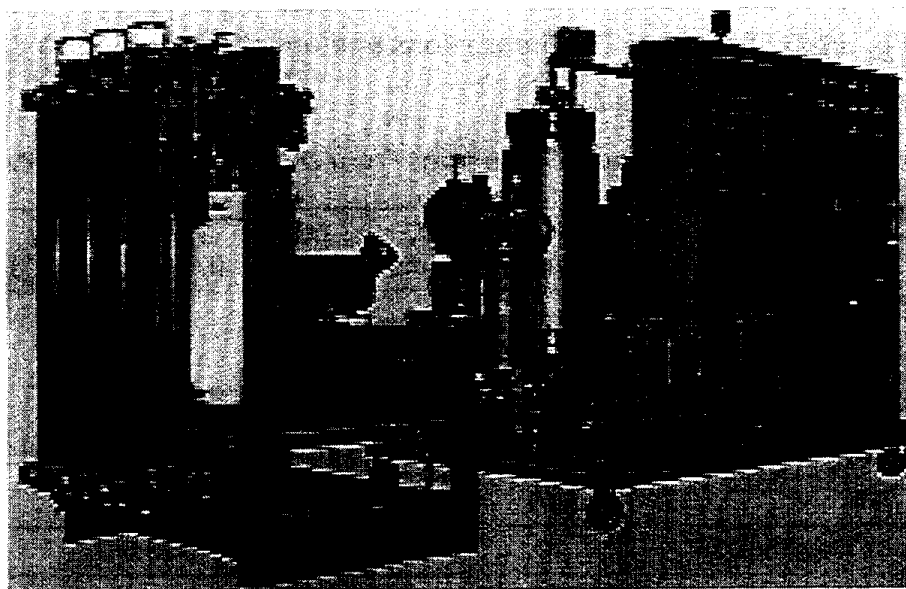


Figure 5-7. HBT UOB™ industrial hydrogen generation system

Table 5-5. System temperatures

Location	Temperature, K (under full load)
UOB™	1755
HTS inlet	560
HTS outlet	577
Condenser/Cooling Unit outlet	286

Table 5-6. System operating parameters and flowrates

Parameter (under full load)	Capacity
Natural gas feed	7.3 kg/h
Natural gas heat rate	106 kW, HHV
Air feed	60 kg/h
Stoichiometric ratio (λ)	0.45
Hydrogen production	1.39 kg/h
Hydrogen heat rate	55 kW, HHV
Total efficiency	0.52

Process and exhaust gas constituent concentrations were measured following the methods summarized in Table 5-7. Concentrations of NO_x, CO, CO₂, O₂, and THC were measured using ARB Method 100. Formaldehyde (HCHO) and air toxic hydrocarbon species, were measured using USEPA Method TO-11 and TO-14, respectively. Benzene, toluene, ethyl benzene, and total xylenes (BTEX) were measured according to ARB Method 410. Ammonia (NH₃) was measured using Bay Area Air Quality Management District (BAAQMD) Source Test Method 1B (ST-1B). Exhaust flow rates were small so they were calculated from the carbon balance in the POX feed and CO₂ in the exhaust stream. A description of the test methods and the emission results are detailed in Appendix A.

A schematic of the UOB™ system, along with the measured concentrations of gases, are shown in Figure 5-8. The sketch shows the sampling locations for the points plotted in the chart.

Table 5-7. Test methods

Analysis	Method
NO _x , CO, CO ₂ , O ₂ , THC	California ARB Method 100, CEM
Hydrocarbon speciation	USEPA T0-14, SUMMA® Canister, GC/MS
Ammonia	BAAQMD ST-1B, 0.1N HCl impingers
Formaldehyde	USEPA T0-11, DNPH cartridges
Natural gas analysis (ASTM D-1945)	Sample collection - USEPA Method 18 Sample analysis - GC/TCD/FID
BTEX	Sample collection - USEPA Method 18 Sample analysis - GC/ FID (Equivalent to California ARB Method 410)
Moisture content	USEPA Method 4

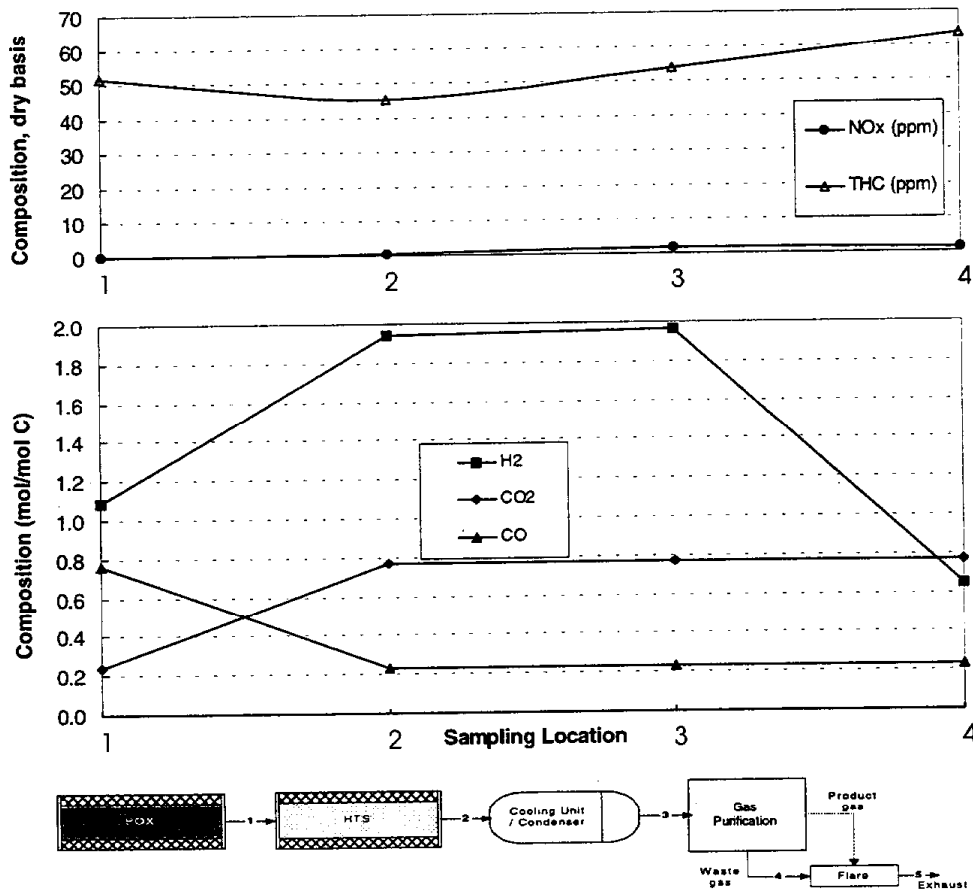


Figure 5-8. Sampling locations and gas compositions for HBT UOB™ system

In Figure 5-8, hydrogen, CO, and CO₂ are given in units of moles per mole of fuel-carbon. Hydrogen increases in the HTS, is separated in the PSA, and reduced in the waste gas. CO, CO₂ and hydrocarbons are concentrated in the PSA waste gas as hydrogen is removed. Essentially no NO_x is produced in the UOBTM system and total hydrocarbons (THC) are below 70 ppm. Flare emissions (location 5) vary with operating conditions and are discussed later.

For these tests, a sub-stoichiometric mixture of air and natural gas were injected into the UOBTM. As discussed in Section 3, the air is preheated within the UOBTM to increase reaction temperatures. This heating improves hydrogen and CO conversion and minimizes unreacted methane. Steam is not added to the industrial UOBTM with natural gas feed. This unit operates at an air/fuel ratio (λ) of 0.46 to provide a margin of safety for carbon formation and to allow for heat losses from the uninsulated reactor vessel. Demineralized water is injected downstream of the UOBTM to quench the reaction and provide steam for the HTS. The system is not equipped with a low temperature shift (LTS) unit; so the HTS is operated at a lower temperature than in a normal POX system (310°C) in order to achieve lower CO levels. To achieve the lower CO levels more CO conversion occurs in the HTS so more heat is liberated. The added heating would decrease the life of the catalyst in a normal operation. After CO reacts with steam to form CO₂ and hydrogen in the HTS, the gas stream is cooled in a condenser. Hydrogen is separated from the condenser product in the PSA.

For test condition C3, only the waste gas from the PSA was burned in a flare. For condition C₂, both waste gas and the hydrogen product gas were burned. The PSA waste gas is similar to the composition of fuel cell anode gas. It contains a mixture of nitrogen, CO₂, and unreacted hydrogen. Although the fuel cell anode gas will have a higher humidity and lower CO content than the PSA waste gas, the fate of the hydrocarbons is the same for the UOBTM system as in a fuel cell system. After the process gas exits the HTS, hydrocarbon species should remain unaffected in the PSA until they are burned. The flare approximates the destruction that might occur when fuel cell anode gas is used as fuel. Test of the UOBTM flare, therefore, provides information on the fate of hydrocarbons similar to that in a fuel cell/POX system.

Figure 5-9 compares the yield of CO and hydrogen with those predicted from equilibrium calculations for the same feed gas composition (natural gas feed with a stoichiometry of $\lambda=0.45$). The measured composition from the POX was near equilibrium levels indicating that the reaction reached completion. The comparison for the HTS exit shows that equilibrium was not reached.

The output of the HTS depends on a number of factors including operating temperature and catalyst age. Due to the constraints of testing, the HTS temperature was not adjusted for optimum CO. The effect on hydrocarbon emissions should be minimal, however, because most hydrocarbon species should be frozen after the quench step. Operating the HTS catalyst at low temperatures increases the hydrogen output; however, the increased heat of reaction from CO conversion decreases the catalyst activity over time. As the catalyst ages, the bed temperature can be raised slightly to accelerate the reaction rate. Fresh catalysts can produce CO levels as low as 2 percent (Moard). If the catalyst activity decreases, CO levels may rise as high as 6 percent. Reversing this effect by raising the bed temperature results in a CO level of 3 to 4 percent. CO levels between 4 and 6 percent were measured from the HTS exit gas. Long term data for a UOBTM showed CO levels of 3.3 percent.

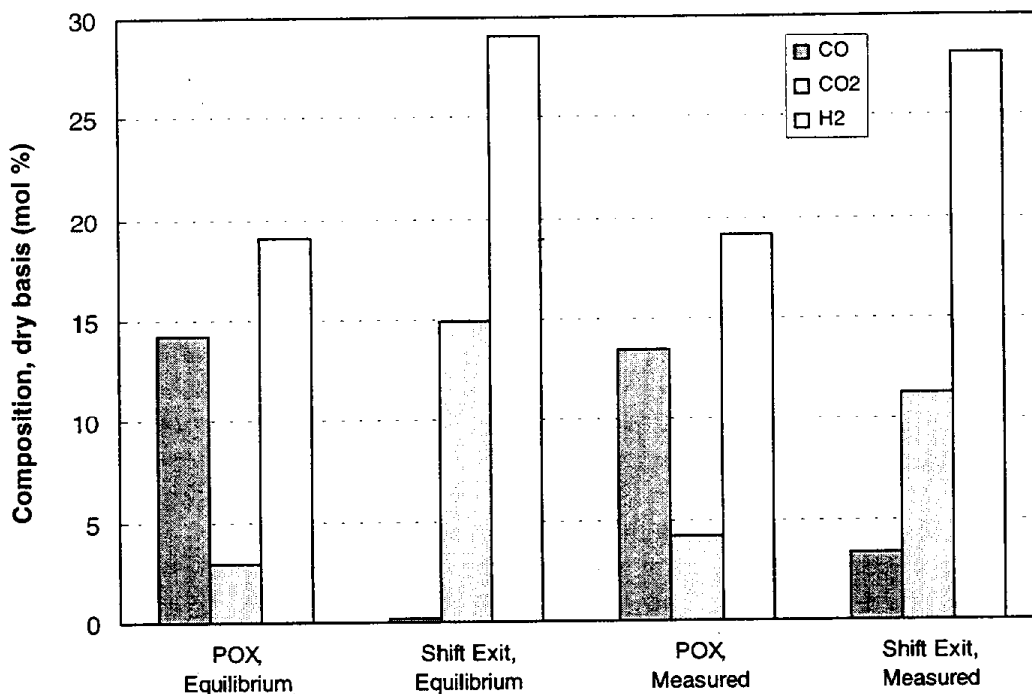


Figure 5-9. Measured versus predicted gas compositions from HBT UOB™ system

Figure 5-10 shows the trace gas pollutant levels in the POX system and flare. Ammonia, a precursor to NO_x in the flare and a potential fuel cell contaminant, was detected in the hot POX and HTS gas streams. Ammonia levels dropped by 99.9 percent after the HTS gas passed through the water condenser, because ammonia is absorbed in the water. Ammonia production is expected to be lower in the vehicle system because the operating pressure will be 3 atm compared to the 10 atm operating pressure of the commercial UOB™ system. The fate of formaldehyde at the HTS exit is similar to ammonia because it is scrubbed by the condenser water. Low levels of formaldehyde were measured in the flare exhaust when burning the PSA effluent, no formaldehyde was detected when the product hydrogen and PSA effluent were burned.

NO_x and total hydrocarbon (THC) concentrations are shown in Figure 5-11. NO_x levels are below 1 ppm in the reducing environment of the POX system. THC levels are below 100 ppm. These levels represent a very high level of carbon conversion in the POX unit. Over 99.5 percent of the carbon is converted to CO or CO_2 .

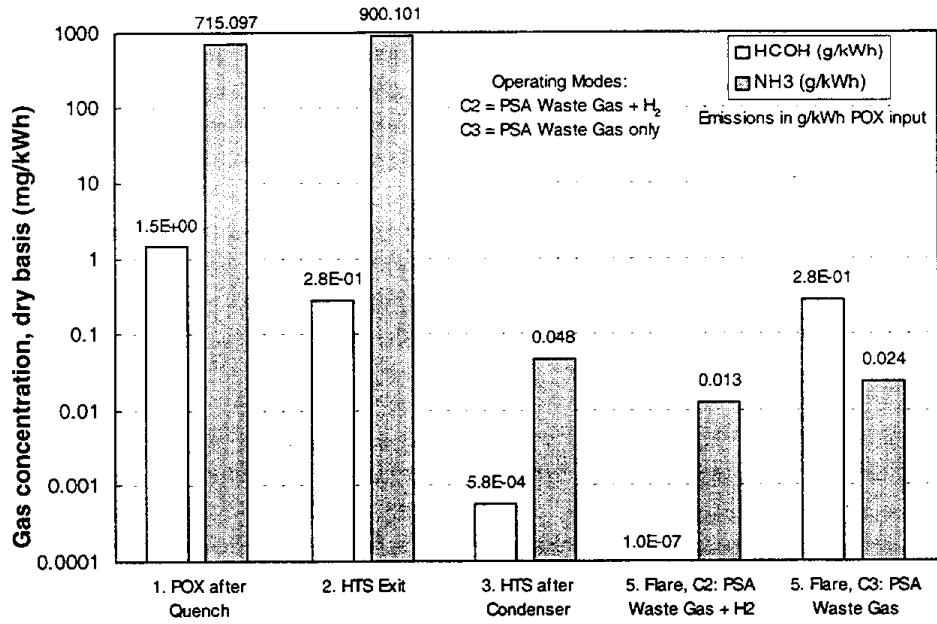


Figure 5-10. Trace gas compositions from HBT UOB™ system

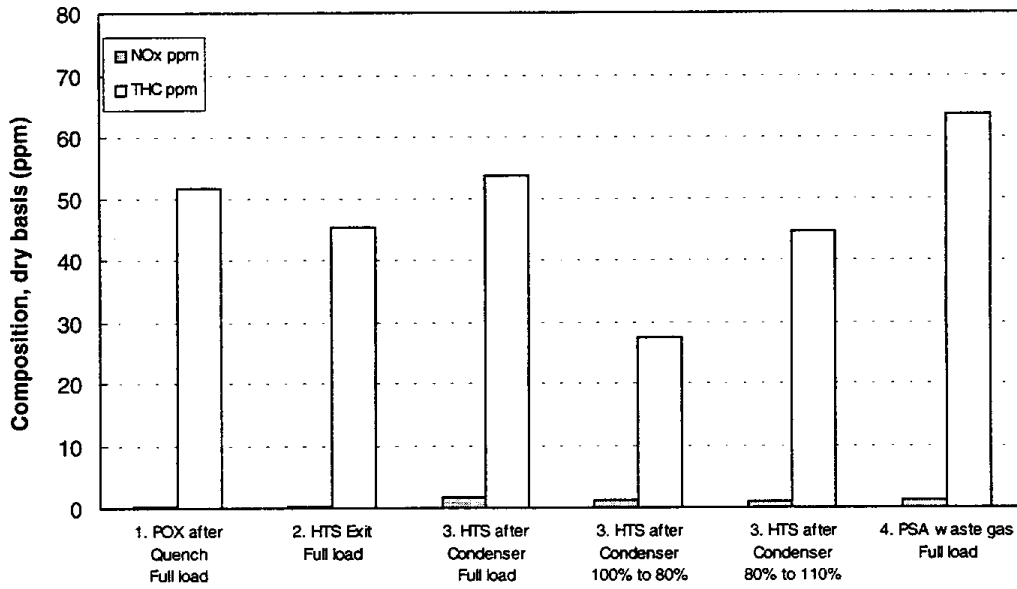


Figure 5-11. Product gas NO_x and THC compositions from HBT UOB™ POX system

Figures 5-12 and 5-13 show the emissions from the pilot start up burner and the UOBTM flare at several operating conditions. Figure 5-12 gives emissions in units of parts per million (ppm) on a log scale, and Figure 5-13 give emissions in units of g/kWh of POX input. The process initially warms up with the pilot natural gas burner (Pilot). The main POX burner then starts and is operated at an oxidizer-fuel ratio near stoichiometric ($\lambda = 0.9$) to further heat the process (POX Pilot). When temperature is high enough, the oxidizer-fuel ratio is lowered to the POX operating point (POX start). The PSA waste gas with or without the product hydrogen is combusted in the flare. Hydrocarbon emissions are highest for the pilot burner during start up when natural gas is burned. Hydrocarbon concentrations from the both the POX and waste gas/hydrogen flare reflect the lower hydrocarbon levels achieved through the POX and HTS processes. NO_x levels are dramatically reduced and CO levels are also lower when the POX start is achieved.

Figure 5-14 shows the concentrations of gases during transient load changes. The load from the HBT UOBTM system was varied from 100 to 80 percent and then 80 to 110 percent. The unit was programmed to respond to a load change with a relatively slow algorithm. The most significant effect was a reduction in hydrocarbon concentration as the load dropped and an increase in hydrocarbon concentration as load increased.

The composition of trace hydrocarbons was measured in the POX gas stream and in the flare exhaust. Gas streams were drawn into SUMMA canisters for 15 minute sampling periods. The gas compositions were analyzed according to EPA methods TO-11 and TO-14. The levels of various hydrocarbons are shown in Table 5-8. Trace hydrocarbons were detected at ppb levels. The saturated hydrocarbons and olefins were below the detection limit of 20 ppm. Determining the mix of C1 through C5 hydrocarbons was, therefore, not possible. Data from the continuous analyzers indicated that the sum of the hydrocarbon concentration was less than 50 ppm.

The presence of oxygenates such as acetone, dioxane, and methyl- tertiary butyl ether (MTBE) appear to be synthesized in the partial oxidation reactor. The oxygenated compounds could be produced in the water condenser phase of the HBT system. However, this unit operates at relatively low temperatures (90°C). In a vehicle fuel cell system, humidification may be accomplished with spray atomization or bubbling the anode gas through a water bath. In a vehicle system the conditions for humidification will be at a somewhat higher temperatures.

Figure 5-15 shows the effectiveness of the flare in reducing emissions. CO emissions are reduced by over 99.9 percent. This reduction efficiency occurs because CO burns readily and because high levels of CO are in the fuel gas stream. The anode gas from a PEMFC will have much lower levels of CO, and the reduction efficiency will not be as high. Hydrocarbons emissions were reduced by 85 percent in the flare. Hydrocarbon levels were very low in the flare gas feed so these lower removal efficiencies are expected. These results would be similar to those found in anode gas from a fuel cell.

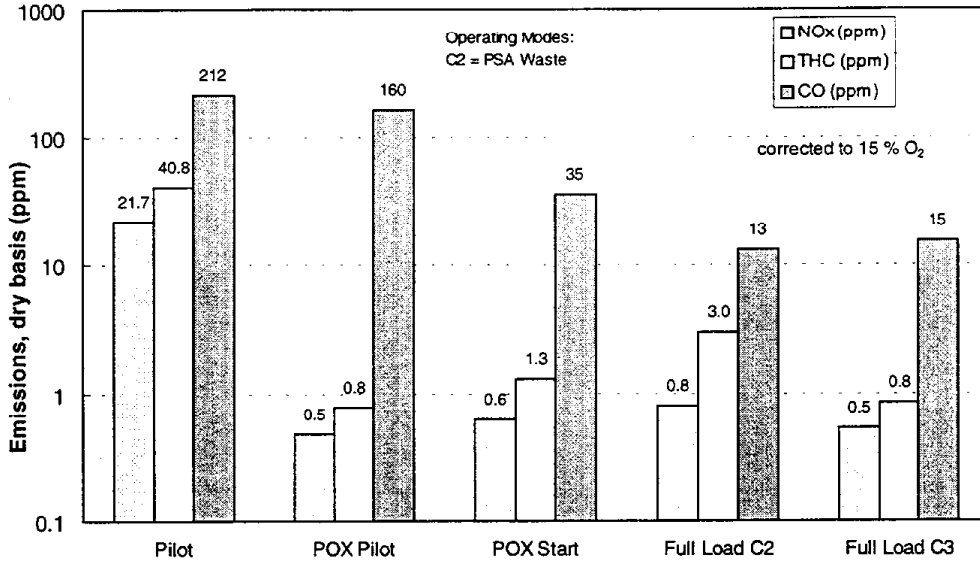


Figure 5-12. Emissions from HBT UOB™ start-up burner and flare (corrected to 15% O₂)

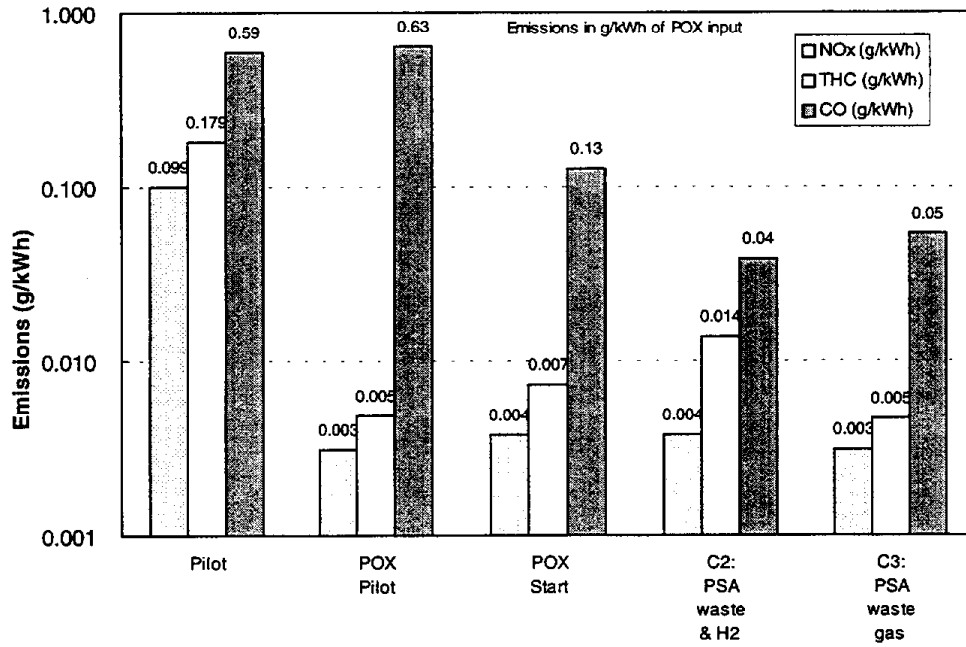


Figure 5-13. Emissions from HBT UOB™ start-up burner and flare (g/kWh POX input)

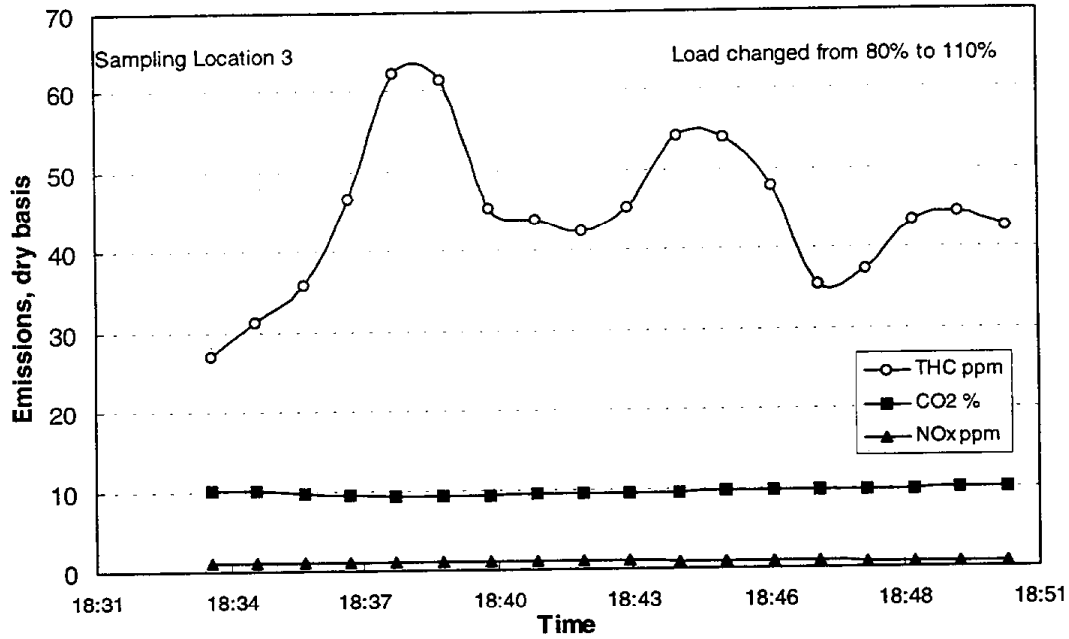


Figure 5-14. Effect of load change on HBT UOB™ gas compositions

Table 5-8. Trace hydrocarbons in the gas stream and flare emissions from the HBT UOB™ system (mg/kWh), by U. S. EPA TO-14 and BASTM-1B methods

Component	HTS Exit	Flare PSA Waste Gas	Flare PSA Waste Gas with H ₂
1,3 butadiene	<2.47E-05	<7.5E-06	<7.9E-06
acetone	2.15E-04	3.62E-06	8.45E-05
benzene	2.14E-04	4.22E-06	5.69E-06
dioxane	<4.02E-05	<1.18E-05	5.45E-05
ethane	<1.5E-02	<8.4 E-02	<8.4E-02
ethanol	4.20E-05	9.57E-06	1.62E-05
hexane	<3.83E-05	<5.77E-06	<6.24E-06
methane	4.88E-02	<4.5E-02	<4.5E-02
MTBE	<3.29E-05	<9.72E-06	1.76E-05
toluene	5.03E-05	6.32E-06	9.38E-06

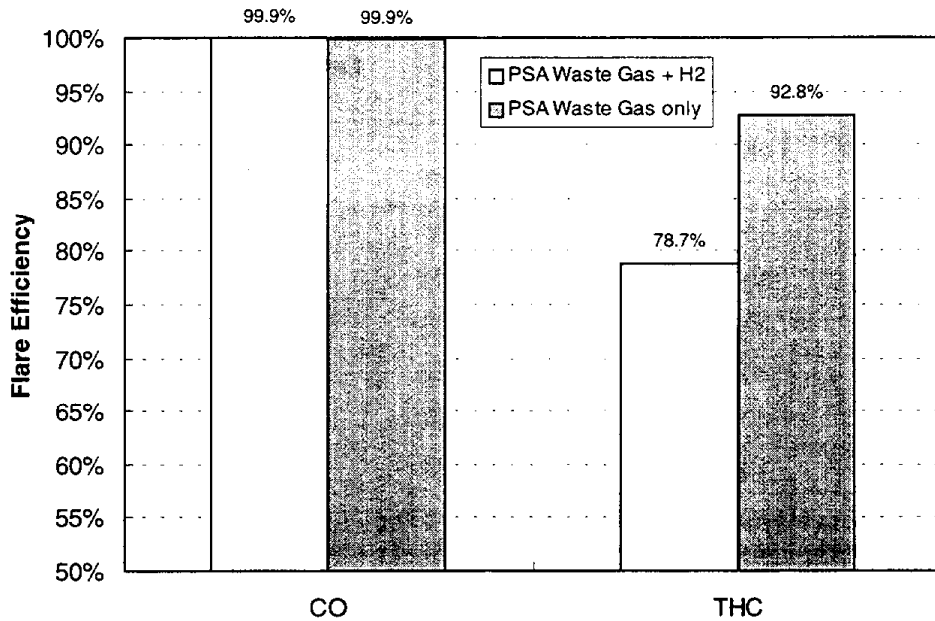


Figure 5-15. Emission reduction efficiency for HBT UOB™ flare

5.4 FZJ METHANOL REFORMER DATA

The Research Center Jülich (FZJ) is developing components for a methanol steam reformer PEMFC system. Their efforts include testing of a catalytic burner with a premixed radiant design. The burner design allows for the complete oxidation of the fuel in the presence of large quantities of inert components. FZJ tested the burner over steady state and transient conditions. Burner fuel included pure methanol to simulate start-up and mixtures of methanol and simulated anode gas, containing H₂, CO₂, and water vapor. Riedel reports the optimal stoichiometry for burner operation as $\lambda=1.1$.

Table 5-9 summarizes the emissions from the FZJ catalytic burner. The data includes operating points with both low and high methanol utilization rates. The hydrogen utilization rate varies with steam reformer configuration to balance the energy demand required for fuel cell operation. The condition with high hydrogen utilization resembles the gas compositions that would be achieved by burning anode gas from a POX system. With a POX system, supplemental fuel may also be added to power the exhaust blower or maintain combustion in the burner.

Table 5-9. Emissions from FZJ catalytic burner ($\lambda=1.1$)

Burner Fuel Feed (mol H ₂ / mol methanol)	Load (kW/m ²)	CO ₂ (mol CO ₂ / mol fuel)	Emissions (mg/kWh) ^a			
			NO _x	HC	CO	HCHO
0/ 1	45		NR ^b	27	6.5	NM ^b
0.5/ 0.5	40	0	0.65	12	4	122
0.8/ 0.2	40	0	1.0	2.5	2.9	40
0.9/ 0.1	40	0	0.55	2	2.6	22
0.8/ 0.2	40	1	NR	7	5.5	NM
0.8/ 0.2	40	2.2	NR	6	11	NM

^a Energy in kWh corresponds to total reformer thermal input in kWh. Data from Riedel.

^b NR = not reported since NO_x levels were generally low, NM = not measured

Inert components had only a minor affect on emissions which indicate that the catalytic burner was effective in oxidizing the fuel. Water vapor did not affect HC and CO emissions while CO₂ resulted in a slight increase in emissions. The presence of CO₂ does not favor equilibrium for CO oxidation because CO could also be formed through a reverse water gas shift reaction with hydrogen and CO₂. Operating the burner with a higher ratio of hydrogen to methanol reduced emissions. NO_x emissions from the burner are very low because it operates in a temperature range from 400 to 800°C.

For the methanol only run, start up time for the burner is 120 sec. Figure 5-16 shows HC and CO emissions during the start up. The CO emissions from the burner are generally lower than those of the HC emissions. This result may be due to the performance of the catalyst in oxidizing CO.

Figure 5-17 shows that the effect of changes in burner load are reached within 80 sec for an H₂/methanol ratio of 0.8. During transient increases in load, hydrocarbon emissions increased by a factor of 3 to 4 before dropping to steady state levels. Similar effects were observed with CO emissions. During load decreases the thermal mass of the burner helps maintain high combustion temperatures which contribute to HC and CO oxidation.

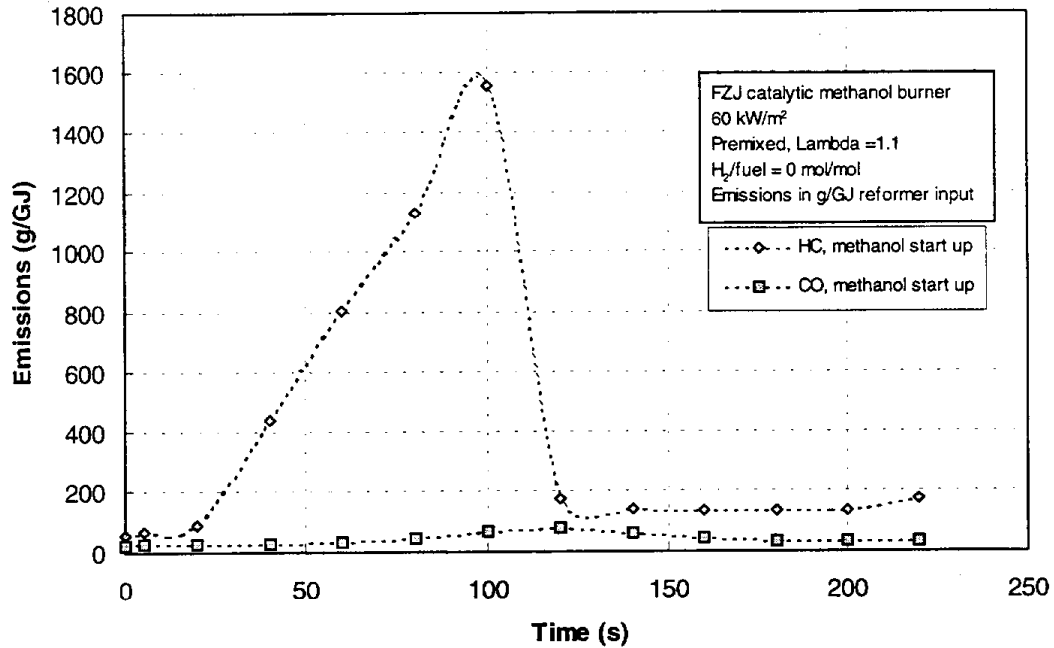


Figure 5-16. Startup emissions from FZJ catalytic burner operating on methanol

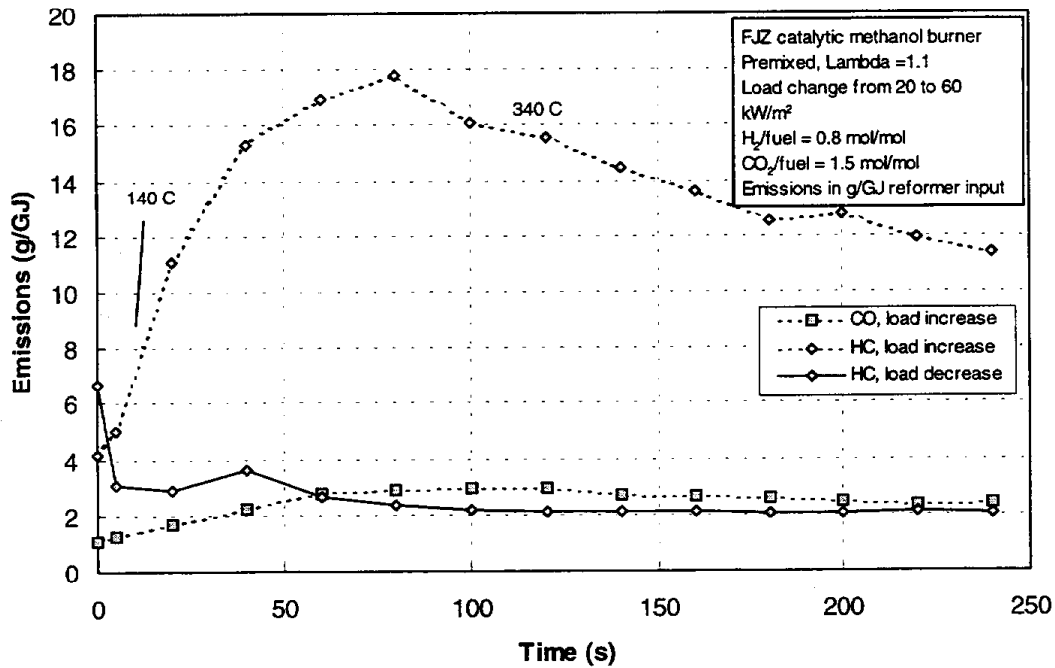


Figure 5-17. Effect of load change on HC and CO emissions with catalytic burner operating on hydrogen/methanol fuel

5.5 PAFC STATIONARY FUEL CELL DATA

Emission data from the ONSI stationary PAFC are shown in Table 5-10. The PAFC power plants operate on natural gas fuel with a steam reformer. The PAFC can tolerate moderate levels of CO. In these tests, the fuel cell feed contained about 2 percent CO. The reformer burns a mixture of natural gas and anode gas. The emissions for the fuel cell are lower than those of conventional natural gas combustion because the majority of the fuel cell gas is hydrogen.

Table 5-10. Emissions from PAFCs (Kordesch, Wimmer)

Fuel Cell	Emissions (mg/kWh _e)		
	NO _x	HC	CO
Stationary 200 kW NG ONSI PC25 PAFC	6 to 300	30 to 70	20 to 50
IFC 100 kW methanol PAFC	ND	10	20

5.6 EMISSION DATA FOR OTHER BURNERS AND ENGINES

Data from other burners and conventional engines provides insight into the expected emissions from fuel cell/reformer systems under some conditions. During start up and warm up periods, reformer burners and POX units operate near stoichiometric conditions. Start up emissions also represent a substantial portion of the emissions from conventional vehicle operations so comparisons are useful.

One example of data on start up emissions comes from tests on the experimental low emission burner shown in Figure 5-18. The burner has an alumina flame holder that is designed to minimize emissions. Figure 5-19 shows that the emissions of CO and HC are much higher during start up. Similar values and trends can be expected in reformer and conditioner burners.

Data from Daimler-Benz on automobile exhaust during start up are shown in Figure 5-20. The emissions are reduced by the vehicle's emission control catalyst. Hydrocarbon reduction efficiencies of 70 to 90 percent are achieved at automobile exhaust temperatures. Similar emission reductions can be expected when a catalytic coating is incorporated into a fuel cell reformer.

Steady state emission data can also be useful for certain operating situations. USEPA AP-42 provides data on the emissions of NO_x, CO, and THC for the combustion of numerous fuels in various combustion devices over a range of stoichiometries. Data were also found for a Capstone turbine.

Al-Garni published response time and temperature data for a catalytic combustors operating on hydrogen-air mixtures. A study of different catalyst types indicated stable combustion over a range from 220 to 320°C at the surface of the combustor and 420°C in the center of the catalyst.

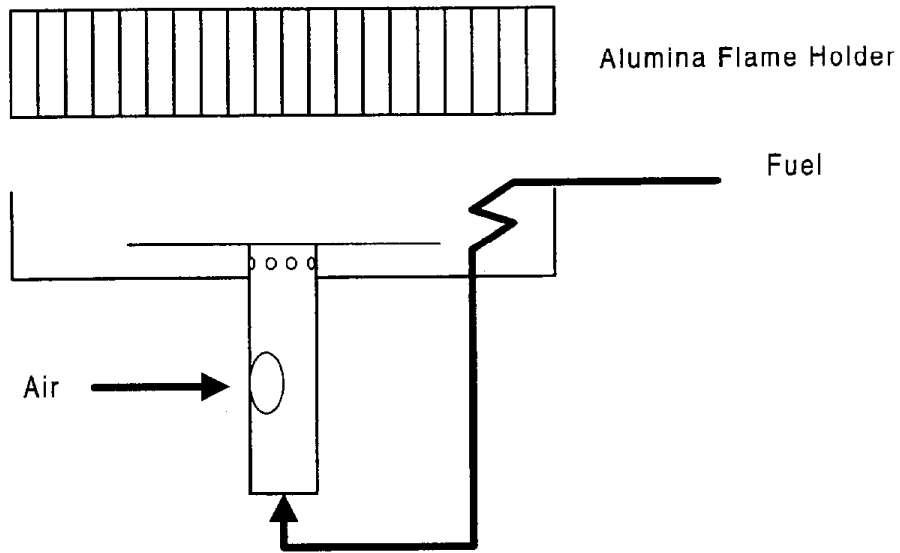


Figure 5-18. Experimental gasoline burner configuration

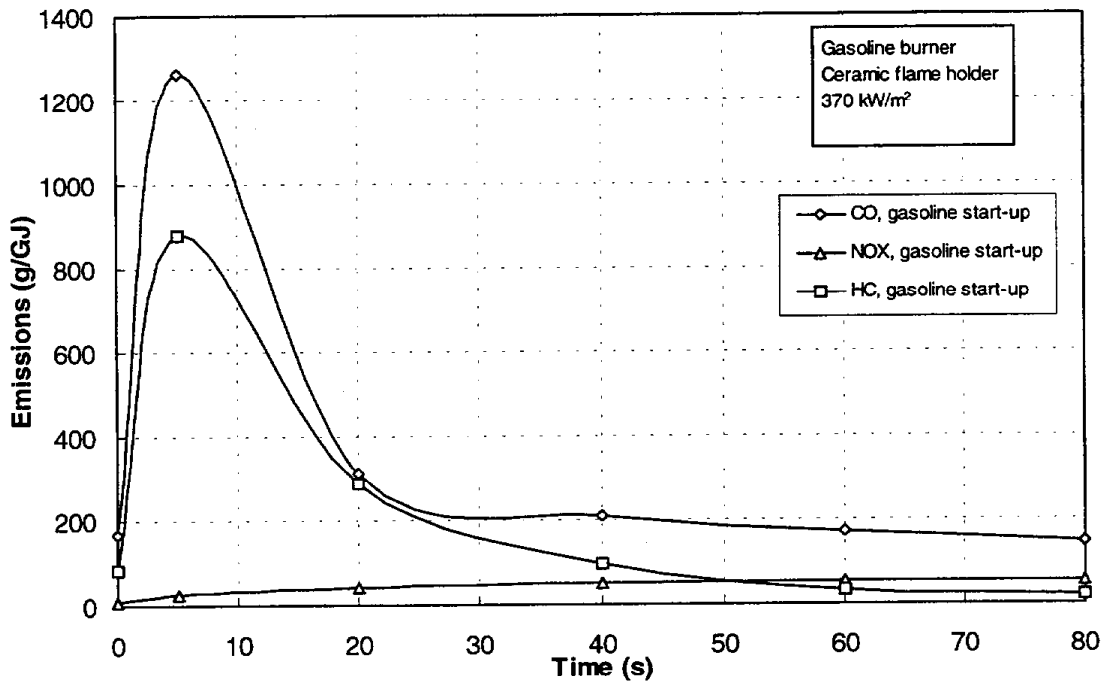


Figure 5-19. Start-up emissions from experimental gasoline burner

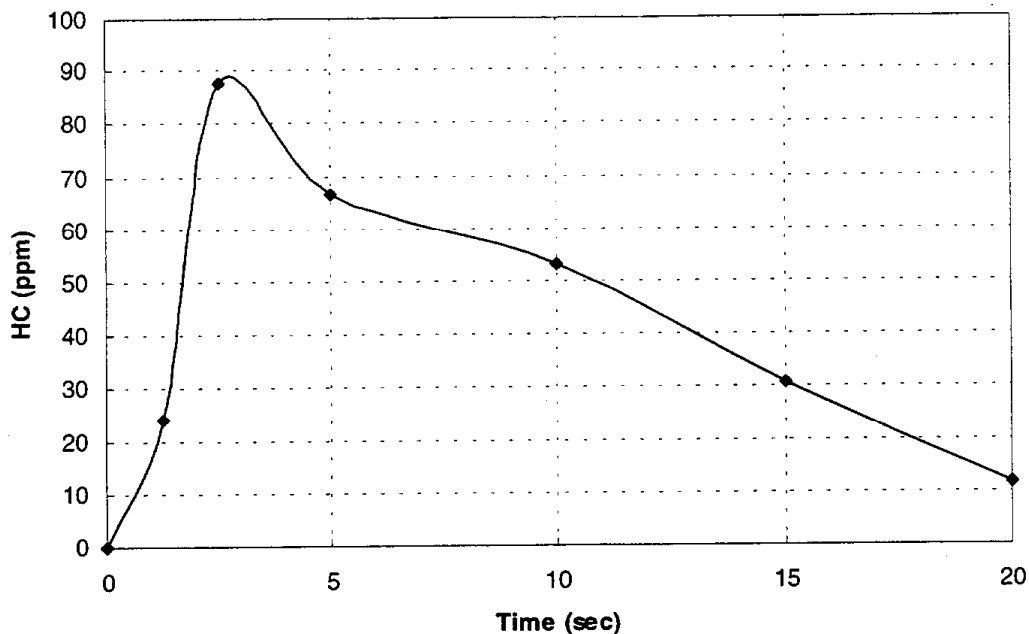


Figure 5-20. Catalyst start up emissions

Van Der Drift reports emissions from a low NO_x hydrogen/methane burner operating at high heat release rates (200 to 2000 kW/m^2). A foam ceramic burner plate operated in a surface combustion mode with premixed air/ fuel mixtures. When burning 80 percent hydrogen with stoichiometry of $\lambda=1.3$, NO_x emissions (corrected to 0% O_2) were 5 ppm at a load of 200 kW/m^2 rising to 55 ppm at 2000 kW/m^2 . The burner achieved relatively low NO_x emissions because the burner operated in a radiant mode, and NO_x emissions due to thermal hot spots were avoided. Flame temperatures, when operating on 80 percent hydrogen and 20 percent natural gas, were 1740°C at 200 kW/m^2 and 2190°C at 2000 kW/m^2 . At low power density, the flame temperature decreases which contributes to lower NO_x .

Emissions were also measured for a non catalytic surface combustion burner designed to operate on 70 to 100 percent hydrogen. NO_x emissions from this burner operating at $\lambda=1.3$ were under 5 ppm (corrected to 0% O_2) with a heat release rate of 1500 kW/m^2 .

The NO_x emission data from reformers is lower than that of other stationary combustion sources such as a gas turbine or EPA AP-42 emission factors for natural gas and diesel combustion. This result is expected because the reformer burner operates at a lower temperature and with a dilute gas stream. The low temperature operation is the dominant feature that lowers NO_x (Reidel).

CO emissions from the HBT UOBTM burner was as low as those from conventional combustion sources. The waste gas from the UOBTM was a mixture of CO and hydrogen and did not contain the low CO that would be expected from PEMFC anode gas. The FZJ burner resulted in much

lower CO emissions since it was burning a mixture of simulated anode gas with 10 percent of the fuel provided by methanol.

5.7 COMPARISON OF EMISSION DATA

Table 5-11 summarizes data from various conventional burners and includes the reformer data that were previously discussed. The emissions are presented on a mass per unit of burner fuel input basis. The emissions from the fuel processors was scaled by taking the ratio of reformer fuel consumption to burner fuel consumption. These emission values are then comparable with other combustion data.

The data in Table 5-11 provide some significant insights towards the emissions from fuel cell powered vehicles. NO_x emissions from fuel cell vehicles and the HBT flare are much lower than those from conventional combustion sources. THC and CO emissions for simple liquid fueled burners during start up are much higher than those emissions from other sources such as boilers and turbines operating at steady state. Emission data from TBB-2 and TBB-3 were consistent. NO_x emissions from the TBB-2 were often below the detection limit.

Table 5-12 shows the emission standards for light- and heavy-duty vehicles as well as stationary sources on a comparable g/GJ basis. This comparison required an assumption of fuel economy to represent engine emissions on a mass per unit energy basis. The fuel consumption for modern heavy-duty engines does not vary by more than 20 percent over the EPA transient test procedure. Light-duty vehicle fuel consumption varies considerably since it depends on the weight of the vehicle. The fuel economy in Table 5-12 for the light-duty car emissions is based on the corporate average fuel economy of 27.5 mpg. The actual emission certification is performed on the city portion of the driving cycle (FUDS) where the fuel economy is about 22 mpg for a combined city and highway fuel economy of 27.5 mpg.

Table 5-11. Summary of burner emission data

Data Source	Operation Mode	Fuel	Emissions (g/GJ Burner) ^a		
			NO _x	CO	THC
Capstone turbine	Steady-state	Natural gas	45	76.5	6
Capstone turbine	Steady-state	Diesel	90	76.5	9
Industrial boilers and heaters emissions					
EPA / AP-42	Steady-state	No. 2 Diesel	86	15.6	2
EPA / AP-42	Steady-state	Natural gas	43	14.5	2
Cleaver-Brooks	Steady-state	Propane	60	14.6	2
ARCADIS Multi-fuel Burner					
Burner VD-1	Steady-state	Gasoline	42	137	80
Burner VD-1, with insulation	Steady-state	Gasoline	41	31	28
Burner VD-1, flame holder	Steady-state	Gasoline	55	152	20
Burner VD-1, flame holder start	Start-up	Gasoline	35	634	615
Burner VD-1	Steady-state	Propane	66	304	97
HBT POX					
Flare Pilot	Pilot burner	Natural gas	28	164	50
UOB™ Pilot	Reformer warm-up	Natural gas	0.9	176	1
UOB™	Reformer start-up	Natural gas	1.0	35	2
UOB™	Full load (C2)	H ₂ /CO ₂ /CO	1.5	15	5
UOB™	Full load (C3)	CO ₂ /H ₂ /CO	1.7	30	3
FZJ - Methanol SR ^b	Steady state	Methanol	0.5	4	11
DOE PAFC TBB-2 ^b					
Reformer burner startup/11 kW	Start-up	Methanol	7	330	25
Reformer burner idle/11 kW	Steady-state	H ₂ /CO ₂ /CO/Methanol	<8	250	11
Reformer burner 25%/19 kW	Steady-state	H ₂ /CO ₂ /CO/Methanol	<6	450	9
Reformer burner 50%/27 kW	Steady-state	H ₂ /CO ₂ /CO/Methanol	8	680	39
DOE PAFC TBB-3 ^b	CBD	H ₂ /CO ₂ /CO/Methanol	3	700	21
IFC Methanol PAFC ^b	Steady-state	H ₂ /CO ₂ /CO	ND ^c	34	17

^aGJ Burner — Fuel energy rate to the burner.

^bEmissions per estimated GJ of anode gas.

^cND = not detected.

Table 5-12. Comparison of vehicle and stationary emission standards on an energy basis

Emission Source	Units	Emissions		
		NO _x	CO	THC
CA light-duty ULEV	g/mi	0.2	1.7	0.04
CA 2000 heavy-duty truck engine	g/bhp-h	4	15.5	1.3
Natural Gas Turbine in SCAQMD ^a	g/bhp-h	0.17	1	0.01
CA light-duty ULEV	g/GJ ^b	37	318	7.5
CA 2000 heavy-duty truck engine	g/GJ	453	1754	147
Natural Gas Turbine in SCAQMD	g/GJ	14.6	86	0.9

^a Emission data for stationary gas turbine meeting SCAQMD Rule 1134 (Unnasch 1996).

^b Emissions on a g per fuel energy input HHV basis.

6. ASSESSMENT OF VEHICLE EMISSIONS

This section presents the estimated emissions for the case studies presented in Section 4. This assessment includes emissions from the vehicle as well as refueling and fuel production. The estimated emissions are compared to emission standards and to the corresponding emissions attributed to operation of battery powered electric vehicles. Emission sources from fuel cell powered vehicles include the following:

- Start-up burner combustion
- Anode gas or reformer burner combustion during normal operation
- Vent emissions
- Condenser water

Section 6.1 presents the emissions from the light-duty vehicle case studies. Section 6.2 identifies refueling and other life-cycle emissions. Light-duty vehicle emissions and refueling emissions are compared to potential emission standards and comparable emissions in Section 6.3. Section 6.4 presents similar comparisons for a wider range of fuel cell types for operation in heavy-duty vehicles.

6.1 LIGHT-DUTY VEHICLE EMISSIONS

Vehicle energy modeling in Section 4 and emission data in Section 5 provide the basis for the emissions assessment in this section. Emissions are estimated for each category of vehicle discussed in Section 4.

6.1.1 POX/PEMFC Emissions

Exhaust from burners is the principle source of emissions from fuel cell powered vehicles with on-board reformers. Additional emissions could occur if gases are purged from the fuel processor system, but these emissions are infrequent or are recycled to the burner. The start up and operating emissions are described separately. An analysis of estimate uncertainty is also presented. Lastly, POX/PEMFC vent and fugitive emissions are discussed.

6.1.1.1 Start-up Exhaust Emissions

Fuel cell system start up requires the fuel processor to warm up to temperature before hydrogen is produced. The start up burner experiences a light off period of about 30 sec where HC and CO emissions are over 500 g/GJ and continues to operate for another 90 sec at a reduced emission

rate. These start up steps produce the largest components of the vehicle's NMOG and CO emissions for a typical duty cycle. Except for the Johnson Matthey Hot Spot™ system, these warmup rates have yet to be achieved in practice.

For a POX system, the start up burner operates near stoichiometry (slightly rich) in order to maintain the reducing conditions in the catalyst beds. The burner is then reduced to a richer stoichiometry, and air is fed to the anode gas burner to complete the combustion process. When the temperature point is reached, the burner is set to the optimum stoichiometry for maximum hydrogen production.

Start-up emissions were calculated from the energy required to warm up the fuel processor using the emissions factors in Table 6-1. The emissions factor data from Section 5 were adjusted with an NMOG reduction factor because the emission data were from burners without catalytic control. Future POX burners will include catalytic afterburners for NMOG and CO control. The emission rates represent an estimated ranking of emissions among the different fuels. Gasoline emissions were estimated from a small burner test. NO_x emissions for other fuels were estimated based on data in Table 5-11, which generally indicate lower emissions for alternative fuels. NMOG emissions for alternative fuels were estimated to be lower since these simpler compounds can burn more completely during the start up phase. NMOG emissions for CNG combustion were estimated to be 10 percent of total hydrocarbons. The energy requirement for heating the POX fuel processor was based on an estimated mass for the POX reactor and the HTS reactor. The volume and mass of the fuel cell and fuel processor system were sized for the system to meet the vehicle energy requirements described in Section 4. Specifically, the heat requirement was estimated by assuming that the 5 mm thick POX reactor wall, the 3 mm thick HTS housing, and the HTS catalyst reach operating temperature in less than 90 seconds. The heat energy input requirements for the 20 kW system were about 35 percent of the 60 kW system. The estimated energy required to warm up 20, 40, and 60 kW POX reactors was 750, 1,300, and 1,900 kJ, respectively. A catalyst is assumed to reduce NMOG and CO emissions during start up.

6.1.1.2 POX/PEMFC Operating Exhaust Emissions

Once the POX system is operating, the hydrogen product gas reacts on the fuel cell anode, and the waste anode gas is burned in a catalytic combustor. The anode gas must be very low in CO and HCs to ensure efficient fuel cell operation. Estimated emission factors for gasoline and alternative-fueled POX/PEMFC vehicles are shown in Table 6-2. NO_x emissions are based on the FZJ data for anode gas combustion. These are confirmed by similar low emissions from the HBT emission tests. A CO concentration of 20 ppm was assumed to be in the anode gas. Emissions are lowered in the catalyst according to the reduction factor shown in Table 6-2. The CO emissions are consistent with those from the FZJ emission data after an estimated reduction factor is taken into account. Data from HBT confirmed that the HC concentrations from the fuel processor are about 50 ppm or 5 ppm on an NMOG basis. After combustion in a flare, these emissions dropped by 60 to 80 percent. NMOG emissions from the HBT flare were less than 1 ppm (15 percent O₂ basis). NMOG emissions from fuels other than natural gas were estimated to be 2 ppm. These emission rates are shown on a g/GJ basis for comparison with other emission data.

Table 6-1. Estimated start-up exhaust emission factors for POX burners

Fuel	Emissions (g/GJ) ^a			NMOG/CO
	NO _x	NMOG	CO	Reduction
Gasoline	42	180	320	80%
Diesel	42	180	320	80%
LPG	30	140	320	80%
Ethanol	35	140	320	80%
CNG	20	10	250	50%
Methanol	20	140	320	80%

^a Emission factors estimated from Table 5-11 and strip chart recordings during start-up.

Table 6-2. Estimated exhaust emission factors for POX/PEMFC anode gas combination during steady state operation

Fuel	Emissions (g/GJ) ^a			NMOG/CO
	NO _x	NMOG	CO ^b	Reduction
Gasoline	0.7	2	28	85%
Diesel	0.7	2	28	85%
LPG	0.7	2	28	85%
Ethanol	0.7	2	28	85%
CNG	0.7	0.5	28	70%
Methanol	0.7	2	28	85%

^aEmissions per GJ of burner energy. NO_x and NMOG data based on Figure 5-3 and Table 5-9.

^bCorresponds to 20 ppm CO into the fuel cell.

Table 6-3 summarizes the emissions from an array of RFG-fueled POX/PEMFC vehicle configurations. The emission values were developed from a second-by-second simulation, which adjusts the burner emissions to take into account the transient load profile of the FUDS cycle. The largest contribution to emissions is the emissions from the start-up burner. As such, the 20 kW hybrid configuration reflected lower emissions. Minor changes are observed in emissions between the different configurations of the RFG vehicle. The system with a methanation reactor has higher CO emissions because the fuel cell model includes a CO tolerant catalyst. Some of the CO is removed in the fuel cell prior to combustion in the anode gas burner, so the effect in absolute terms is minor.

Table 6-3. Simulated exhaust emissions from RFG-fueled POX/PEMFC passenger cars (FUDS cycle)*

Fuel Cell/Engine Type	Gasoline Fuel Cell Only	Gasoline Fuel Cell Dominant Hybrid	Gasoline Load Sharing Hybrid	Gasoline Battery Dominant Hybrid	Gasoline Fuel Cell Dominant Hybrid
Fuel Processor	POX PROX	POX PROX	POX PROX	POX PROX	POX Methanation
Fuel Cell Power (kW)	75	60	40	20	60
<u>Start-up Emissions (g/mi)</u>					
NO _x	0.0037	0.0033	0.0023	0.0013	0.0033
NMOG	0.0032	0.0029	0.0020	0.0011	0.0029
CO	0.0056	0.0051	0.0036	0.0020	0.0051
CO ₂	6.2	5.6	3.9	2.2	5.6
CH ₄	0.0018	0.0016	0.0011	0.0006	0.0016
<u>Operating Emissions (g/mi)</u>					
NO _x	0.0024	0.0023	0.0022	0.0022	0.0023
NMOG	0.0015	0.0012	0.0012	0.0009	0.0013
CO	0.014	0.014	0.013	0.013	0.026
CO ₂	237	232	229	216	235
CH ₄	0.0088	0.0080	0.0056	0.0031	0.0080
<u>Total Emissions (g/mi)^b</u>					
NO _x	0.0060	0.0056	0.0046	0.0034	0.0057
NMOG	0.0047	0.0041	0.0032	0.0020	0.0041
CO	0.020	0.019	0.017	0.015	0.019
CO ₂	243	238	228	218	237
CH ₄	0.0106	0.0096	0.0067	0.0037	0.0096

*Component and vehicle mass given in Table 4-6.

^bEmission estimates depend upon many factors. Uncertainty is approximately ±50 percent.

Table 6-4 shows the projected exhaust emissions for POX/PEMFC vehicles operating on alternative fuels. All of the case studies are for 60 kW fuel cells with a small battery for start up and peak power requirements. The main effect from alternative fuels was a difference in fuel processor efficiency. Because most of the hydrocarbons are cracked in the POX unit, the effect of fuel choice on NMOG emissions is only important for methanol, CNG, and ethanol. For CNG, the very low NMOG content of the fuel significantly reduces the vehicle NMOG emissions. The emissions from a CNG vehicle with reduced weight, fuel capacity, and range were also estimated. Weight reduction resulted in a small decrease in emissions which was proportional to the energy consumption over the driving cycle. With methanol vehicles, the principal unreacted hydrocarbon is methanol. This component is absorbed in the condenser

water prior to being burned by the anode gas burner. This effect is expected to a lesser extent with ethanol because ethanol can dissociate in the POX reactor into C₂ hydrocarbons, such as ethane. These estimates are model predictions based on a wide variety of assumptions. While the results are shown to a considerable degree of precision to reflect the effect of modeling assumptions, the uncertainty in the estimates is on the order of ±50 percent. When actual vehicles are built and tested, the emissions will be affected by parameters other than the modeling assumptions so the relative ranking of emission estimates, which are both low and fairly close, may not resemble the ranking of actual vehicle emissions.

Table 6-4. Simulated exhaust emissions for alternative-fueled POX/PEMFC vehicles (FUDS cycle) (fuel cell dominant hybrid)^a

Component	Diesel	LPG	Ethanol	CNG ^b	CNG	Methanol
Fuel Cell/Engine Type	PEMFC	PEMFC	PEMFC	PEMFC	PEMFC	PEMFC
Fuel Processor	POX PROX	POX PROX	POX PROX	POX PROX	POX PROX	POX PROX
Fuel Cell Power (kW)	60	60	60	60	60	60
<u>Start-up Emissions (g/mi)</u>						
NO _x	0.0034	0.0023	0.0028	0.0017	0.0017	0.0017
NMOG	0.0029	0.0029	0.0023	0.0004	0.0004	0.0023
CO	0.0051	0.0051	0.0051	0.0120	0.0120	0.0051
CO ₂	5.8	5.2	5.7	4.6	4.6	5.5
CH ₄	0.0016	0.0016	0.0016	0.0240	0.0240	0.0016
<u>Operating Emissions (g/mi)</u>						
NO _x	0.0023	0.0023	0.0023	0.0023	0.0024	0.0023
NMOG	0.0012	0.0012	0.0012	0.0005	0.0005	0.0007
CO	0.014	0.014	0.014	0.018	0.018	0.014
CO ₂	243	214	232	191	195	226
CH ₄	0.0080	0.0080	0.0080	0.0120	0.0120	0.0080
<u>Total Emissions (g/mi)^c</u>						
NO _x	0.0057	0.0046	0.0051	0.0040	0.0040	0.0040
NMOG	0.0041	0.0035	0.0035	0.0009	0.0009	0.0030
CO	0.019	0.019	0.019	0.028	0.028	0.019
CO ₂	249	219	238	196	200	232
CH ₄	0.0096	0.0096	0.0096	0.0360	0.0360	0.0096

^aComponent and vehicle mass given in Table 4-7.

^bRange limited to 420 kM (260 mi) to reduce vehicle weight.

^cEmission estimates depend upon many factors. Uncertainty is approximately ±50 percent.

6.1.1.3 POX/PEMFC exhaust emission uncertainty analysis

An uncertainty analysis was performed on the estimate for the gasoline POX/PEMFC vehicle to evaluate the sensitivity of emission estimates to vehicle and emission control parameter assumptions. Estimate ranges for assumed parameters were incorporated into a statistical forecast model. The Crystal Ball software (Decisioneering) represents input assumptions as estimated probability curves and predicts the outcome of the model for a wide range of input assumptions. This approach presents the uncertainty of a model outcome as a probability curve rather than multiple “what if” cases. The following parameters were varied in the model.

- Start up burner emission rates
- Operating emission rates
- Battery operating strategy
- Reformer size
- Catalyst efficiency during start up
- Catalyst efficiency during cycle operating
- Reformer start up time
- Vehicle weight

For each parameter, a range of values was assumed, and a probability was associated with each value. Figures 6-1 and 6-2 show the input assumptions for catalyst efficiency and reformer size. The probability refers to the distribution of the x-axis value within the range of possible outcomes. In the case of catalyst efficiency, Figure 6-1 indicates that the estimated NMOG reduction factor is between 5 and 45 percent with a minimum value of 5 percent. The reduction factor represents the quantity of hydrocarbons remaining after the catalyst and corresponds to 100 minus the catalyst efficiency in percent. The most likely reduction factors are estimated to be between 10 and 20 percent and some allowance is made for less optimal catalyst performance. In Figure 6-2, the probability distribution is based on one-third of vehicles each having 20, 40, and 60 kW POX reformers. The x-axis value corresponds to the energy required to warm up the reformer.

Figure 6-3 shows the probability distribution of estimated NMOG emissions for a gasoline POX/PEMFC vehicle. The statistical forecasting model predicts the results for 6000 random samples based on the assumptions listed above. The model performs a random sampling of all input parameters (with uncertainty assumptions) and calculates NMOG emissions for each sampling point. The value of each input assumption selected by random sampling from eight different input assumptions profiles. These input assumptions reflect the estimated uncertainty for each input parameter. NMOG emissions are shown as a probability distribution. 80 percent of the NMOG forecasts are below 0.004 g/mi.

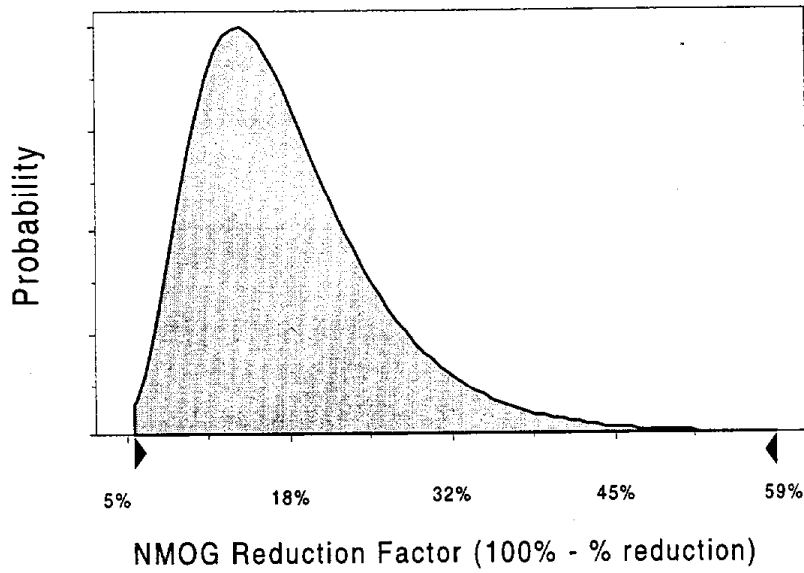


Figure 6-1. Input assumptions for catalyst emission reduction factor

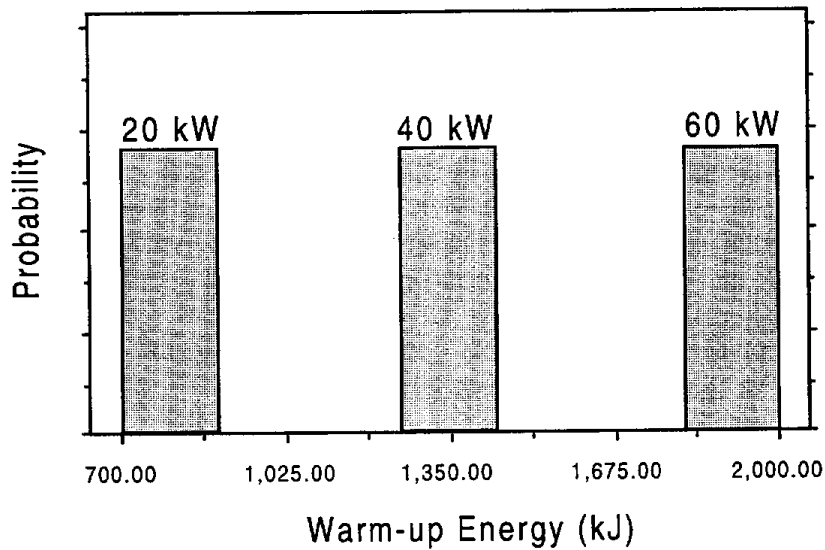


Figure 6-2. Reformer warm-up energy for 20, 40, and 60 kW POX reformers (energy in kJ)

Forecast: Total NMOG Emissions

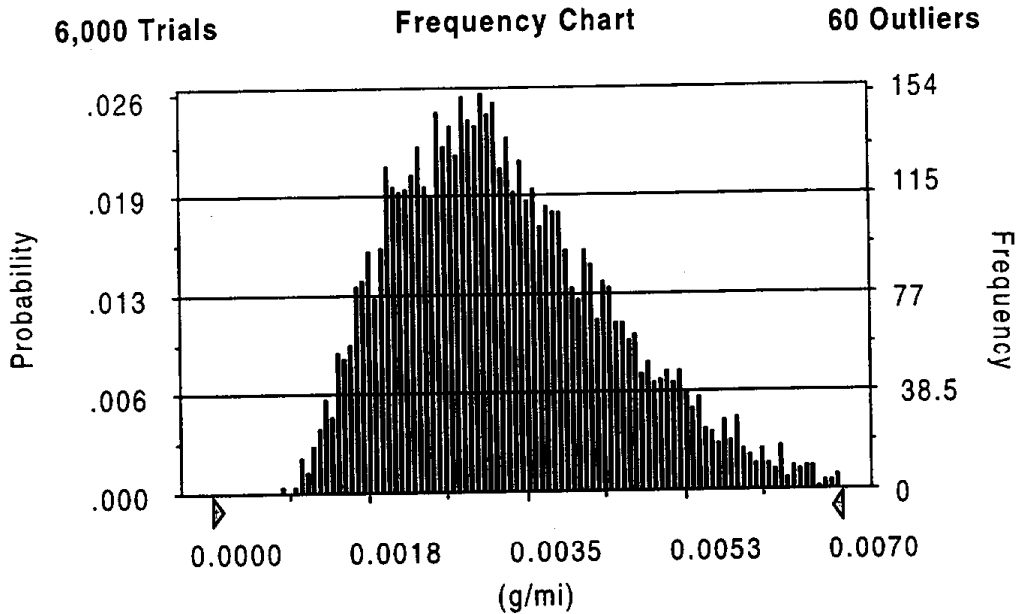


Figure 6-3. Probability distribution of NMOG emission estimates from light-duty RFG POX/PEMFC hybrid and range-extender hybrid, fuel-cell vehicles

Figure 6-4 shows the sensitivity of assumptions on the estimate of total NMOG emissions. The most significant factor is the reformer size which affects the size of the POX reactor and the energy required to heat the reactor. The next most important factor is the efficiency of the catalytic burner in further reducing the NMOG emissions from start-up. Similarly, the effectiveness of the catalyst in controlling operating emissions as well as the NMOG levels emitted from the POX unit are important but not as critical as start-up emissions. The relative outcome of this analysis is similar to results for light-duty vehicles with internal combustion engines. Variations in burner emissions during transient load changes are considered for the two power management strategies discussed in Section 4. Both operating strategies assume that no supplemental fuel is required for the reformer or compressor/expander. The different strategies affect the reformer load and rate of energy consumption during the driving cycle. Changes in reformer load were estimated to have only a moderate effect on emissions, since the fuel cell would be adversely affected by an increase in hydrocarbons from the fuel processor. The emission simulation values in this study assume an operating strategy that favors low emissions. Operating strategies that rely on significant burner trim can result in much higher emissions. The analysis of input assumption indicates that reformer size and start up emissions have a significant effect on total NMOG emissions. Reformer size translates directly into energy consumption and start up fuel combustion. Vehicle operating strategy and reformer HC emissions.

Sensitivity Chart

Target Forecast: Total NMOG Emissions

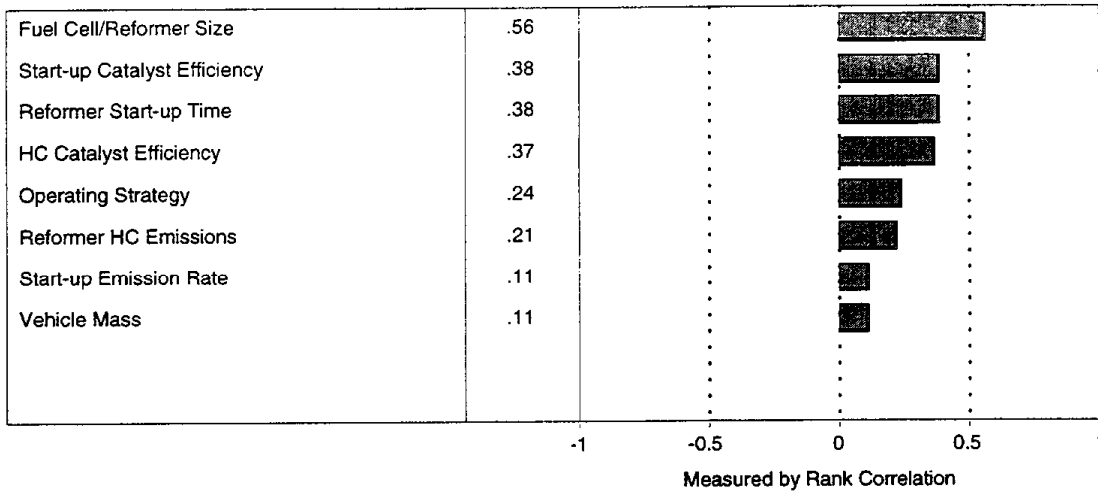


Figure 6-4. Sensitivity of POX/PEMFC vehicle NMOG exhaust emission projections; reformer size affects start-up emissions for 20, 40, and 60 kW fuel cells

The start up emission rate ranks low on the emission sensitivity chart since the range in start up emissions is assumed to be between 150 and 250 g/GJ which is consistent with emission data. A greater uncertainty is estimated for the efficiency of the catalytic burner during start up, therefore the potential impact on emissions is greater. Vehicle mass affects the total energy demand for the fuel cell system over the driving cycle. This energy demand affects the fuel demand during normal operation after start up where emissions are low.

Several assumptions are key to producing low emissions from fuel cell power systems. Burning supplemental fuel to power the expander during normal operation would increase emissions since the combustor will be designed to operate on dilute hydrogen from the fuel cell anode gas. However, such an operating mode is not expected. Since the PEMFC has such stringent requirements levels of CO and hydrocarbon contaminants entering the combustor during normal operation must be very low. Hydrocarbon control during start up is very important for maintaining low emissions. This operating constraints also applies to conventional gasoline fueled vehicles.

6.1.1.4 POX/PEMFC Vent and Fugitive Emissions

Another source of vehicle emissions is condenser tank discharges, coolant, and engine oil. Fuel cell powered vehicles will not have any engine oil which is a significant source from drips as well as oil change related discharges. Condenser tanks may release condensate periodically. The

water that is collected from the fuel cell system will be filtered prior to reuse in the vehicle system. The filter could collect traces of soot. Most of the condensed water will be recycled into the POX unit, and the amount of condensate discharge represents a small fraction of the total water used in the system. An analysis of the water from the HBT emission testing indicated the hydrocarbons were below the detection limit of 10 ppm. These data suggest that emissions from vehicle condensate are not an issue. Fuel cell powered vehicles will have radiators that are similar to those on gasoline powered vehicles. A mixture of water vapor and coolant would be released during venting. Such events are relatively infrequent and are not a significant issue with gasoline powered vehicles. Similarly, radiator venting would be inconsequential with fuel cell powered vehicles.

6.1.2 Methanol Steam Reformer and ATR with PEMFC Exhaust Emissions

A methanol steam reformer with a PEMFC requires warm up of the reformer for system start up and continuing operation of the reformer burner during vehicle operation to provide heat for the reforming reaction. These sources of emission are discussed separately. Vent and fugitive emissions are also discussed below.

6.1.2.1 Methanol ATR and SR/PEMFC Start-up Exhaust Emissions

Start up requirements for a low temperature methanol steam reformer/PEMFC consist of warm up of the burner, reformer catalyst, PROX, and fuel cell. During start-up, the vehicle operates on battery power. The catalytic burner operates on pure methanol until the reformer has reached 260°C where methanol dissociates into CO and hydrogen. The burner catalyst warms up through direct contact with the combustion products, and the reformer catalyst is heated through conduction from the burner. Data from the FZJ indicate a start up time of 120 sec. Because the reformer does not produce hydrogen gas until it is at operating temperature, preheating components such as the PROX unit and PEMFC, if required, can be accomplished with steam that is generated from the burner exhaust. Emission estimates for a methanol steam reformer were based on data from the FZJ. Additional hydrocarbon and CO control of 80 percent was estimated assuming that an optimized catalyst or burner modifications would be implemented. Table 6-5 shows exhaust emission factors that were estimated for the methanol ATR and steam reformer systems.

Table 6-5. Estimated start-up emission factors for methanol ATR and steam reformer burners

Fuel	Emissions (g/GJ)			NMOG/CO
	NO _x	NMOG	CO	Reduction
Methanol ATR	10	140	320	80%
Methanol SR	10	180	320	80%

6.1.2.2 Methanol ATR and steam reformer/PEMFC operating exhaust emissions

A catalytic combustor provides heat energy for the external reformer of both an ATR system and a steam reformer. The ATR allows more rapid start up since methanol can be burned directly in the catalyst material. As in the case of the POX system, all of the product gases from the ATR pass through the PEMFC and therefore must contain low levels of CO and hydrogen. Excess anode gas from the fuel cell can be burned to provide thermal energy for the ATR. Both the ATR and steam reformer can be operated without supplemental methanol in the burner. The ratio of methanol to anode gas in the reformer feed is a design detail that can vary from system to system. Emissions from the reformer operating with 10 percent methanol feed were estimated from the FZJ data. Emission assumptions for the methanol reformer systems are shown in Table 6-6. Table 6-7 shows the vehicle emissions over the FUDS cycle on a g/mi basis. Emissions were estimated for the fuel cell dominant hybrid configuration with different fuel processor systems. The SR/PROX system operates the reformer on waste anode gas only and does not use supplemental methanol fuel. This is the same approach as used by the NECAR 3. The SR/PROX burner trim system uses supplemental methanol during increases in reformer load, consequently, NMOG increases during vehicle operation. THE ATR system combines steam reforming with partial oxidation of methanol at the low temperatures required for the methanol steam reformer. The battery dominant hybrid configuration with a 20 kW fuel cell results in the lowest emissions. Start up emissions are lower since the reformer has a lower mass for the smaller fuel cell. CO₂ emissions for the battery dominant hybrid are also lower since fuel consumption is reduced. Emissions measurements from NECAR 3 were reported by dbb (Cooper). Testing was performed over the FTP and did not include cold start. NO_x and CO were both reported as 0.00 g/mi. Total hydrocarbons, excluding methanol and formaldehyde but including methane, were 0.005 g/mi. Cold start emissions would presumably result in total emissions over the 0.01 g/mi SULEV limit. These results are the first data for a fuel cell powered passenger car with an on-board reformer. Changes in water management and condensers may also reduce emissions further in future vehicles.

Methanol SR/PEMFC Vent and Fugitive Emissions

Vent and fugitive emissions for methanol SR and ATR systems will be similar to those for POX systems. Methanol fuel can be trapped in the reformer exit gas. This methanol water mixture will be recycled into the reformer and will not result in a vehicle emission.

Table 6-6. Estimated operating exhaust emissions for methanol ATR and steam reformer burners

Fuel	Emissions (g/GJ)			NMOG/CO Reduction
	NO _x	NMOG	CO	
Methanol ATR	10	2	28	85%
Methanol SR H ₂ /CH ₃ OH =0.9	10	10	28	85%
Methanol SR 0 methanol feed	10	2	28	85%

Table 6-7. Simulated exhaust emissions from alternative-fueled POX/PEMFC passenger cars (FUDS cycle)^a

Fuel Cell/Engine Type	Methanol Fuel Cell Dominant Hybrid	Methanol Battery Dominant Hybrid PEMFC			
Fuel Processor	SR PROX burner trim	ATR PROX	SR/membrane	SR PROX	SR PROX
Fuel Cell Power (kW)	60	60	60	60	20
<u>Start-up Emissions (g/mi)</u>					
NO _x	0.0009	0.0008	0.0008	0.0008	0.0003
NMOG	0.0032	0.0011	0.0029	0.0029	0.0011
CO	0.0056	0.0051	0.0051	0.0051	0.0019
CO ₂	5.5	5.5	5.5	5.5	2.1
CH ₄	0.0018	0.0016	0.0016	0.0016	0.0006
<u>Operating Emissions (g/mi)</u>					
NO _x	0.0017	0.0019	0.0017	0.0017	0.0017
NMOG	0.0037	0.0010	0.0006	0.0006	0.0006
CO	0.011	0.011	0.021	0.011	0.010
CO ₂	172	190	170	172	165
CH ₄	0.0088	0.0080	0.0080	0.0080	0.0030
<u>Total Emissions (g/mi)^b</u>					
NO _x	0.0026	0.0027	0.0025	0.0025	0.0020
NMOG	0.0069	0.0021	0.0034	0.0034	0.0016
CO	0.016	0.017	0.026	0.016	0.012
CO ₂	178	195	175	178	167
CH ₄	0.0096	0.0096	0.0106	0.0096	0.0036

^aComponent and vehicle mass given in Table 4-8.

^bEmission estimates depend upon many factors. Uncertainty is approximately ±50 percent.

6.1.3 DMFC Emissions

6.1.3.1 DMFC Exhaust Emissions

DMFCs produce no combustion emissions. Methanol is catalyzed on the anode to produce CO₂. Fuel that passes through the membrane is oxidized on the cathode. A mixture of water, methanol, and CO₂ are circulated to the vehicle water/methanol tank and CO₂ is separated and vented. Cathode air is also vented and CO₂ related to methanol crossover is released with the cathode air. The cathode air contains only water, oxygen depleted air, and water vapor.

6.1.3.2 DMFC Vent and Fugitive Emissions

The vent from the water/methanol tank is the principal source of emissions from the DMFC. These emissions consist of CO₂ from the anode reaction and traces of methanol vapor. The vapor pressure of methanol/water mixtures is very low, so relatively little methanol will be in the vapor phase. A vapor control system for a DMFC might consist of the following:

- CO₂ separator which removes gaseous CO₂ with traces of methanol vapor from methanol water mixture
- Water trap to collect remaining methanol vapor; the water can provide make-up water for vehicle use
- Carbon absorption canister to remove traces of methanol, if required; the carbon absorption canister can be purged with fresh cathode air

Emission estimates for the DMFC vehicle are shown in Table 6-8. Other than almost undetectable traces of methanol, the DMFC produces no criteria pollutants.

6.1.4 Effect of Off-Cycle Operation, Deterioration, and Failure Modes on Emissions

Estimates of emissions are based on an analysis of fuel processor performance and related emissions during start-up and normal operation. Reformer operation was based on theoretical judgements combined with limited test data. These emissions are affected by factors such as vehicle operating cycle, transient load changes, deterioration with age, and system failures.

High NO_x emissions from fuel cell powered vehicles are unlikely, even during failure modes or off-cycle operation. NO_x emissions during normal operation will be very low since the fuel source for catalytic burners in fuel cell systems is waste anode gas. Even a failure in the catalytic burner would not result in an increase in NO_x emissions since operating temperatures are assured to be low; the composition of anode and cathode gas has a low heating value and is diluted with nitrogen and CO₂. If the catalytic burner fails, the air compressor will lose over 30 percent of its power and air supply to the fuel cell and reformer will drop with a large drop in power.

Fuel cell load requirements depend upon the vehicle driving cycle or driver behavior and the type of hybrid configuration. Transient operation and load changes have the greatest effect on fuel cell systems with no battery or a small battery. The fuel cell only and fuel cell dominant hybrid configurations, described in Section 4, will experience the greatest variations in reformer output as the fuel cell must match the road load power requirement with little or no supplemental battery power. The battery dominant hybrid and load sharing hybrid will require smaller changes in fuel cell and reformer output to match driving requirements. The battery provides power to meet rapid transient load changes, so the reformer does not need to respond as quickly to load changes.

Table 6-8. Emissions for DMFC passenger cars^a

Fuel Cell/Engine Type	Methanol DMFC Fuel Cell Only	Methanol DMFC Battery Dominant Hybrid
Fuel Processor		
Fuel Cell Power (kW)	72.9	20
<u>Start-up Emissions (g/mi)</u>		
NO _x	0.0000	0.0000
NMOG	0.0000	0.0000
CO	0.0000	0.0000
CO ₂	0.0	0.0
CH ₄	0.0000	0.0000
<u>Operating Emissions (g/mi)</u>		
NO _x	0.000	0.000
NMOG	0.0001	0.0001
CO	0.0000	0.0000
CO ₂	183	180
CH ₄	0.0000	0.0000
<u>Total Emissions (g/mi)^b</u>		
NO _x	0.0000	0.0000
NMOG	0.0001	0.0001
CO	0.0000	0.0000
CO ₂	183	180
CH ₄	0.0000	0.0000

^aComponent and vehicle mass given in Table 4-8.

^bEmission estimates depend upon many factors. Uncertainty is approximately ±50 percent.

During a change in load, the flow rates of air, fuel, and steam into the reformer must match the load requirements. A change in heat transfer to the reformer reactants must also occur. As process conditions change in the reformer, temperature distributions within the reactor can vary and potentially lead to incomplete reactions. This would result in increased HC and CO in the reformer product gas. Data on the effect of load changes and transient operation from reformers is limited.

PEMFC's require extremely low CO in the anode feed mixture. A failure in the CO clean up portion of the fuel processor would greatly reduce power and efficiency to the extent that the

vehicle would not operate well. Consequently, CO cannot increase during transient operation or as a result of catalyst failures in a driveable vehicle. Systems for removing CO during load changes have not been completely developed at this time. If the requirement to clean up CO during all types of load changes proves to be too technically challenging, then hybrid operation is an option for fuel cell vehicles. The key emission issue with fuel cell vehicles is NMOG. The catalytic burner is expected to reduce NMOG emissions.

6.1.4.1 Methanol Steam Reformer Systems

In a steam reformer system, the reformer burner provides heat energy for the reforming reaction. Sources of fuel are excess hydrogen from the fuel cell anode, and possibly, supplemental methanol, which are both combusted in the catalytic reformer burner.

Data from a laboratory reformer shows a pronounced effect of load change on emissions. As indicated in Section 5.4, the FZJ experimental methanol steam reformer experienced a four fold increase in HC and a three fold increase in CO emissions as the load was increased from 20 to 60 kW. As the load increased, a time delay of 100 seconds occurred in conjunction with an increase in the reformer temperature. Decreasing the load resulted in a reduction in emissions as excess heat energy in the reformer was available for converting a smaller amount of reformer feed gas. The FZJ steam reformer was operated on a mixture of simulated anode gas and methanol. The design goal for commercial methanol SR systems is to operate the reformer only on anode waste gas and not use supplemental methanol as fuel. Consequently, the effect of load changes on reformer emissions will be diminished as the source of HCs and CO entering the reformer is eliminated. NECAR 3 operates without supplemental methanol feed to the reformer burner. An important uncertainty for methanol SR systems is whether supplemental fuel can be eliminated from all operating conditions.

Changing load can also increase the amount of unreacted methanol in the reformer product gas that passes through the fuel cell, water condenser, and reformer burner. It is likely that too high a methanol concentration in the reformat will adversely affect fuel cell operation. Consequently, operating modes that lead to inefficient reformer operation and high levels of methanol in the reformer product gas will need to be avoided, in order to maintain good vehicle driveability. Excess methanol from the fuel cell will likely be trapped in a water condenser after the fuel cell, before it is burned in the reformer burner. This water is recycled back to the reformer. Water is trapped both after the reformer and after the fuel cell. Excess water may be recovered in the fuel cell system. Under some operating conditions, excess water may need to be discarded and the water would contain traces of methanol. However, water recovery in fuel cell systems is very challenging, so it is likely that approaches to managing water recovery and preventing releases will be developed.

6.1.4.2 POX System

Data on the effect of load changes on emissions is also limited for POX systems. THC in the exit gas composition from the HBT stationary reformer was monitored during load changes (Section 5.3). As loads increased, THC in the reformer product gas increased by a factor of two,

from 30 to 60 ppm. During a decrease in reformer load, THC in the product gas did not increase. In vehicle systems, the effect of load changes has not yet been quantified.

Since the POX system is exothermic (unlike the steam reforming reaction), there is no opportunity for burning supplemental fuel in the reformer to provide additional heat energy for load changes. Other approaches may be used to provide additional heat energy to quickly respond to transients. Varying reformer stoichiometry is a possible approach for increasing reforming temperatures. The ability to adjust stoichiometry and steam flow to affect temperature as well as gas flow would allow flexibility in controlling POX systems; however, POX developers have yet to be tested the effect of operating strategies on reformer product gas compositions or emissions.

6.1.4.3 Effect of Load Changes on Emissions

The effects of transient load changes on emissions were evaluated for the POX/PEMFC and methanol SR/PEMFC emission estimates for passenger cars. NMOG emissions vary during changing operating conditions. The effect of operating transients on HC emissions is not well known. For example, vehicles could be driven over conditions with more stops and starts and harder accelerations than the FUDS cycle. Operating conditions for a vehicle system could result in NMOG emissions from the reformer and fuel cell system that need to be controlled with a supplemental catalyst in the anode gas burner. Given the need to maintain a product gas to the PEMFC that contains low CO, as well as low NMOG, the effect of off cycle driving on emissions must be limited.

The effect of load changes was incorporated into the CYCLEMASTER emissions model; however, these estimates have not been validated against vehicle fuel processor operation. The key assumptions for the emissions estimates in Section 6.3 are the NMOG emissions rate and the emissions reduction factor from the catalytic anode gas burner. Figure 6-5 shows the estimated effect of an assumed 50 percent increase in the emission rate during transients (high transient) for a gasoline POX/PEMFC system.

Higher emissions levels, due to system deterioration, were also estimated for the CNG and gasoline POX systems as shown in Figure 6-5. CNG operation results in low NMOG, since the fuel consists primarily of methane.

Supplemental fuel could be burned in the catalytic burner or compressor/expander of either a POX/PEMFC or SR/PEMFC system, in order to make up for a shortfall in energy to power the compressor during a change in load. However, such designs are not contemplated at this time. Electric motor assist would provide supplemental compressor power. Supplemental fuel could also be burned to provide additional energy for a low temperature steam reformer system. Newer designs do not make use of this burner trim; however, it could be a feature that is used for extreme operating conditions. A more desirable strategy, from an emissions perspective, would be to draw less power from the fuel cell and use waste anode gas to provide additional fuel for the reformer. The actual opportunities for using burner trim depend upon the design details and operating strategy for a SR/PEMFC system. Figure 6-6 shows the effect of assumptions on load change, burner trim operation, start-up emissions, and burning supplemental fuel in the burner

(with burner trim) for a methanol SR/PEMFC system. NMOG emissions remain relatively low for increased transient effects. It is assumed that methanol will be absorbed in water in the condenser after the fuel cell so NMOG emissions are lower than those from other fuels.

Constraints on fuel cell performance, in the presence of some hydrocarbons or methanol, may require operating strategies that do not result in the rapid load changes that could increase emissions. However, the effect of hydrocarbons on fuel cell performance is not well documented and high levels of some hydrocarbon species may not affect fuel cell operation.

6.1.4.4 Effect of Deterioration and System Failures

A more significant risk for increasing emissions is a failure in the catalytic burner or a diminished efficiency in reducing NMOG due to deterioration. The catalytic burner converts unreacted hydrogen and air to water vapor which provides additional energy for the compressor expander. It is likely that the catalyst will also play a role in reducing NMOG emissions. A partial failure of the catalyst could reduce its effectiveness in reducing NMOG, even though it was still burning hydrogen, and expander performance was not notably affected. The effectiveness of the catalyst in controlling start up NMOG could also deteriorate.

The impact of a reduced effectiveness in the burner catalyst for controlling NMOG is illustrated in Figures 6-5 and 6-6. The high emissions assumptions include increased effect of transients, increased start-up energy requirements, and a reduction in the effectiveness of the catalytic burner. A reduction in the effectiveness of the catalyst from 80 to 20 percent during start-up, and from 85 to 20 percent during normal operation, was assumed. A 50 percent increase in emissions during transit operation was assumed. The result for the high emissions assumptions is an increase in total emissions from 0.004 to 0.025 g/mi for a gasoline POX/PEMFC system. Since the NMOG fraction of natural gas is much lower, the effect of reduced catalyst performance is not expected to increase NMOG emissions above 0.01 g/mi as shown in Figure 6-5. For a methanol SR/PEMFC system, reducing the effectiveness of the catalytic burner also increases NMOG emission to 0.025 g/mi. For the "high transient" cases, a 50 percent increase in transient NMOG was assumed while start-up and catalyst assumptions were not changed.

Data on the durability of catalytic burners is unknown at this time. Factors that can affect burner durability include contaminants in the fuel, thermal shock, and extreme temperature conditions. Such operating conditions could occur in fuel cell vehicles. Contaminants such as sulfur are assumed to be removed in the clean up system on a POX vehicle. However, during start up, the effectiveness of sulfur removal systems may be limited, so some contaminants could affect the catalytic burner over time. Another operating condition that could affect catalytic burners is the transition from start up to reforming. During the initial portion of start up for POX systems, air and fuel may be burned at a relatively lean stoichiometry to generate heat. After start-up, the reformer must operate at its design point and produce a mixture of hydrogen and other gases. Initially, the CO content of the reformer product gas may be too high, so the gas may need to be burned in the catalytic burner rather than fed to the fuel cell. The amount of heat energy released would be much higher than during normal fuel cell operation. High levels of heat release in the catalytic burner could affect its performance over time.

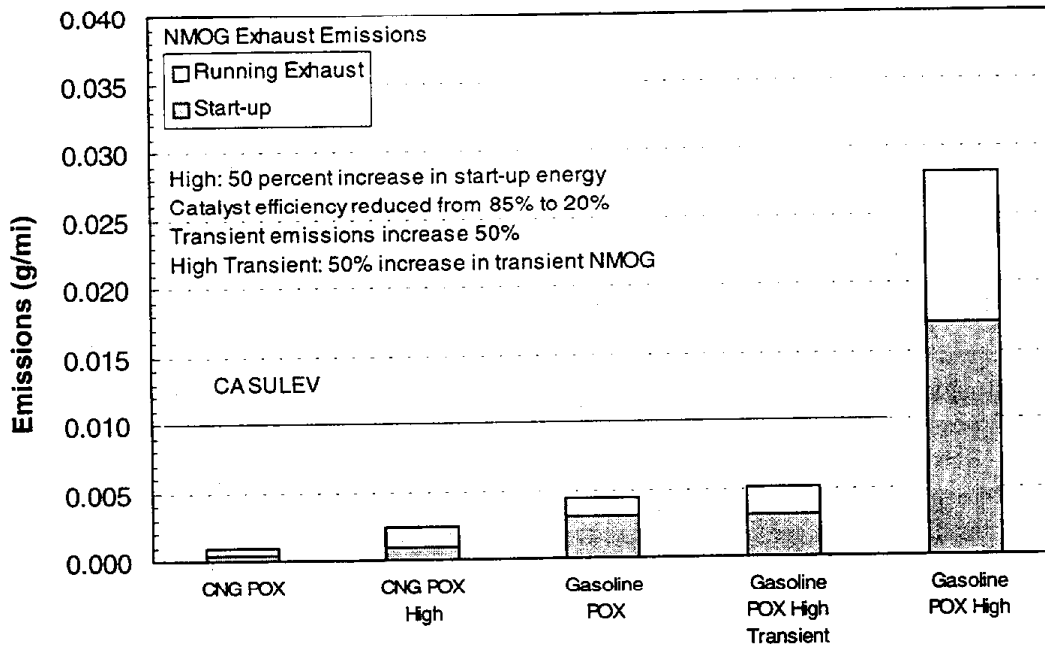


Figure 6-5. Effect of assumptions on emissions from POX/PEMFC vehicles

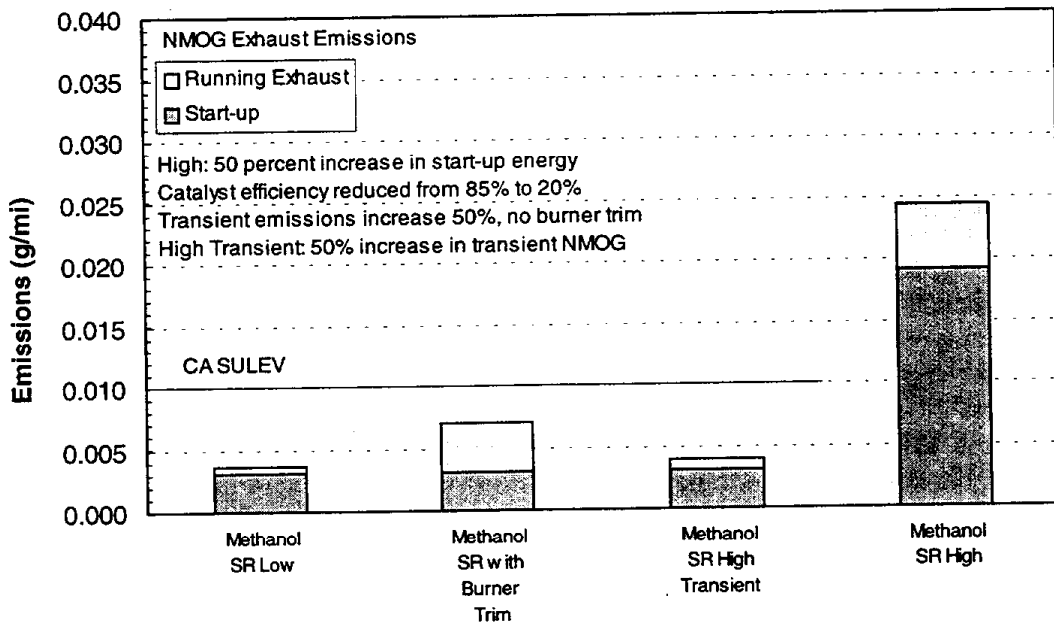


Figure 6-6. Effect of assumptions on emissions from methanol SR/PEMFC vehicles

POX reactors are less susceptible to fuel quality issues and temperature excursions since there is no catalyst in the reforming section. An ATR and methanol SR system must maintain a more stable operating temperature. The durability of such systems has not been determined at this time. Presumably, a catastrophic failure in the reformer would prevent vehicle operation and therefore, would not result in increased emissions.

Figures 6-5 and 6-6 provide estimates for potential increases in emissions from fuel cell vehicles. The effect of extended operation and transients on emissions is not known at this time. However, the sensitivity of fuel cells to contaminants will likely limit the potential for increased emissions from fuel cell powered vehicles.

6.2 LIGHT-DUTY VEHICLE FUEL CYCLE EMISSIONS

The total life cycle emissions from fuel production and refueling impact the emission inventories for vehicles. Fuel cell powered vehicles may need to meet the emission regulations which require zero evaporative emissions. While this source of hydrocarbons can be eliminated with closed fueling systems, other portions of the fuel production chain can still contribute to emissions. An ARB study on fuel-cycle emissions identified the emissions from fuel production, distribution, and vehicle refueling for a variety of fuels (Unnasch). The emissions are stated on a gram per volume of fuel basis and can be applied to the fuel cell vehicle cases in this study. Refueling and evaporative emissions can be significant sources of hydrocarbons; however, such emissions are likely to be eliminated by ARB standards for vehicles to qualify for the lowest emission categories.

Most of the emissions associated with fuel production are only weakly associated with throughput. For example, oil refining results in HC emissions; however, reducing the amount of gasoline consumed by vehicles will not affect refinery emissions in the near term in the South Coast Air Basin or California, as the refineries will continue to run at capacity. This argument corresponds to the discussion of marginal emissions in the ARB fuel cycle study.

Emissions that depend more clearly on fuel throughput include tanker truck emissions and refueling emissions. This study includes the following sources in the comparison of fuel cycle emissions:

- Tank truck emissions
- Electric power for CNG compression
- Refueling spillage and CNG disconnect losses
- Fuel cycle CO₂

Other emissions are subject to interpretation and can arguably be excluded from a marginal fuel cycle analysis. The marginal fuel cycle analysis appeared to be the key comparison when the status of ZEVs was considered in California. Table 6-9 shows the power plant emissions related to battery powered ZEVs as presented in the ARB study on fuel-cycle emissions. These values are shown for reference and are not compared directly to the emissions from fuel cell powered

vehicles because the ZEV emissions encompass a broad range of assumptions on power generation mix and marginal emission assumptions. Further comparisons are made to the Super ULEV standard described in Section 1.

Table 6-9. Power plant emissions from battery powered electric vehicles

Source	NO _x	NMOG	CO	CO ₂	CH ₄
80/20 charging year 2010 g/kWh ^a	0.048	0.008	0.043	258	0.007
EV emissions (g/mi)	0.012	0.002	0.01	65	0.002

^a Emissions were based on CEC modeling of power plant dispatching. Emissions are shown on a g in SCAB per total kWh consumed as reported in Unnasch (1996). EV energy consumption assumed in the CEC model was 0.25 kWh/mi. Higher energy consumption values have also been observed.

Assuming that evaporative emissions are eliminated from fuel cell vehicles, one may conclude that spillage will be the most significant emission source. Table 6-10 presents spillage emission estimates for conventional IC engine vehicles and fuel cell vehicles. The analysis is based on a constant spill volume and a refueling volume that corresponds to the fuel economy and fuel heating value. Methanol, CNG, ethanol, and LPG vehicles will be fueled at about the same frequency as conventional gasoline vehicles, while gasoline and diesel vehicles will require about one half of the fuel for the same range and should be filled less frequently because it is unlikely that the vehicle fuel tank will be reduced significantly in size. Today's diesel fueled cars do not have significantly smaller fuel tanks, and the driver is able to take advantage of greater range. The combination of fuel spillage and refueling volume determines the spillage on a g/gal basis. All of the spilled fuel evaporates to produce air emissions. The spillage and projected refueling emissions are shown in Figure 6-7 on a g/volume basis. The refueling vapor loss portion of the emissions should be eliminated with ARB regulations. Emissions from diesel vapor losses are so low that they are currently not required to be controlled. Methanol and ethanol vapor emissions are also very low.

Table 6-11 shows the NO_x emissions from transporting fuels by tanker truck. The fuel transport emissions represent less than 10 percent of the total emissions.

Table 6-10. Light-duty vehicle NMOG spillage emissions^a

Fuel	Fill Volume (L)	Spillage/fill (THC, mL)	Spillage (g/L)	Vapor Losses (g/L)	Spillage (g/g)	Vapor (g/g)
Gasoline ICE	35	2.4	0.049	0.0926	0.0069%	0.0129%
Gasoline FC	25	2.4	0.069	0.0926	0.0096%	0.0129%
Diesel FC	25	2.4	0.083	0.0042	0.0096%	0.0005%
LPG FC	35	2.0	0.029	3.8710	0.0057%	0.7742%
Methanol FC	35	2.4	0.054	0.0088	0.0069%	0.0011%
Ethanol FC	30	2.4	0.063	0.0057	0.0080%	0.0007%
CNG FC	60	3.0	0.007	0.0000	0.0050%	0.0000%

^aFill volume was estimated from fuel tank size. Spillage and vapor loss from Unnasch, 1996.

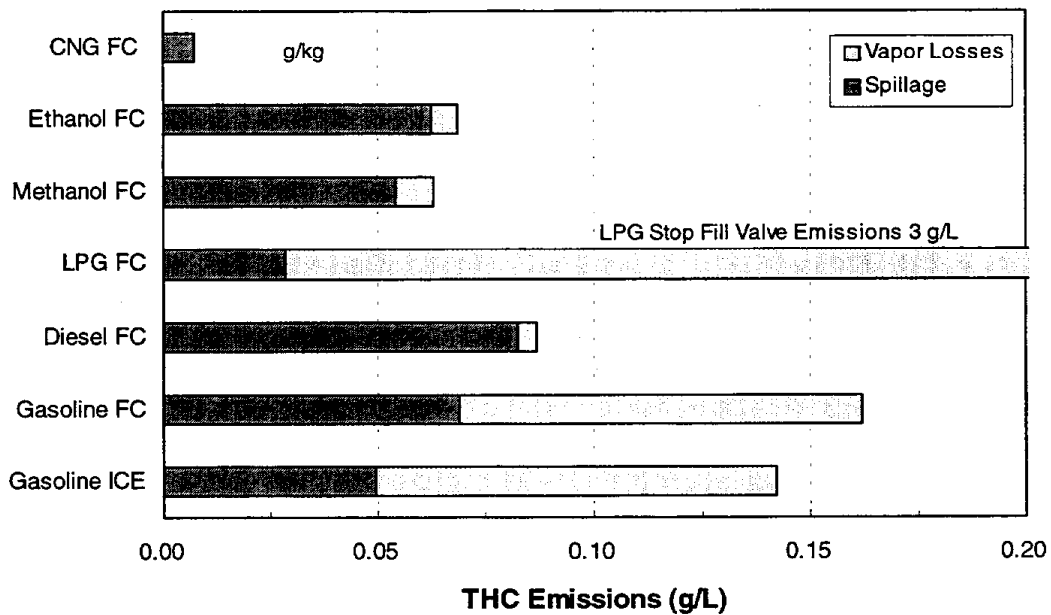


Figure 6-7. Light-duty vehicle refueling emissions (g/gal). Vapor losses would need to be eliminated to qualify for SULEV certification.

Table 6-11. Fuel transportation NO_x emissions

Fuel	Truckload (gal)	Distance (mi)	Transport NO _x	
			(g/L)	(g/mi)
Gasoline ICE	8500	50	0.0143	0.00235
Gasoline POX	8500	50	0.0143	0.00143
Diesel POX	7080	50	0.0171	0.00169
LPG POX	10000	50	0.0121	0.00149
Methanol SR	7800	50	0.0156	0.00267
DMFC	7800	50	0.0156	0.00301
Ethanol POX	7800	50	0.0156	0.00236
CNG POX	—	50	0.0009	0.00024

^a Truck emissions estimated from year 2010 truck with 9 g/mi NO_x emissions which corresponds to 2 g/bhp-h.

6.3 TOTAL LIGHT-DUTY VEHICLE EMISSIONS

Figure 6-8 shows the NMOG emissions for the leading light-duty vehicle systems. The emissions are well below those from ULEVs and within the range of the proposed SULEV standard. The dominant source of emissions is refueling spillage. Refueling spillage may be controlled for SULEVs, but these requirements have not been determined at this time. The technologies that are below the SULEV standard including refueling emissions are the CNG POX, LPG POX, and DMFC. The DMFC will not be commercially available for several years. The LPG technology would need to control refueling venting emissions. These emissions are already controlled with automatic stop fill devices in the Netherlands. The sum of fuel spillage and exhaust are greater than 0.01 g/mi for all the liquid fuel options.

Figure 6-9 shows the NO_x emissions from light duty vehicles. The emissions from the vehicle are well below SULEV standards. Tank truck exhaust used to deliver the fuel and pipeline compressor emissions are small compared to vehicle exhaust.

Global CO₂ emissions are shown in Figure 6-10. The data include direct emissions from the vehicle and from the fueling cycle emissions. Vehicle CO₂ emissions are determined from the vehicle fuel economy and the carbon content of the fuel. Direct emissions from ethanol fueled vehicles are zero since the carbon in the fuel was recently removed from the atmosphere. Fuel cycle CO₂ emissions include fossil fuel inputs for ethanol production. Higher estimates of fuel cycle CO₂ have also been published for ethanol fuel production.

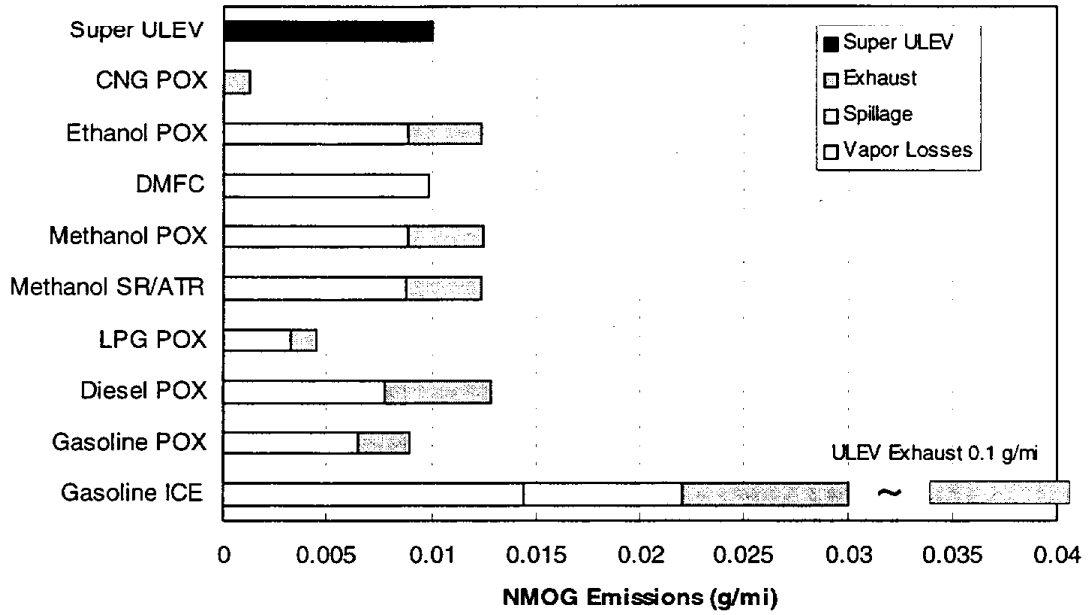


Figure 6-8. Light-duty vehicle NMOG emissions (g/mi)

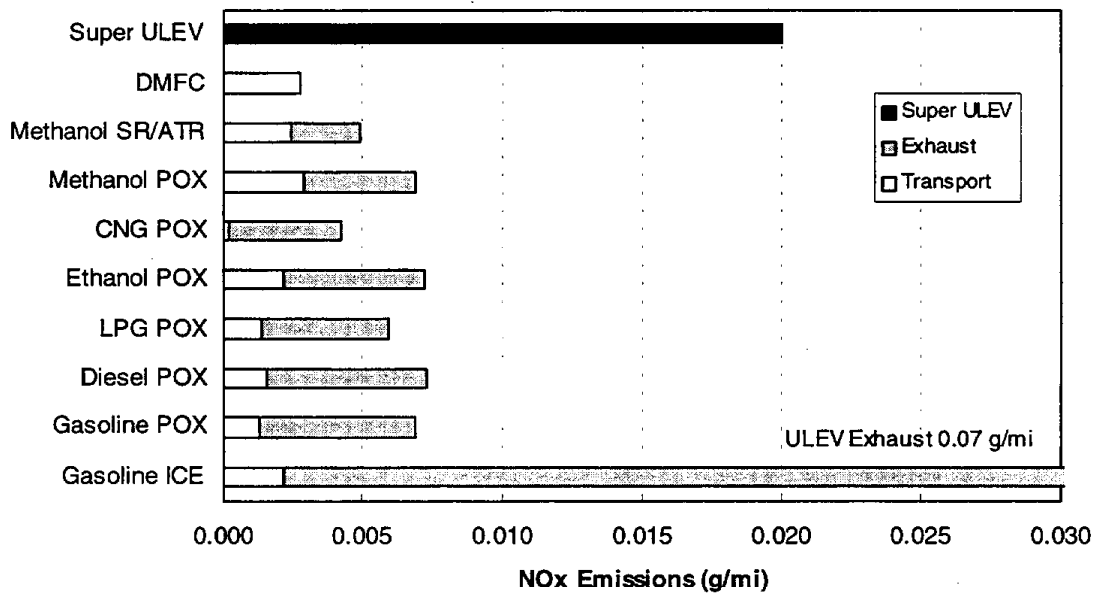


Figure 6-9. Light-duty vehicle NO_x emissions (g/mi)

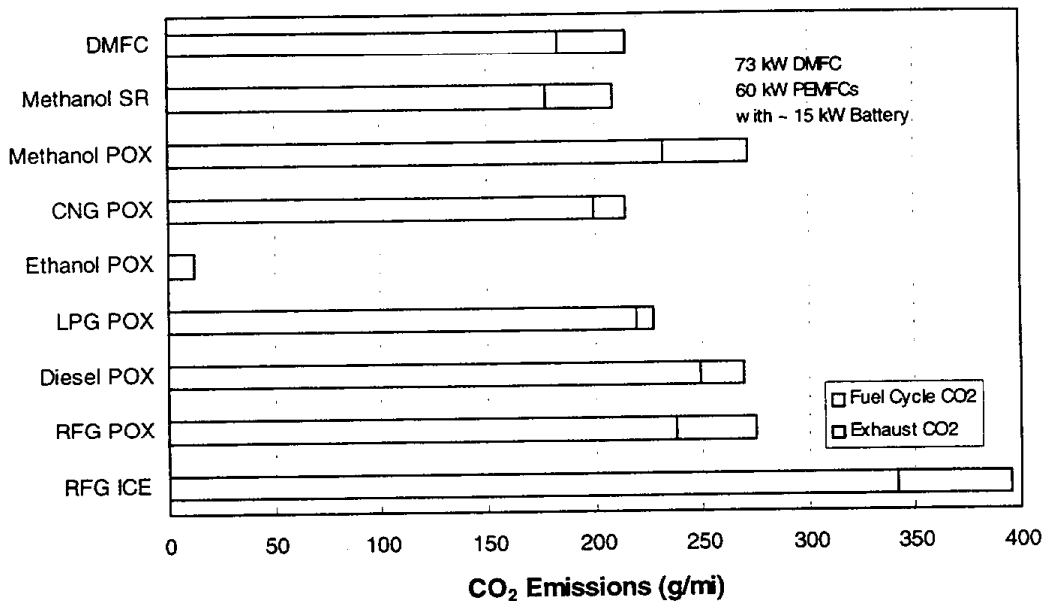


Figure 6-10. Light-duty vehicle CO₂ emissions (g/mi)

6.4 HEAVY-DUTY VEHICLE EMISSIONS

Heavy-duty vehicle case studies include PEMFC, PAFC, and SOFC technologies with low temperature methanol steam reformers, high temperature steam reformers, and a POX fuel processor. This comparison provides a broad overview of the effect of different reformer and fuel cell technologies in emissions.

6.4.1 Heavy-Duty Vehicle Exhaust Emissions

Table 6-12 shows the assumptions for start-up emissions. Catalytic NMOG and CO reduction was assumed for the steam reformer technologies. The extent of emission reduction was estimated to be lower than that for light-duty vehicles because heavy-duty vehicles are expected to operate over longer lifetimes with harder duty cycles. Furthermore, start-up emissions are not such a critical portion of heavy-duty vehicle operation, so emission control requirements would be lower.

Table 6-13 shows the operating emission assumptions for heavy-duty vehicles. The IFC PAFC operates with a high temperature steam reformer, so higher NO_x emission rates are assumed. Data from the IFC system indicates NO_x below the detection level. The estimated NO_x levels in Table 6-13 are consistent with detection limits for the test data presented in Section 5. Emission levels for the low temperature methanol SR and POX/PEMFC systems are estimated from the FZJ data as was the case for the light-duty vehicle analysis. NO_x emissions are higher for the SOFC with the high temperature turbine. PAFCs are less sensitive to CO emissions. Therefore, fuel processors for PAFCs will provide less CO clean up and CO emissions could be higher.

Data from the IFC PAFC system indicate CO levels that were about twice the levels required for the PEMFC system. The CO and NMOG assumptions combined with the reduction factor in Table 6-13 are consistent with the data for the IFC PAFC system.

Table 6-12. Estimated start-up exhaust emission factors for heavy-duty vehicles

Fuel/Technology	Emissions (g/GJ) ^a			NMOG/CO Reduction
	NO _x	NMOG	CO	
Methanol SR PEMFC	20	180	320	40%
Methanol SR PAFC	20	180	320	40%
CNG SR PEMFC	20	10	320	40%
Diesel POX PEMFC	40	180	250	40%
Diesel POX SOFC	40	180	320	0%

^aEmission factors estimated from Table 5-11 and strip chart recordings during start-up.

Table 6-13. Operating exhaust emission factors for heavy-duty vehicles

Fuel/Technology	Emissions (g/GJ) ^a			NMOG/CO Reduction
	NO _x	NMOG	CO ^b	
Methanol SR PEMFC	0.7	1.5	28	60%
Methanol SR PAFC	1.5	17	57	60%
CNG SR PAFC	1.5	0.5	57	60%
Diesel POX PEMFC	0.7	2	28	60%
Diesel POX SOFC	20	2	34	0%
Methanol/FC PAFC	ND	17	34	0%

^aEmissions per GJ of burner energy. NO_x and NMOG data based on Figure 5-3 and Table 5-9.

^bCorresponds to 20 ppm CO into the fuel cell.

The SOFC system operates at higher temperatures. The effluent from the SOFC is burned in a turbine. The emissions would be similar to those from a turbine; however, the hydrocarbons will be pre-combusted in the fuel processor. The turbine will be burning a mixture of CO and hydrogen. NO_x emissions are lower than those from a conventional natural gas turbine but higher than a low temperature catalytic burner.

Table 6-14 shows the estimated start up and operating emissions for fuel cell powered transit buses. The estimates for the PAFC systems are consistent with engine test data. The projected emissions are lower than those from the Phase III Georgetown bus since more advanced systems will operate without burner trim. The slightly lower CO and NMOG emissions for the PEMFC systems are due to the fuel cell gas clean up requirements. This analysis compares projections based on PAFC power plant tests with analytical estimates for other technologies. While the PEMFC and SOFC systems require further development, the constraints on the operation of the PEMFC assure that CO and NMOG emissions must be close to the indicated projections.

Table 6-14. Simulated heavy-duty bus exhaust emissions^a

Component	Methanol Fuel Cell Only	Methanol Hybrid	Methanol Hybrid	CNG Hybrid	Diesel Hybrid	Diesel Hybrid
Fuel Cell/Engine Type	PEMFC	PEMFC	PAFC	PAFC	PEMFC	SOFC
Fuel Processor	low T SR	Low T SR	High T SR	High T SR	POX	POX
Fuel Cell Power (kW)	205	100	100	100	100	100
<u>Start-up Emissions (g/mi)</u>						
NO _x	0.006	0.003	0.006	0.003	0.006	0.007
NMOG	0.029	0.014	0.029	0.001	0.015	0.029
CO	0.051	0.025	0.051	0.021	0.027	0.051
CO ₂	18.4	7.4	18.4	8.1	10.2	11.7
CH ₄	0.005	0.003	0.005	0.042	0.003	0.003
<u>Operating Emissions (g/mi)</u>						
NO _x	0.018	0.016	0.017	0.018	0.019	0.430
NMOG	0.015	0.000	0.017	0.018	0.019	0.037
CO	0.287	0.032	0.033	0.036	0.037	0.075
CO ₂	1770	1601	1646	1505	1965	1572
CH ₄	0.027	0.013	0.027	0.210	0.014	0.016
<u>Total Emissions (g/mi)^b</u>						
NO _x	0.0236	0.0189	0.0223	0.0212	0.0247	0.4364
NMOG	0.0443	0.0142	0.0455	0.0189	0.0338	0.0661
CO	0.3387	0.0568	0.0844	0.0572	0.0641	0.1257
CO ₂	1788	1610	1664	1513	1975	1583
CH ₄	0.0321	0.0154	0.0321	0.2520	0.0168	0.0192

^aComponent and vehicle mass given in Table 4-13.

^bEmission estimates depend upon many factors. Uncertainty is approximately ±50 percent.

6.4.2 Heavy-Duty Vehicle Fuel Cycle and Total Emissions

Emissions for fuel cell technologies were compared to typical emissions from heavy-duty transit buses. Fuel cycle emissions represent a lower fraction of the overall emissions. Table 6-15 shows the refueling assumptions for spillage emissions. Quick disconnect dry break fueling systems for buses result in lower spillage losses over the typical large volumes of fuel that are dispensed. The role of transport NO_x is similar to that for light-duty vehicles. Fuel cell powered buses achieve a hundred-fold reduction in NO_x compared to the advanced diesel buses.

Exhaust and fuel cycle CO₂ emissions are shown in Figures 6-11 through 6-13. The reduction in CO₂ emissions is proportional to the fuel economy of the vehicles.

Table 6-15. Heavy-duty bus NMOG refueling spillage (emissions per fill)

Fuel	Fill Volume (L)	Spillage/fill* (THC, mL)	Spillage (g/L)	Vapor Losses (g/L)	Spillage (g/g)	Vapor (g/g)
Diesel ICE	160	2	0.011	0.0042	0.0015%	0.0006%
Diesel FC	160	2	0.011	0.0042	0.0013%	0.0005%
Methanol FC	200	2	0.008	0.0018	0.0010%	0.0002%
CNG FC	600	4.0	0.001	0.0000	0.0007%	0.0000%

*Spillage estimated for dry-break fueling hardware for transit buses. Trapped volume which is vented was measured for a CNG fill fitting.

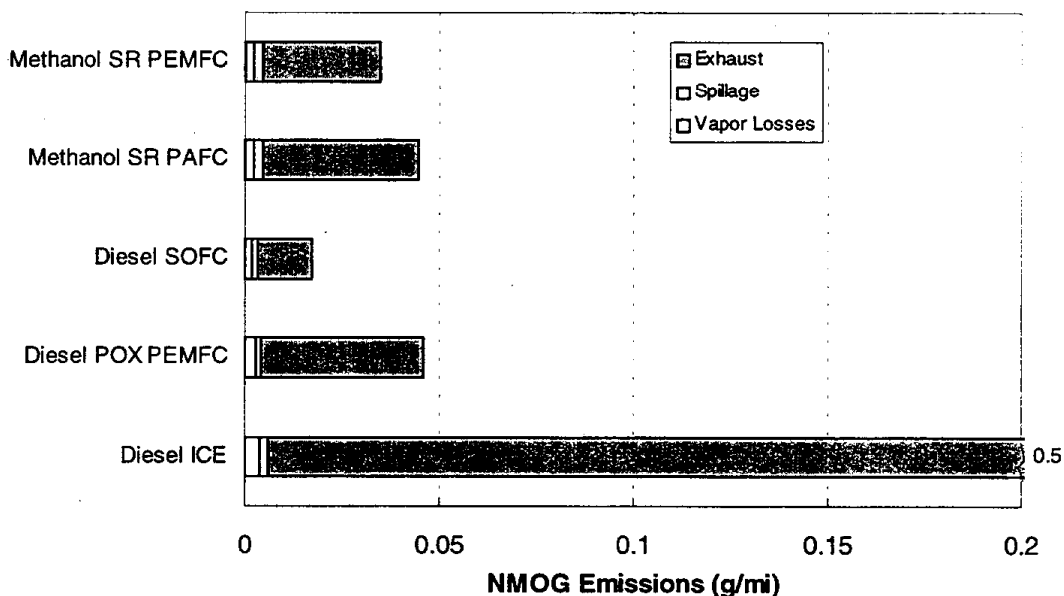


Figure 6-11. Heavy-duty bus NMOG emissions (g/mi)

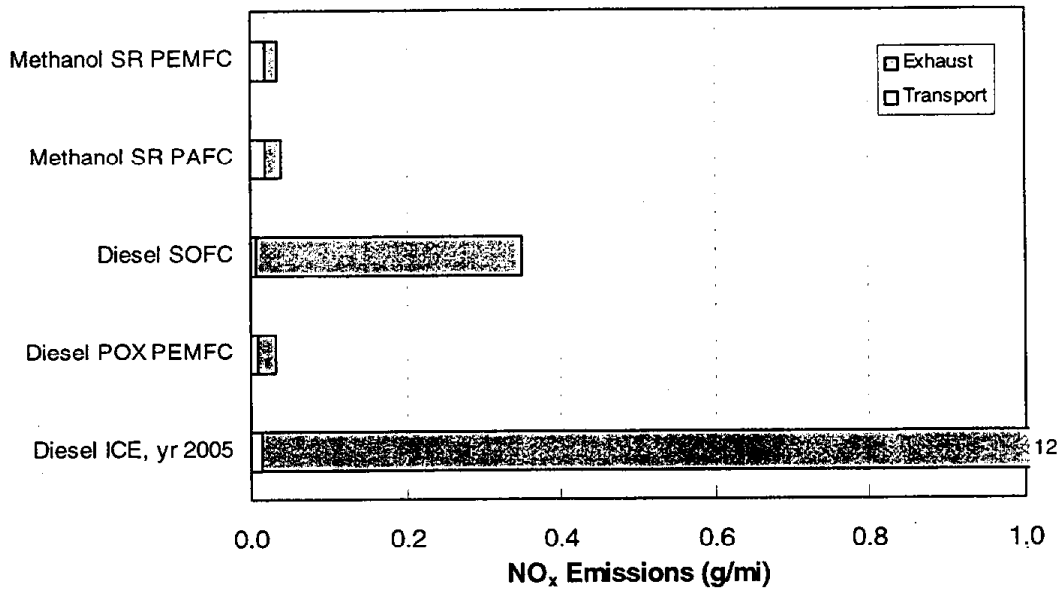


Figure 6-12. Heavy-duty bus NO_x emissions (g/mi)

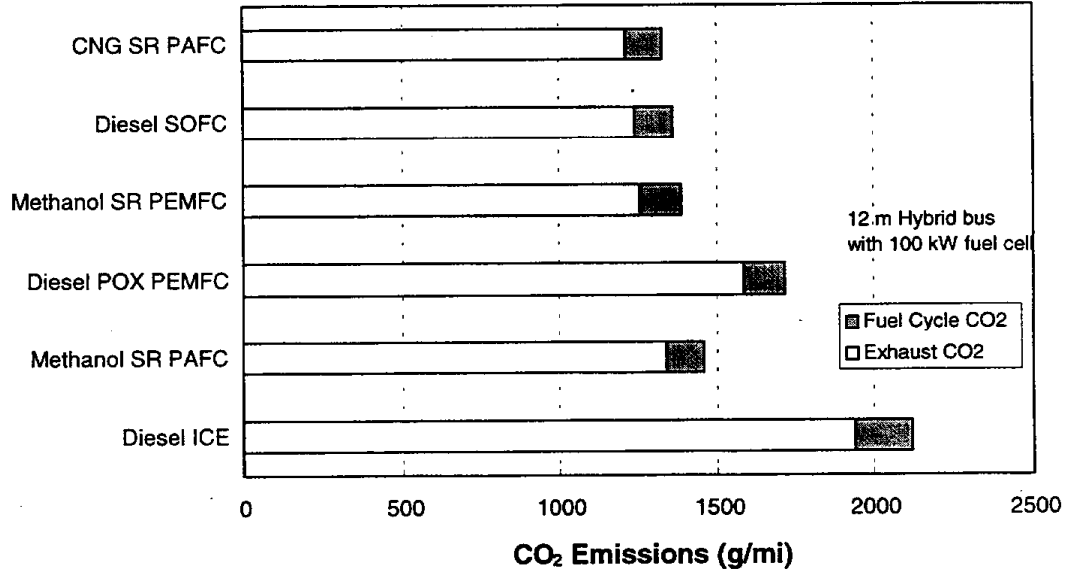


Figure 6-13. Heavy-duty bus CO₂ emissions (g/mi)

7. CONCLUSIONS

Fuel cell powered electric propulsion is a technically feasible alternative to the internal combustion (IC) engine for light and heavy-duty vehicle applications. Fuel cells operate on hydrogen which can be produced from a variety of fuels with on-board fuel processors, called reformers. The emissions from reformers are much lower than those from internal combustion engines.

In this study, an evaluation of fuel cell and reformer technologies resulted in the following conclusions:

- PEMFCs are most suitable for light duty vehicle operation because of their high efficiency and power density, low temperature operation, and status of development
- The fuel processor/reformer system must produce a hydrogen rich gas with low (20 ppm) levels of CO in order to allow efficient operation of PEMFCs. This requirement adds to the complexity of a fuel cell system.
- Both partial oxidation (POX) and methanol steam reformer systems are feasible for integrated operation with proton exchange membranes fuel cells (PEMFCs) in passenger cars and heavy-duty vehicles. Low and high temperature steam reformers have been demonstrated in prototype vehicles and a POX/PEMFC system has operated in the laboratory. PEMFCs are also suitable for heavy-duty vehicle operation.
- Direct methanol fuel cells (DMFCs) do not require reformers which makes them attractive for vehicle applications. However, DMFC development has not advanced to the scale suitable for passenger cars.
- Solid oxide fuel cells (SOFCs) would operate with high efficiency and do not require gas clean up systems. SOFC development has also not advanced to the scale required for vehicle applications.
- Phosphoric acid fuel cells (PAFCs) are too bulky for light-duty vehicle operation but are feasible for heavy-duty vehicles such as buses with a variety of reformer and fuel options
- Molten carbonate fuel cells (MCFCs) are too bulky and require too much gas processing for vehicle applications

The assessment of fuel cell reformer emissions included case studies for a range of light- and heavy-duty vehicle options. Light-duty vehicle case studies included POX and steam reformer systems for PEMFC as well as DMFCs. The POX/PEMFC system has multi-fuel capability the emissions from RFG, diesel, LPG, CNG, ethanol and methanol fueling were evaluated. Both the DMFCs, which operate on methanol without a reformer, and PEMFCs, which operates on methanol with low temperature steam reformers and autothermal reformers, were also considered.

The following conclusions were reached for the light-duty vehicle case studies:

- Emissions from PEMFC powered vehicles can be lower than ARBs proposed SULEV emission standard including both exhaust and fuel cycle emissions. NO_x emissions are inherently low, but control of NMOG emissions is required for some fuel processor systems.
- Refueling spillage and exhaust NMOG put some vehicles at or above the SULEV standard
- The feed gas purity requirements of the PEMFC assure very low emissions from the vehicle during normal operation. The PEMFC is sensitive to CO and HC concentrations. Therefore, the fuel processor must remove these contaminants. The remaining waste gas contains hydrogen with a mixture of water vapor, nitrogen, and CO_2 . The resulting emissions from burning the fuel cell anode gas are almost below detection levels. The primary source of NMOG and CO emissions is the burner during start-up.
- Natural gas POX/PEMFC vehicles can meet the standard with little or no emission control but will incur a weight penalty due to the high pressure gas cylinders.
- Refueling spillage contributes a significant portion of the NMOG emissions for methanol, ethanol, gasoline, diesel, and LPG systems
- NMOG emissions will likely need to be controlled from gasoline, diesel, ethanol, and LPG POX PEMFC systems and some methanol steam reformer systems
- A PEMFC system with a low temperature steam reformer or ATR will be the most efficient system that will be available in the near term with a potential efficiency improvement of 80 percent over a comparable ICE vehicle
- CO_2 emissions will be reduced by 25 to 40 percent over those from internal combustion engines
- Sulfur control in POX/PEMFC systems and the effect of trace methanol contaminants for low temperature steam reformer systems are among the many issues that need to be resolved before such fuel cell systems can become commercially viable.

Case studies for heavy-duty vehicles included PEMFCs with low temperature methanol steam reformers, PAFCs with high temperature reformers operating on methanol and natural gas, PEMFC with diesel POX, and an SOFC with a POX fuel processor. The following conclusions were reached for heavy-duty vehicles case studies:

- NO_x, CO, and NMOG emissions from fuel cell powered buses have been demonstrated to be far below those from diesel buses. NO_x levels are as low as one-hundredth of diesel levels while NMOG levels are about one tenth of diesel levels with modest exhaust gas clean-up.
- Fuel cell operation results in a 20 to 30 percent improvement in fuel economy which translates directly to a 20 to 30 percent reduction in CO₂ emissions.

8. REFERENCES

- Adam Opel AG, Energie für die Mobilität ven morgen, Brennstoffzellen-technologie, January 1999.
- A. D. Little, "Multi-fuel Reformers for Fuel Cells Used in Transportation. Multi-Fuel Reformers: Phase 1 -- Final Report," DOE Report DOE/CE/50343-2, May 1994.
- Appleby, A.J., *Fuel Cell Handbook*, Van Nostrand Reinhold, 1989.
- Amphlett, J., et al., "On Board Hydrogen Purification for Steam Reformation/PEM Fuel Cell Vehicle Power Plants," *International Journal of Hydrogen Energy*, Vol. 21, No. 8, pp 673-678, 1996.
- ARB, "Proposed Amendments to California Exhaust and Evaporative Emission Standards and Test Procedures for Passenger Cars, Light-Duty Trucks, and Medium-Duty Vehicles, LEV II," *California Air Resources Board Staff Report: Initial Statement of Reasons*, September 1998.
- Baker, B. S., et al., "Selective Removal by Methanation of Carbon Monoxide from a Mixture of Gases Containing Carbon Dioxide," U.S. Patent 3615164, 1971.
- Ballard Power Systems, Web Page, www.ballard.com and 1996 Annual Report.
- Barbir, F., Tradeoffs in Ambient/Pressurized PEM Systems," SAE Fuel Cells for Transportation TOPTEC, Cambridge Massachusetts, March 1998.
- Barrigh, J., Ballard Generation Systems, personal communication, November 1998.
- BØgild Hansen, J., "Fuel Processing for Mobile Fuel Cell Applications," in Proceedings from Fuel Cells for Traction Applications, Royal Swedish Academy of Engineering Sciences, IVA-R 408, February 1994.
- Borroni-Bird, C. E., "Fuel Cell Commercialization Issues for Light-Duty Vehicle Applications," Proceedings of the Fourth Grove Fuel Cell Symposium, September 1995, *Journal of Power Sources*, Vol. 61, July 1996.
- Brady, S., "40 Foot PAFC Hybrid Electric Bus," SAE Fuel Cells for Transportation TOPTEC, Cambridge Massachusetts, March 1998.
- Burke, A., "Ultracapacitors: Cost-Effective HEV Power Management," SAE TOPTEC Making Hybrid Electric Vehicles Commercially Viable," New York, New York, May 1998.

Callaghan, V. M., "100 kW PAFC Fuel Cell Power System," SAE Fuel Cells for Transportation TOPTEC, Cambridge Massachusetts, March 1998.

Colsmann, G., "Verfahrenstechnische Optimierung der Brenngaserzeugung für Brennstoffzellen in Kraftfahrzeugen", (Process Engineering Optimization of Combustion Gas Production for Fuel Cells in Vehicles), Research Center Jülich GmbH (FZJ), Report No. Jül-3127, ISSN 0944-2952, October 1995.

Cooper, R. and G. Feasey, "Summary of dbb's MeOH Fuel Cell Engine Development Activities," SCAQMD Reformer Conference, November 20, 1998.

Decisioneering, Crystal Ball Manual, Denver, CO, 1996.

DeLuchi, M., "Hydrogen Vehicles: An Evaluation of Fuel Storage Performance, Safety, Environmental Impacts, and Cost," University of California, Davis, 1989.

Düsterwald, H. G., "Untersuchung eines Methanolreformerkonzepts unter den besonderen Bedingungen der Dynamik und Langzeitstabilität beim Einsatz im Brennstoffzellen-Pkw," (Investigation of a methanol reformer concept under dynamic and steady state conditions for use with fuel cells in passenger cars), Research Center Jülich (FZJ) Report No. Jül-3452, ISSN 0944-2952, November 1997.

Edwards, N., et al. "Fuel Cell System for Transport Applications Including On-Board HotSpot™ Reformer," SAE Fuel Cells for Transportation TOPTEC, Cambridge, Massachusetts, March 1998.

Ekdunge, P. and M. Råberg, "The Fuel Cell Vehicle Analysis of Energy Use, Emissions, and Cost," International Journal of Hydrogen Energy, Vol. 23, No. 5, pp 381-385, 1998.

EPRI, "Solid Oxide Fuel Cells," Electric Power Research Institute R&D Report, BR-106591, 1996.

Ernst, W., "Reformate-Fueled PEM Fuel Cells," SAE Fuel Cells for Transportation TOPTEC, March 1998.

Fitzgerald, B.G., Booz-Allen & Hamilton, personal communication, August 1996.

Ganser, B., "Verfahrensanalyse: "Wasserstoff aus Methanol und dessen Einsatz in Brennstoffzellen für Fahrzeugantriebe," (Process Engineering Analysis: Hydrogen from Methanol and use in Fuel Cells for Vehicle Power), Research Center Jülich GmbH (FZJ), Report No. Jül-2748, ISSN 0944-2952, March 1993.

Golunski, S., "Hot Spot™ Fuel Processor, Advancing the Case for Fuel Cell Powered Cars," Platinum Metals Review, 42, (1),2-7, 1998.

Gottesfeld, S., et al., "Polymer Electrolyte Direct Methanol Fuel Cells: An Option for Transportation Applications," 1996 Fuel Cell Seminar, November 1996.

Gottesfeld, S., "Polymer Electrolyte Direct Methanol Fuel Cells: Developments for Portable Power and Potential Transportation Applications," *1998 Fuel Cell Seminar*, November 1998.

Halpert, G., Jet Propulsion Laboratory, personal communication, June 1997.

Halpert, G., "Update of Direct Methanol Fuel Cell Development," Windsor Workshop on Transportation Fuels, June 1997 (b).

Heiler, F., "Mercedes-Benz Fuel Cell Research Car Debuts at Frankfurt Show," Media Information, Daimler-Benz, September 1997.

Howard, P. F., "Ballard Zero Emission Fuel Cell Bus Engine," Proceedings of the 12th International Electric Vehicle Symposium, December 1994.

Hydrogen and Fuel Cell Letter, "Chicago Transit Unveils Ballard Hydrogen Fuel Cell Bus, Fleet Test to Start Next Year," Volume X, Number 10, October 1995.

HyWeb, *Hydrogen Gazette*, www.hywebde, Ludwig Bölkow System-technik, GmbH, 1998.

James, B. D., "Technology Development Goals for Automotive Fuel Cell Power Systems," Prepared by Argonne National Laboratory for DOE, Final Report ANL-94/44, August 1994.

Kalhammer, F. R., et al., "Performance and Availability of Batteries for Electric Vehicles: A Report of the Battery Technical Advisory Panel," prepared for ARB, December 1995.

Kawatsu, S., et al., "PEFC R&D Technology at Toyota," *1996 Fuel Cell Seminar*, November 1996.

Krumpelt, M., and C.C. Christianson, "An Assessment and Comparison of Fuel Cells for Transportation Applications," Argonne National Laboratory, 1989.

Kumar, R., and S. Ahmed, "Fuels Processing for Transportation Fuel Cell Systems," Argonne National Laboratory Report ANL/CMT/CP-84932, July 1995.

Lai, J., "Bidirectional DC to DC Converters for Fuel Cell Systems," SAE Fuel Cells for Transportation TOPTEC, Cambridge, Massachusetts, March 1998.

Lancaster, P., "Ballard Receives \$4 Million Order from Delphi to Supply Fuel Cells for Chrysler," News Release, Ballard Power Systems, February 1997.

Ledjeff-Hey, K. and A. Heinzl, "Critical Issues and Future Prospects for Solid Polymer Fuel Cells," Proceedings of the Fourth Grove Fuel Cell Symposium, September 1995, *Journal of Power Sources*, Vol. 61, July 1996.

Menser, R. and B. Höhle, "Verfahrensanalyse der Stromerzeugung für Fahrzeugantriebe mit Methanol als Energieträger und Brennstoffzellen als Energieumwandlungssystem," (Process Engineering Analysis of Vehicle Power Production with Methanol as an Energy Carrier and Fuel

Cells as an Energy Conversion System), Research Center Jülich GmbH (FZJ), Report No. Jül-3445, ISSN 0944-2952, October 1997.

Meyer, A., "Ambient Pressure PEM Systems," SAE Fuel Cells for Transportation TOPTEC, March 1998.

Mitchell, W. L., "CO Clean-Up and Fuel Cell Performance on Gasoline/Ethanol Fuel Processor Reformate," SAE Fuel Cells for Transportation TOPTEC, Cambridge Massachusetts, March 1998.

Mitchell, W. L., "Development of an Integrated Reformer/Fuel Cell Power System for Petroleum and Alcohol Fueled Vehicles: Part 1 - Brassboard Demonstration," *1998 Fuel Cell Seminar*, November 1998.

Murphy, T. C., et al., "Electro-chemical Capacitor Developments," *Electric & Hybrid Vehicle Technology*, UK & International Press, 1996.

O'Brien, C. and S. Hochgreb, "Thermodynamic Analysis of Fuel Processing," Western States Section/The Combustion Institute, 1997 Spring Meeting, April 1997.

Ogden, J. M., T. G. Kreutz, and M. Steinbugler, "Fuels for Fuel Cell Vehicles: Vehicle Design and Infrastructure Issues," SAE Paper 982500, October 1998.

Patil, P., "The Role of Alternative Fuels in the New Generation of Vehicles," SAE Paper 952379, October 1995.

Powers, C. A., and M. R. Wool, "User's Manual, Aerotherm Chemical Equilibrium Computer Program, (ACE81)," Acurex Corporation, Aerotherm Division, Mountain View, California, Acurex Report UM-81-11/ATD, August 1981.

Randhava, S. S., "Selective Catalytic Methanation of a Gaseous Mixture Containing Carbon Monoxide," U.S. Patent 3663162, 1972.

Rehg, T., "High-Efficiency, High-Power Density, Co-Tolerant PEM Fuel Cell Stack System," Fuel Cells for Transportation, DOE Research and Development Abstracts, April 1999.

Reinkingh, J., "Hot Spot Fuel Processor," SAE Fuel Cells for Transportation TOPTEC, Cambridge Massachusetts, March 1998.

Riedel, E., "Untersuchung und Entwicklung eines katalytischen Brenners zur Beheizung eines Kompaktreformers," (Investigation and Development of a Catalytic Burner for Heating a Compact Reformer), Research Center Jülich GmbH (FZJ), Report No. Jül-3240, ISSN 0944-2952, June 1996.

Roan, V., "Energy and Power Management for Fuel Cell Vehicles," SAE Fuel Cells for Transportation Topotec, March 1993.

Roman, D., "Ballard, Ford, Daimler-Benz to Join Forces to Develop Fuel Cell Technology for Future Vehicles in over C\$600 Million Transaction," News Release, Ballard Power Systems, December 1997.

Rostrup-Nielsen, J., R., Christiansen, L., J., "Fuel Cell Power Plants for High Efficiency - Principles and Status," Presented at the 1991 International Symposium on Energy and Environment, August 1993, Helsinki.

Srinivasan, S., Los Alamos National Laboratory, personal communication, August 1996.

Taylor, D., Southern California Edison, personal communication, September 1998.

Teagan, P., "The Environmental Benefits of Fuel Cell Technology," World Fuel Cell Council, July 1992.

Thomas, C. E., "Overview of Hydrogen Production Options for Fuel Cell Vehicles," Seventh Annual U.S. Hydrogen Meeting, Alexandria, Virginia, April 1996.

Thomas, C. E. et al., "Societal Impacts of Fuel Cell Options for Fuel Cell Vehicles," SAE Paper 982496, October, 1998.

Twigg, M., *Catalyst Handbook*, Wolfe Publishing, 1989.

Unnasch, S., "Evaluation of Fuel-Cycle Emissions on a Reactivity Basis," Acurex Environmental Final Report FR-96-114, prepared for California Air Resources Board, ARB Contract Number A166-134, September 1996.

Unnasch, S., et al., "Reclamation of Automotive Batteries: Assessment of Health Impacts and Recycling Technology, Task 1: Assessment of Recycling Technology," ARB Contract Number 93-323, Final Report, March 1995.

Van Der Drift, A., "Low-NOx Hydrogen Burner," *International Journal of Hydrogen Energy*, Vol 21, No. 6, pp. 445-449, 1996.

Westinghouse, "Solid Oxide Fuel Cell, Breakthrough Technology for Highest Efficiency Power Generation", 1997.

Wimmer, R., Emission Characterization of a Fuel Cell powered Bus, SAE Paper 980680, February 1998.

Wimmer, R., Integration Issues and Test Results of an FC/Battery System," SAE Fuel Cells for Transportation TOPTEC, Cambridge, Massachusetts, March 1998(b).

Woods, R. R., "Fuel-Flexible Fuel Processor," *1998 Fuel Cell Seminar*, November 1998.

Woods, T., Booz-Allen & Hamilton, personal communication, August 1996.

Yolota, K., and T. Misono, "11 MW Fuel Cell Plant Operation Interim Report," 1992 Fuel Cell Seminar Program and Abstracts, November 1992.

